

**VALIDATION OF COMPUTER-GENERATED RESULTS WITH
EXPERIMENTAL DATA OBTAINED FOR TORSIONAL
VIBRATION OF SYNCHRONOUS MOTOR-DRIVEN
TURBOMACHINERY**

A Thesis

by

NIRMAL KIRTIKUMAR GANATRA

Submitted to the Office of Graduate Studies of
Texas A&M University
in partial fulfillment of the requirements for the degree of

MASTER OF SCIENCE

May 2003

Major Subject: Mechanical Engineering

**VALIDATION OF COMPUTER-GENERATED RESULTS WITH
EXPERIMENTAL DATA OBTAINED FOR TORSIONAL
VIBRATION OF SYNCHRONOUS MOTOR-DRIVEN
TURBOMACHINERY**

A Thesis

by

NIRMAL KIRTIKUMAR GANATRA

Submitted to Texas A&M University
in partial fulfillment of the requirements
for the degree of

MASTER OF SCIENCE

Approved as to style and content by:

John Vance
(Chair of Committee)

N. K. Anand
(Member)

Jay Walton
(Member)

J. Weese
(Interim Head of Department)

May 2003

Major Subject: Mechanical Engineering

ABSTRACT

Validation of Computer-Generated Results with Experimental Data Obtained for Torsional Vibration of Synchronous Motor-Driven Turbomachinery. (May 2003)

Nirmal Kirtikumar Ganatra, Dipl., K. J. Somaiya Polytechnic, Bombay, India;

B.E., University of Bombay, India

Chair of Advisory Committee: Dr. John Vance

Torsional vibration is an oscillatory angular twisting motion in the rotating members of a system. It can be deemed quite dangerous in that it cannot be detected as easily as other forms of vibration, and hence, subsequent failures that it leads to are often abrupt and may cause direct breakage of the shafts of the drive train. The need for sufficient analysis during the design stage of a rotating machine is, thus, well justified in order to avoid expensive modifications during later stages of the manufacturing process. In 1998, a project was initiated by the Turbomachinery Research Consortium (TRC) at Texas A&M University, College Station, TX, to develop a suite of computer codes to model torsional vibration of large drive trains. The author had the privilege of developing some modules in Visual Basic for Applications (VBA-Excel) for this suite of torsional vibration analysis codes, now collectively called *XLTRC-Torsion*. This treatise parleys the theory behind torsional vibration analysis using both the Transfer Matrix approach and the Finite Element approach, and in particular, validates the results generated by *XLTRC-Torsion* based on those approaches using experimental data available from tests on a 66,000 HP Air Compressor.

Dedicated to my loving parents for providing me with the best of everything I could ever ask for, and for inculcating values and morals in me that I will treasure all my life.

ACKNOWLEDGEMENTS

It is with great pleasure and felicity that I am presenting this thesis on “Validation of Computer-Generated Results with Experimental Data obtained for Torsional Vibration of Synchronous Motor-Driven Turbomachinery”.

I would like to express my sincere thanks to my research advisor Dr. John Vance for giving me the cherished opportunity to work under his guidance. I would be lacking on my part if I failed to express my appreciation to Mark Corbo (No Bull Engineering) and Charles Yeiser (Rotor Bearing Technology and Software) for providing me with the data for the 66,000 HP Texaco Air Compressor that was required to consummate this research project.

I fall short of words to express a sense of gratitude towards Andrew Conkey for helping me grasp the basics during the initial programming stages of the project. I would also like to thank Asit Singhal (Atlas Copco US Inc.) and Avijit Bhattacharya (Turbomachinery Lab, Texas A&M University) for their much solicited guidance in programming the software for this project. It should be noted that the computer codes, *XLTRC-Torsion*, have been and are still being developed by graduate students advised by Dr. Vance. Therefore, *XLTRC-Torsion* also makes use of several subroutines developed by others.

Last but not the least, I would like to thank the members of the Turbomachinery Research Consortium (TRC) at Texas A&M University for exhibiting faith in this project by allocating the necessary research funds, without which this project would not have materialized.

TABLE OF CONTENTS

	Page
ABSTRACT	iii
DEDICATION.....	iv
ACKNOWLEDGEMENTS.....	v
TABLE OF CONTENTS.....	vi
LIST OF TABLES.....	viii
LIST OF FIGURES	ix
INTRODUCTION	1
LITERATURE REVIEW	6
ANALYTICAL MODELING OF THE DRIVE TRAIN.....	10
General Guidelines for Modeling of Rotors for Torsional Analysis.	14
NUMERICAL SOLUTION TECHNIQUES.....	17
Transfer Matrix Method.....	17
Finite Element Method.....	21
Formulation of Element Inertia and Stiffness Matrices	22
System Inertia and Stiffness Matrix	26
Solution Methods for the Eigenproblem.....	27
Contrariety between Transfer Matrix and Finite Element Techniques	30
TIME TRANSIENT ANALYSIS.....	32
Starting a Synchronous Motor.....	34
Modeling and Analysis.....	36
Run-up Calculations.....	37
Transient Calculations.....	38
Integration of the Torque Vector.....	42
Types of Forcing Torque.....	43

	Page
Campbell Diagrams.....	47
Driving Torque Definition for Use in Transient Analyses.....	49
CUMULATIVE FATIGUE ASSESSMENT AND PREDICTING	
NUMBER OF STARTS	62
VALIDATION OF CODE-GENERATED RESULTS WITH	
ANALYSIS AND TEST DATA	69
66,000 HP Air Compressor Train	69
Analytical Model of the Drive Train.....	71
Undamped Torsional Natural Frequency Calculation.....	81
Campbell Diagrams.....	84
Mode Shapes	88
Transient Analysis Results	94
Cumulative Fatigue Analysis	118
CONCLUSION.....	130
NOMENCLATURE	133
REFERENCES	139
VITA.....	144

LIST OF TABLES

TABLE	Page
1 Geometric Data for the Five Inertia, Transfer Matrix Model	72
2 Geometric Data for the Seventy-four Inertia, Transfer Matrix Model....	73
3 Geometric Data for the Five Inertia, Finite Element Model	75
4 Geometric Data for the Seventy-four Inertia, Finite Element Model	76
5 Comparison of Undamped Torsional Natural Frequency Results	82
6 Transient Analysis Input Data for the Five inertia, Transfer Matrix Model	96
7 Transient Analysis Input Data for the Seventy-four inertia, Transfer Matrix Model	97
8 Transient Analysis Input Data for the Five inertia, Finite Element Model	98
9 Transient Analysis Input Data for the Seventy-four inertia, Finite Element model	99
10 Comparison of Estimated and Actual Run-Up Times	101
11 Summary of Results of Transient Torque Analyses	117
12 Comparison of Predicted Lives Calculated Using Fatigue Analysis	129

LIST OF FIGURES

FIGURE	Page
1 Lumped Parameter Model for Torsional Vibration Analysis	11
2 A Single Branch System with a Gear Pair	13
3 Point of Rigidity.....	15
4 Torsional Inertia and Stiffness Elements of the nth Station	18
5 Synchronous Motor Torque Input.....	44
6 Pulsating Frequency of a Synchronous Machine	45
7 Arbitrary Frequency as a Function of Rotor Speed.....	45
8 Torque as an Arbitrary Function of Time	47
9 Torsional Interference Diagram (Campbell Diagram).....	48
10 “Dummy” Air Compressor Train Under Study, with Assumed Values	51
11 Geometry Plot of a Five-Disk Train	52
12 Campbell Diagram.....	53
13 Run-Up Plot of the Motor.....	54
14 Torque Plot Using Definition of Driving Torque in Eq. (78), with No Damping Considered	55
15 Torque Plot Using Definition of Driving Torque in Eq. (75), with No Damping Considered	57
16 Torque Plot Using Definition of Driving Torque in Eq. (78), and Considering Damping	58
17 Torque Plot Using Definition of Driving Torque in Eq. (75), and Considering Damping	59

FIGURE	Page
18 Air Compressor Train – Schematic.....	69
19 Five Inertia Model of the Air Compressor Train	80
20 Seventy-four Inertia Model of the Air Compressor Train	81
21 Run-Up and Transient Torque Graphs Plotted Using Data From Experiments	83
22 Campbell diagram from Corbo et al. [15].....	85
23 Campbell Diagram for the Five Inertia Model Using Transfer Matrix Method	86
24 Campbell Diagram for the Seventy-four Inertia Model Using Transfer Matrix Method.....	86
25 Campbell Diagram for the Five Inertia Model Using Finite Element Method	87
26 Campbell Diagram for the Seventy-four Inertia Model Using Finite Element Method.....	87
27 Mode Shapes for the Five Inertia Model Using Transfer Matrix Method	89
28 Mode Shapes for the Seventy-four Inertia Model Using Transfer Matrix Method	90
29 Mode Shapes for the Five Inertia Model Using Finite Element Method	91
30 Mode Shapes for the Seventy-four Inertia Model Using Finite Element Method.....	92
31 Mode Shape for first mode (14.00 Hz) from Corbo et al. [15].....	93
32 Mode Shape for second mode (34.00 Hz) from Corbo et al. [15]	93
33 Motor Torque Characteristic Curve	95

FIGURE	Page
34 Compressor (Load) Torque Characteristic Curve	95
35 Run-Up Curve for the Five Inertia, Transfer Matrix Mode	102
36 Run-Up Curve for the Seventy-four Inertia, Transfer Matrix Model	102
37 Run-Up Curve for the Five Inertia, Finite Element Model	103
38 Run-Up Curve for the Seventy-four Inertia, Finite Element Model	103
39 Run-Up Curve Plotted Using Data From Experiments	104
40 Transient Torque Plot for 5 Inertia, Transfer Matrix Model at Station No. 1 (Motor Rotor)	105
41 Transient Torque Plot for 74 Inertia, Transfer Matrix Model at Station No. 27 (Motor Rotor)	106
42 Transient Torque Plot for 5 Inertia, Finite Element Model at Node No. 1 (Motor Rotor)	108
43 Transient Torque Plot for 74 Inertia, Finite Element Model at Node No. 27 (Motor Rotor)	108
44 Transient Torque Plot for the 66,000 Hp Air Compressor Plotted Using Data From Experiments	109
45 A Closer View of the Transient Torque Plot for the 66,000 Hp Air Compressor at Resonant Speed to the First Torsional Natural Frequency Plotted Using Data From Experiments	110
46 A Closer View of the Transient Torque Plot for the 66,000 Hp Air Compressor at Resonant Speed to the First Torsional Natural Frequency Predicted by the Five Inertia, Transfer Matrix Model	112
47 A Closer View of the Transient Torque Plot for the 66,000 Hp Air Compressor at Resonant Speed to the First Torsional Natural Frequency Predicted by the Seventy-four Inertia, Transfer Matrix Model	113

FIGURE	Page
48 A Closer View of the Transient Torque Plot for the 66,000 Hp Air Compressor at Resonant Speed to the First Torsional Natural Frequency Predicted by the Five Inertia, Finite Element Model	114
49 A Closer View of the Transient Torque Plot for the 66,000 Hp Air Compressor at Resonant Speed to the First Torsional Natural Frequency Predicted by the Seventy-four Inertia, Finite Element Model	115
50 A Closer View of the Transient Torque Plot for the 66,000 Hp Air Compressor at Resonant Speed to the First Torsional Natural Frequency Predicted by Corbo et al. [16]	116
51 Fatigue Analysis Results for 5 Inertia, Transfer Matrix Model at Station No. 1 (Motor Rotor) with Diameter = 21.069"	119
52 Fatigue Analysis Results for 5 Inertia, Transfer Matrix Model at Station No. 1 (Motor Rotor) with Diameter = 13.17"	120
53 Fatigue Analysis Results for Experimental Transients Applied on 5 Inertia, Transfer Matrix Model at Station No. 1 (Motor Rotor) with Diameter = 13.17"	122
54 Fatigue Analysis Results for 74 Inertia, Transfer Matrix Model at Station No. 27 (Motor Rotor) with Diameter = 13.17"	124
55 Fatigue Analysis Results for Experimental Transients Applied to the 74 Inertia, Transfer Matrix Model at Station No. 27 (Motor Rotor) with Diameter = 13.17"	125
56 Fatigue Analysis Results for 5 Inertia, Finite Element Model at Element No. 1 (Motor Rotor) with Diameter = 21.069"	126
57 Fatigue Analysis Results for 5 Inertia, Finite Element Model at Element No. 1 (Motor Rotor) with Diameter = 13.17"	127
58 Fatigue Analysis Results for 74 Inertia, Finite Element Model at Element No. 27 (Motor Rotor) with Diameter = 13.17"	128

INTRODUCTION

Torsional vibration is an oscillatory angular motion that causes relative twisting in the rotating members of a system. This oscillatory twisting motion gets appended to the steady rotational motion of the shaft in a rotating or reciprocating machine. Systems in which some driving equipment drives a number of components, thus enabling them to rotate, are often subjected to constant or periodic torsional vibration. This necessitates the analysis of the torsional characteristics of the system components.

Often, if the frequency of a machine's torque variation matches one of the resonant torsional frequencies of the drive train system, large torsional oscillations and high shear stresses can occur within the vibrating components. If a machine experiencing such torsional vibration is continuously operated, an unwarranted fatigue failure of weak system components is imminent. One of the major obstacles in the measurement and subsequent detection of torsional vibration in a machine is that torsional oscillations cannot be detected without special equipment. However, prediction of torsional natural frequencies of a system and consequent design changes that avoid the torsional natural frequencies from occurring in the operating speed range of a machine is necessary. Oscillatory behavior of a system component experiencing torsional vibration, however, may often be of little interest to the designer unless it affects the basic functions expected of the system. The stresses occurring within components are of paramount importance as

they determine the structural integrity and life of the machine. This helps determine the allowable limit of the torsional vibration. Many a time, torsional vibration produces stress reversals causing metal fatigue and gear tooth impact forces.

Turbomachinery drive trains driven by synchronous motors or diesel engines generally experience torsional fluctuations that arise due to the torsional impulses generated in the machine. These impulses, then, produce torsional vibrations in the rotating machine components. When these vibrations encounter a torsional natural frequency of the system, resonance occurs in the machine often leading to direct failure of the weakest machine components. This torsional vibratory motion is usually limited by the damping due to fluids such as oil or water in contact with the rotating members, internal machine resistance, or resistance imposed by a torsional damper attached to the machine.

When two or more different machines are coupled together, wherein one drives another operating as a single unit, any deviation from pure rotation in one would be transmitted to some extent to other components. It is important to note that the natural frequencies of the coupled system will be different from that of each individual machine taken into account. It does not matter whether each component is individually safe, since perilous torsional vibrations can still originate as a result of the combination. One can, thus, state examples of an engine-generator, motor-compressor or a motor-pump combination. There will be potentially dangerous torsional vibrations in the combination, at distinct speeds and loads in different parts of the combined equipment.

Though the identification of the torsional vibration phenomenon is not new, it still remains one of great importance when designing turbomachinery. It may be noted that this problem persists since the available knowledge, though limited, is not fully put to use and complex machineries are combinations of existing individual machines which in combination may produce undesirable vibration characteristics.

Curbing dangerous shaft failures that occur due to torsional vibration are hardly the main cause of concern for equipment manufacturers, for whom satisfactory operation means a lot more than avoidance of such mechanical failures. Wear and tear of components, excessive noise and vibration are some of the other undesirable effects that may occur. The growing need for making machines more efficient and productive by increasing speed and loads, while trying to significantly reduce weights for ease of transportation and cut down on costs leads to a sizeable number of vibration problems. High loads may also occur in covert forms such as machine start-ups and process changes.

The torsional characteristics of a system greatly depend on the stiffness and inertia in the train. While some properties of the system can be changed, generally the system inertia cannot be altered as required. Consider the simple case of a pump, whose inertia properties are greatly dependent upon the sizes and thicknesses of its impellers, shafts, driving motors etc. This is important since a change in geometries and overall sizes in order to favor torsional characteristics may obscure consideration of characteristics like the pump hydraulics and lateral vibrations. Besides, the selection of the driver, which is primarily based on the power and load requirements, can hardly be

dictated based on torsional characteristics.. The typical engineering objectives of torsional vibration analysis are listed below [1]:

1. Predicting the torsional natural frequencies of the system.
2. Evaluating the effect of the natural frequencies and vibration amplitudes of changing one or more design parameters (i.e. "sensitivity analysis").
3. Computing vibration amplitudes and peak torque under steady-state torsional excitation.
4. Computing the dynamic torque and gear tooth loads under transient conditions (e.g., during machine startup).
5. Evaluating the torsional stability of drive trains with automatic speed control.

Early predictions of torsional characteristics of a piece of machinery would greatly reduce costs if the results of the analyses are judiciously utilized. This can be effected by studying these results and incorporating the changes on paper early during the design stage rather than embarking upon final testing of the product without these considerations and suggesting expensive changes later. The software used for predicting torsional natural frequencies and similar other characteristics should be capable of modeling important properties of the system besides being cost effective in terms of time [34]. It should also be able to incorporate various components like dampers, absorbers, multiple shafts, branches, etc. that affect the dynamic performance of a system. This, however, leads to a trade-off between the amount of time and money spent in generating a model using the software and the degree of accuracy gained by making the model to incorporate finer aspects of the system. Thus, a useful design tool for torsional analysis

should allow quick generation of a model and provide precise results that are satisfactory within pre-determined limits of accuracy [34].

LITERATURE REVIEW

A review of the available literature on torsional vibration analysis identifies the following:

1. History of torsional vibration analysis
2. Modeling of torsional system components
3. Transfer Matrix and Finite Element methods of torsional vibration analysis
4. Methods for prediction of machine life using cumulative fatigue theories

A chronological and informative discussion about the history of torsional vibration analysis is presented in Wilson [2]. It recognizes that early failures in marine and aeronautical drive trains presented the need for torsional vibration analysis.

A trial and error technique called the Holzer's method was developed in early 1900s' for determining the natural frequencies and mode shapes of torsional systems. Assuming a trial frequency and starting at one end of the drive train, with this technique, one can progressively calculate the torque and angular displacement of each station to the other end. If the torque thus calculated is zero at the other end (the boundary condition), the assumed frequency is the natural frequency and the corresponding angular displacement defines the mode shape. The original method does not account for torsional damping and hence can only be used for systems with negligible damping. Rotating machinery seldom contains a large amount of torsional damping, but some special couplings are designed to add damping. The numerous degrees of freedom to be accounted for while analyzing actual machinery make the Holzer's method advantageous

if all the degrees of freedom are to be accounted for with physical coordinates. However, one can often neglect the higher damped modes as they are of lesser importance in design even though the system may have many degrees of freedom. The Transfer Matrix method, the application of which has been described in detail in Pestel and Leckie [3] and Sankar [32], is an extension of the Holzer's method. The method is modified by writing equations relating angular displacements to the internal forces in a matrix form and using complex variables to handle the damping.

Using the modal approach as illustrated in Lund [4] and Childs [5-7], one can efficiently analyze the transient response of drive trains with many degrees of freedom. One can conceive the modal analysis as a linear transformation of the system equations of motion from the "physical" or "actual" coordinates to "modal" or "principal" coordinates. Once the equations have been transformed in this way, a truncated series of these "modal" coordinates may be used to describe the dynamic behavior of the system using information about modes from a prior natural frequency analysis. The main advantage of using the modal approach is that the linear transformation can be "designed to suit" such that it uncouples the system equations of motion. This method, thus, leads to a substantial cutting down of computation time by decreasing the problem size by using just a few low frequency modes for modal representation. However, the main disadvantage of this method is that localized damping (e.g. at a shaft coupling) is not correctly modeled.

Eshleman [8] applied the modal approach in order to determine the torsional response of internal combustion engine drive trains that are subjected to constant and

pulsating torques. Anwar and Colsher [9] extended the modal approach to incorporate damping and backlash found in gears and couplings for torsional vibration analysis of large systems. They have presented a detailed discussion on the analysis of startup of drive trains employing a synchronous motor.

The torsional characteristics of the rotor system can also be modeled using the Finite Element method. As in the transfer matrix method, a complex structure is regarded as a finite assemblage of discrete continuous elements. The basic aim of the modeling is to obtain the component equations of motion in the form of a large matrix. The Finite Element method provides a systematic way of obtaining these equations, with virtually no restrictions on the system geometry, in a form suitable for computer implementation. The procedure for derivation of the element inertia and stiffness matrices has been outlined right from the basics in Rao [10]. These element matrices are then assembled to form the system inertia and stiffness matrices. Various methods for solving the system equations thus obtained are discussed in Bathe [11]. Squires [12] elicits the Finite Element method for determining torsional eigenvalues as well as eigenvectors, besides describing the modal method in which he uses undamped modes with truncation to determine the transient response.

Corbo and Malanoski [13] touch almost all possible aspects, viz. modeling for torsional analysis, undamped and damped torsional natural frequency analyses, considerations for Variable Frequency Drives (VFDs), forced response analysis, transient analysis, etc. that should to be considered while designing rotating machinery in order to avoid failures due to torsional vibration. Wachel and Szenasi [14] is another such

comprehensive resource of useful information on modeling and analysis of drive trains for torsional vibration. Corbo et al [15, 16] enumerate an explicit procedure for design that can be used for avoiding problems arising due to torsional vibration in all forms of synchronous motor-driven turbomachinery. Their procedure, which includes an exhaustive practical example, lists detailed guidelines that a designer can follow while performing synchronous motor startup analyses, determination of shaft size, surface finish, stress concentration, notch sensitivity, design safety factors, etc. They advocate the use of the strain life-theory of failure as opposed to the conventional stress-life approach using Miner's rule to determine the life of the machine, defined in terms of the number of startups the machine can survive. Shigley and Mischke [17] give a generalized procedure for design of shafts under fatigue loading. The relations for determining the values of various factors like those used to account for surface finish, size, etc. in the determination of number of machine startups presented in this treatise have also been taken from [17]. Material properties like modulus of elasticity, true stress and strain at fracture during tensile test, elastic and plastic strain components for different metals have been obtained from [18]. Lipson and Juvinall [19] present notch sensitivity curves to be used under different types of fatigue loading. Notch sensitivity curves for a stepped shaft element under torsional loading have been incorporated into *XLTRC-Torsion*.

ANALYTICAL MODELING OF THE DRIVE TRAIN

The primary objectives warranting rotordynamic modeling and analysis of a system may be diversified based on the aspects of shaft dynamics that need to be predicted. In case of torsional vibration, prediction of the system torsional critical frequencies, determination of torsional mode shapes and prediction of the torque and stress values reached in the shafts of the system rotor, which may then lead to useful interpretation and appropriate design modification are the objectives usually sought. Rotordynamic analyses can be classified as either linear or non-linear analyses, steady state or transient analyses and static or dynamic analyses.

A turbomachinery drive train is often a complicated arrangement of the drive unit, couplings, gearboxes, and one or more driven units, each of which can be represented by masses/inertias and elastic components. Accounting for these components into a model provides the facility for analyzing the model mathematically by considering it as an equivalent system that can be subject to dynamic analysis. This equivalent model, also called the lumped parameter model, comprises of lumped masses/inertias connected by massless elastic springs that represent the flexibility of shafts and couplings (Fig. 1). Usually, components of larger diameters may be considered rigid and be represented as inertias, whereas long slender shafts may be represented as torsional springs. The judgement of number of "stations" or segments into which a long shaft of constant diameter may be lumped depends on the highest mode of interest. The usual procedure for such "lumping" of shafts is to divide each shaft section into equal parts

("beams") and lump their masses into disks at the end of each beam. As a general rule, one takes the number of stations N to be at least one more than the number of natural frequencies of interest.

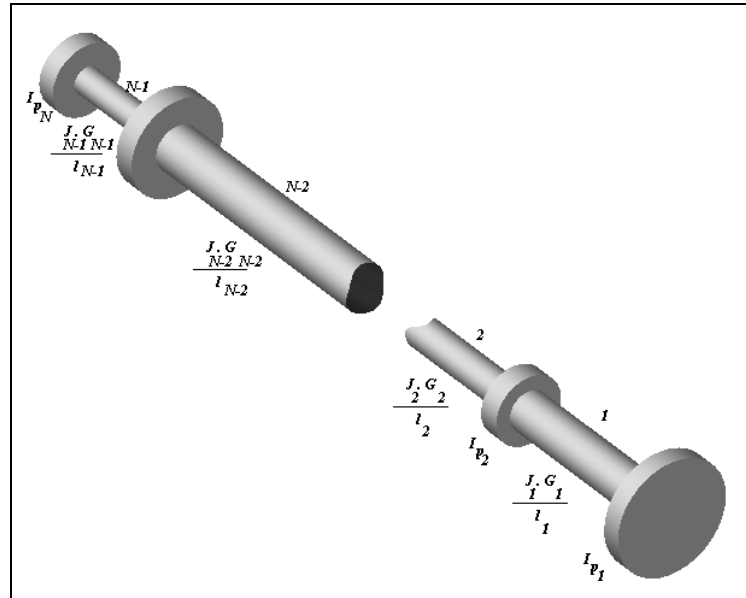


Fig. 1 Lumped parameter model for torsional vibration analysis, Vance [1]

The equation for determining the torsional stiffness of a shaft section may simply be written as

$$K = \frac{J \cdot G}{l} \quad \text{lb}\cdot\text{in}/\text{rad} \quad (1)$$

The value of J , also known as the polar area moment of inertia, is generally easily calculated. It is the area moment of inertia about the Z-axis (perpendicular to the section)

and is mathematically represented in the general form as $J = \int_A r^2 dA$. Here, r is called the instantaneous radius, while dA is the differential area. It can be noted that since $r^2 = x^2 + y^2$, one has the relation $J = I_{XX} + I_{YY}$, with I_{XX} and I_{YY} being the area moment of inertias about the X and Y-axes respectively on the sectioned plane.

One can, thus, write the equation for the polar area moment of inertia for a circular cross-section with a concentric hole in the center as

$$J = \frac{\pi \cdot (d_o^4 - d_i^4)}{32} \quad \text{in}^4 \quad (2)$$

The dissipation of vibration energy within the system is represented by viscous dampers present in the model. The dampers that are denoted by C_n ($1 \leq n \leq N - 1$) represent the energy dissipated in the relative twisting motion of the shafts, whereas those denoted by B_n ($1 \leq n \leq N$) represent the energy dissipated in the bearings, fluid impellers, etc. with an absolute angular velocity dependent torque. These viscous dampers are assumed to produce a torque that is linearly proportional to the angular velocity acting across the damper, but in the opposite sense.

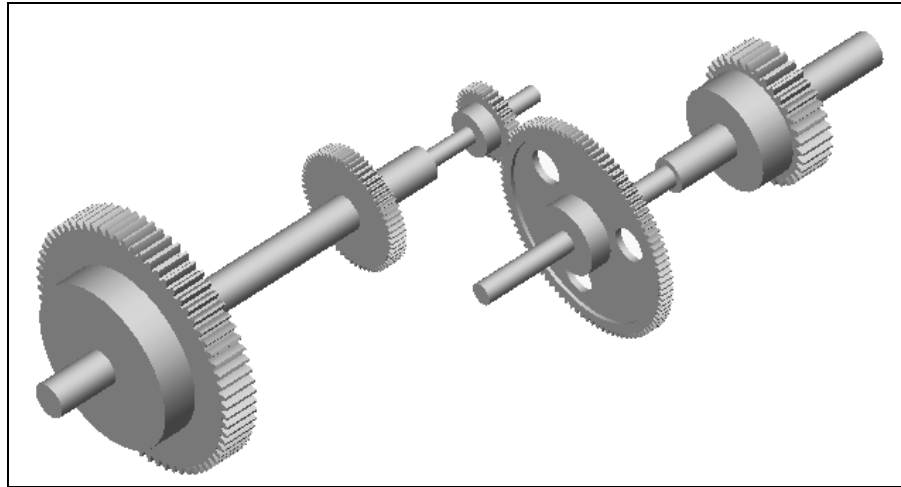


Fig. 2 A single branch system with a gear pair

If there are gear trains or similar speed modifying devices in the system (Fig. 2), the effective stiffness and inertias of the model are altered. Conventionally, all parameters are referred to the shaft speed of the driver station 1. The mass moment of inertia and stiffness parameters of every other station are then calculated as,

$$I_n = G_n^2 \cdot I'_n \quad (3)$$

$$K_n = G_n^2 \cdot K'_n \quad (4)$$

Modeling for torsional analysis involves discretization of the rotor in a typical Finite Element fashion. Here it is important to recognize that the basic mechanism in the case of torsional vibration is that of twisting of the shaft, and hence elementary one-dimensional “beams” may be used for torsional analysis. Due to this, torsional analysis is comparatively easier to perform than its lateral associate is. Complete torsional vibration analysis involves determination of the torsional natural frequencies and mode shapes of

the rotor, plotting the Campbell diagram based on the former results, performing a steady-state forced response analysis on the system with the exciting torques at their respective frequencies considered, and performing a transient analysis on the system to determine time-transient response of the system to the exciting torques.

General Guidelines for Modeling of Rotors for Torsional Analysis [13]

Listed below are a few guidelines that lead to successful modeling of the rotor system:

1. Disk elements should be located axially at the center of gravity of the impeller represented by them. Correct impeller inertias can be determined by using solid modeling software.
2. For extremely rigid disk elements, one should assume the portion of the shaft lying within that element to have zero deflection. One should, thus, calculate shaft element lengths up to the face, and not the center of gravity, of such impellers.
3. For disk elements that are not extremely rigid, their stiffening effect on the shaft carrying them is modeled by assuming that the shaft ends at the “point of rigidity” [20] within the impeller (Fig. 3). The shaft is assumed to deflect in its normal fashion till this point, whilst no deflection is assumed beyond that point. Equations for locating the point of rigidity for several common configurations can be found in Nestorides [20].

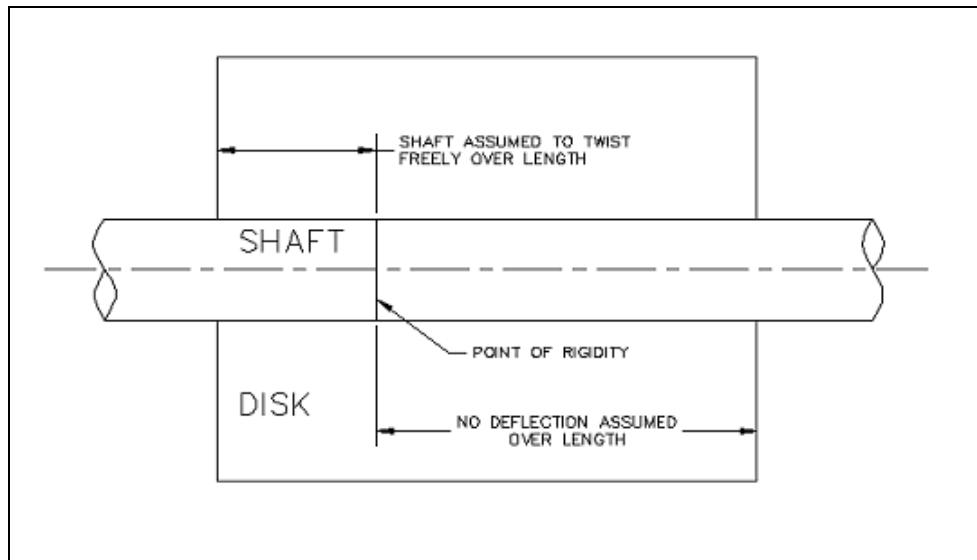


Fig. 3 Point of rigidity. Corbo and Malanoski [13]

4. A shaft joined to a non-rigid coupling or an impeller by an interference fit should be assumed to twist freely over a length equal to one-third of the overlap. The remainder of the shaft should be assumed rigid.
5. A shaft joined to a non-rigid coupling or an impeller by a keyed joint should be assumed to twist freely over a length equal to two-thirds of the overlap. The remainder of the shaft should be assumed rigid.
6. Some solution algorithms may not take the inertia of the shaft into account. In such a scenario, one should add one-half of the shaft inertia to each disk on the ends of the shaft element. In cases where the shaft inertia is a sizeable number when compared with the inertia of major disks in the system, one should divide the shaft element into

a number of disks and smaller shaft elements. Each disk should then represent a portion of the shaft inertia.

7. Couplings should be modeled as two disks with the coupling stiffness acting between them. The inertia of each such disk should be kept equal to one-half of the coupling inertia.
8. Flanges should be modeled as shaft elements with diameters equal to their bolt circle diameters.
9. The accuracy of a model increases with the number of elements when a distributed inertia is divided into a number of shaft and disk elements.
10. Although gear teeth have innate flexibility, usually they can be considered torsionally rigid. Gear tooth flexibility plays a role only in the calculation of very high natural frequencies or in systems having multiple gear meshes. Nestorides [20] gives equations to help account for gear tooth meshes.
11. “Wet” inertias should be considered for elements such as impellers and propellers that are operating in water. Although Corbo and Malanoski [13] state that they have used dry inertias for pump impellers with considerable accuracy in predictions, it is a general practice to assume “wet” inertias of impellers and propellers to be 20-25% more than their actual inertias for torsional analysis.

NUMERICAL SOLUTION TECHNIQUES

Presently, two analysis techniques are predominantly being used for analyzing torsional vibration in drive trains, viz. the Transfer Matrix method and the Finite Element method. A brief description of each of these methods has been presented in this chapter.

Transfer Matrix Method

The traditional Holzer's method for calculation of the natural frequencies of a system uses a numerical table for analysis. The Transfer Matrix method, which is an extension of the Holzer's method, uses matrices for analysis of torsional vibration. This method can be used to calculate the torsional natural frequencies of many different eigenvalue problems.

The basic concept governing the Transfer Matrix method is to express the state variables like torques and angular displacements at a station in the rotor model in terms of the variables of the previous station. While doing this, one conventionally moves from left to right, thus developing a chain-like relationship between variables of the subsequent stations. It, thus, becomes easy to predict the equations for torque and angular displacement at a particular station, if the same for the previous station in the line are known. Then, if the matrices of all the stations are multiplied together proceeding from left to right, the torque and the angular displacement at the rightmost station can be expressed in terms of the variables of the leftmost station. The elements of

the transfer matrices contain the eigenvalue. The boundary conditions at the rightmost end are obtained if this eigenvalue is legitimate.

Generally, in the case of torsional vibration, the boundary condition for torque at each end of the rotor is zero. For performing eigenvalue analysis, the amplitude of angular displacement at the rotor ends is arbitrary, as the eigenvalues do not depend on the amplitude of angular displacement. Having said this, the ratio of these amplitudes at each end is characterized by the eigenvector corresponding to each eigenvalue. This eigenvector can be used to determine the "mode shape" or the relative positions of the model inertias at the occurrence of each eigenvalue.

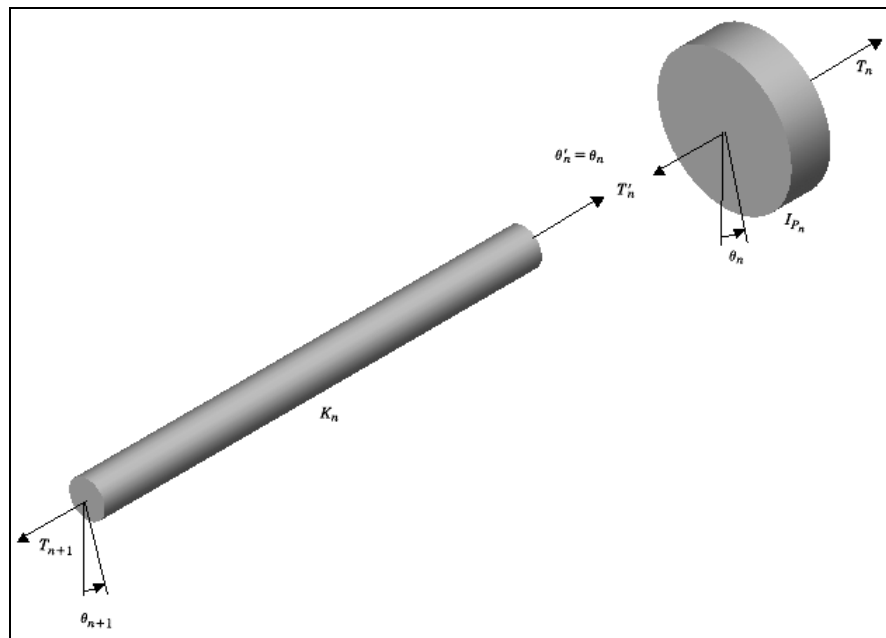


Fig. 4 Torsional inertia and stiffness elements of the nth station, Vance [1]

Figure 4 from Vance [1] shows the n th station of the model represented as comprising of an inertia element and a stiffness element. The left end of the inertia element has unprimed angular displacement and torque, while the corresponding parameters on the right end are primed. One can, thus, write the equation for the torque acting on the right of the n th inertia neglecting damping as obtained from Newton's Second Law or Lagrange's equation as follows:

$$T'_n = I_n \ddot{\theta}_n + T_n \quad (5)$$

Substituting a solution of the form $\theta_n(t) = \bar{a}_n e^{st}$ in the above equation and adding the identity $\theta'_n = \dot{\theta}_n$, one obtains transfer equations for the n th inertia in terms of the eigenvalues s . Here, \bar{a}_n is the amplitude of the oscillation at the n th station and s is the corresponding eigenvalue:

$$\begin{Bmatrix} \theta'_n \\ T'_n \end{Bmatrix} = \begin{bmatrix} 1 & 0 \\ I_n s^2 & 1 \end{bmatrix} \begin{Bmatrix} \theta_n \\ T_n \end{Bmatrix} \quad (6)$$

Let us denote the 2×2 transfer matrix of inertia defined by Eq. (6) as $[T_I]_n$.

As the torsional stiffness element has been assumed massless, torques on its ends are equal. Thus,

$$T_{n+1} = T_n \quad (7)$$

The torsional stiffness and internal damping resist the shaft torque. Hence,

$$T'_n = K_n (\theta_{n+1} - \theta_n) \quad (8)$$

Solving Eq. (8) for θ_{n+1} allows this equation and Eq. (7) to be written as,

$$\begin{Bmatrix} \theta_{n+1} \\ T_{n+1} \end{Bmatrix} = \begin{bmatrix} 1 & \frac{1}{K_n} \\ 0 & 1 \end{bmatrix} \begin{Bmatrix} \theta'_n \\ T'_n \end{Bmatrix} \quad (9)$$

Eq. (9) defines the shaft transfer matrix for the n th shaft as $[T_s]_n$.

Substitution of Expression (6) into Eq. (9) gives

$$\begin{Bmatrix} \theta_{n+1} \\ T_{n+1} \end{Bmatrix} = [T_{sl}]_n \begin{Bmatrix} \theta_n \\ T_n \end{Bmatrix} \quad (10)$$

where,
$$[T_{sl}]_n = [T_s]_n [T_l]_n \quad (11)$$

is evaluated by matrix multiplication. Here $[T_{sl}]_n$ is the transfer matrix of the n th station.

Now let $n = N$ in Eq. (6), let $n + 1 = N$ in Eq. (10), so $n = N - 1$, and so on.

Successive substitutions are made until the left end of the drive train is reached where $n = 1$.

Hence,
$$\begin{Bmatrix} \theta'_n \\ T'_n \end{Bmatrix} = [T_0] \begin{Bmatrix} \theta_1 \\ T_1 \end{Bmatrix} \quad (12)$$

Here,
$$[T_0] = [T_l]_N [T_{sl}]_{N-1} \dots [T_{sl}]_1 \quad (13)$$

Equation (13) is the overall Transfer Matrix for the drive train, which is of the second order for torsional vibration, unregimented by the number of stations incorporated into the model.

The Polynomial Transfer Matrix method by Murphy [21] treats the elements of the transfer matrices as polynomials in s , while storing their coefficients as arrays in the computer. On carrying out the polynomial multiplication in Eq. (13), one gets Eq. (12). The (2,1) element of $[T_0]$ is then taken as the characteristic polynomial of the system,

the roots of which are the eigenvalues. Once the characteristic polynomial is determined in this way, the eigenvalues can be computed by a rootfinder algorithm, one like the Bairstow's method [22].

The eigenvectors corresponding to the calculated eigenvalues are obtained by computing successive values of θ_n from Equations (12) and (13), substituting 1, 2, 3, .. for N , and with s equal to the previously computed eigenvalue.

Finite Element Method

Besides the Transfer Matrix technique, the Finite Element method can also be used to model the torsional characteristics of a turbomachinery drive train. The theory underlying the Finite Element method is to assume that a complex structure is composed of a finite assemblage of a number of discrete adjacent elements, with the goal of obtaining the component equations of motion. The Finite Element method provides an efficient method of formulating these equations with almost no limitations on the geometry, concurrently being highly adaptable to computer programming.

Defining a Finite Element model means setting up the spatial locations of "nodal points", where the angular displacements are to be determined and external torques applied. The continuity of shaft properties is then used to tie the shaft elements at appropriate node points. Point inertias are added at nodal points where necessary to consummate the model. Then, the element mass and stiffness matrices are assembled to obtain the global mass and stiffness matrices.

Formulation of Element Inertia and Stiffness Matrices [10]

Let us assume a single, uniform shaft element with the following properties: length L , mass density γ , shear modulus of elasticity G , area moment of inertia J about the twist axis. Let us also assume a linear variation of the twist angle θ between the two ends of the element. Based on this linear variation, the angular displacement at any point along the element would be

$$\theta(x, t) = N_1(x)\theta_1(t) + N_2(x)\theta_2(t) \quad (14)$$

The functions N_1 and N_2 are called shape functions or interpolation functions. The shape functions are determined by assuming that they are the static angular displacement patterns conforming to the boundary conditions. Based on $\theta(0, t) = \theta_1(t)$ and $\theta(L, t) = \theta_2(t)$, the shape functions N_1 and N_2 must satisfy

$$\begin{aligned} N_1(0) &= 1, & N_1(L) &= 0 \\ N_2(0) &= 0, & N_2(L) &= 1 \end{aligned} \quad (15)$$

The generic differential equation of motion for the shaft may be stated as

$$\frac{\partial}{\partial x} \left(GJ \frac{\partial \theta}{\partial x} \right) + F = \gamma \frac{\partial^2 \theta}{\partial t^2} \quad (16)$$

Since this is static displacement, the external forces F must add up to zero. Besides, the time-dependent transient terms would also be zero. For a continuous isotropic element, the product GJ is constant. Hence, the differential equation can now be written as:

$$\frac{\partial^2 \theta(x, t)}{\partial x^2} = 0 \quad (17)$$

Integrating the above equation twice, and setting it equal to Eq. (14) gives

$$N_1(x)\theta_1(t) + N_2(x)\theta_2(t) = C_1x + C_2 \quad (18)$$

Applying the boundary conditions,

$$N_1 = 1 - \frac{x}{L}, \quad N_2 = \frac{x}{L} \quad (19)$$

Then, angular displacements in the element may be written as:

$$\theta(x,t) = \left(1 - \frac{x}{L}\right)\theta_1(t) + \frac{x}{L}\theta_2(t) = \theta_1(t) + \frac{x}{L}(\theta_2(t) - \theta_1(t)) \quad (20)$$

Lagrange's equations of motion may be used to determine the equations of motion for the element. These can later be interpreted into the mass and stiffness matrices for the element. Since there are no non-conservative forces,

$$\frac{d}{dt} \left(\frac{\partial T}{\partial \dot{\theta}_j} \right) - \frac{\partial T}{\partial \theta_j} + \frac{\partial V}{\partial \theta_j} = 0 \quad j=1,2 \quad (21)$$

where, T is kinetic energy

and V is potential energy.

The kinetic energy of the elemental piece is given by

$$T(t) = \frac{1}{2} \int_0^L \gamma I [\dot{\theta}(x,t)]^2 dx \quad (22)$$

Substituting Expression (20) differentiated once with respect to time, one gets

$$\begin{aligned} T(t) &= \frac{1}{2} \int_0^L \gamma I \left[\left(1 - \frac{x}{L}\right) \dot{\theta}_1(t) + \frac{x}{L} \dot{\theta}_2(t) \right]^2 dx \\ T(t) &= \frac{1}{2} \frac{\gamma I L}{3} \left[\dot{\theta}_1^2(t) + \dot{\theta}_1(t) \dot{\theta}_2(t) + \dot{\theta}_2^2(t) \right] \end{aligned} \quad (23)$$

The potential energy (strain energy) for the elemental piece is

$$V(t) = \frac{1}{2} \int_0^L GJ \left[\frac{\partial \theta(x,t)}{\partial x} \right]^2 dx \quad (24)$$

Substituting Expression (20) differentiated once with respect to x,

$$V(t) = \frac{1}{2} \int_0^L GJ \left[-\frac{1}{L} \theta_1(t) + \frac{1}{L} \theta_2(t) \right]^2 dx \quad (25)$$

$$V(t) = \frac{1}{2} \frac{GJ}{L} [\theta_1^2(t) - 2\theta_1(t)\theta_2(t) + \theta_2^2(t)]$$

Using Equations (23) and (25) in Lagrange's equations, the following two equations of motion result

$$\left(\frac{\gamma IL}{3}\right)\ddot{\theta}_1(t) + \left(\frac{\gamma IL}{6}\right)\ddot{\theta}_2(t) + \left(\frac{GJ}{L}\right)\theta_1(t) - \left(\frac{GJ}{L}\right)\theta_2(t) = 0 \quad (26)$$

and,

$$\left(\frac{\gamma IL}{6}\right)\ddot{\theta}_1(t) + \left(\frac{\gamma IL}{3}\right)\ddot{\theta}_2(t) - \left(\frac{GJ}{L}\right)\theta_1(t) + \left(\frac{GJ}{L}\right)\theta_2(t) = 0 \quad (27)$$

which in the matrix form may be written as $[m]\{\ddot{\theta}(t)\} + [k]\{\theta(t)\} = 0$,

where the element stiffness matrix is $[k] = \frac{GJ}{L} \begin{bmatrix} 1 & -1 \\ -1 & 1 \end{bmatrix}$ (28)

The element mass matrix $[m_c] = \frac{\gamma IL}{6} \begin{bmatrix} 2 & 1 \\ 1 & 2 \end{bmatrix}$ (29)

is called the "consistent" mass matrix since the same shape function is used to derive the stiffness and mass matrices. It may be observed that the mass matrix has dynamic coupling between the node points.

An elucidation leads to the "lumped" mass matrix that has no mass coupling between nodes with the assumption that the node points are so close that the lumped mass matrix would sufficiently define the actual continuous mass distribution. The method involves simply "lumping" or adding the off-diagonal terms in the consistent mass matrix with the diagonal terms. This may be visualized as placing half of the total shaft section inertia at each node point. The lumped mass matrix for the element may, thus, be written as

$$[m_L] = \frac{\gamma IL}{2} \begin{bmatrix} 1 & 0 \\ 0 & 1 \end{bmatrix} \quad (30)$$

where the differential equations of motion for an element are

$$\left(\frac{\gamma IL}{2} \right) \ddot{\theta}_1(t) + \left(\frac{GJ}{L} \right) \theta_1(t) - \left(\frac{GJ}{L} \right) \theta_2(t) = 0 \quad (31)$$

and

$$\left(\frac{\gamma IL}{2} \right) \ddot{\theta}_2(t) - \left(\frac{GJ}{L} \right) \theta_1(t) + \left(\frac{GJ}{L} \right) \theta_2(t) = 0 \quad (32)$$

If there are speed-modifying devices such as gear trains in the drive train, they impose constraints on the shaft speeds of each element, which modify the effective inertia and stiffness parameters in the model. Conventionally, all parameters are referred to the shaft speed of the driver. Hence, the inertia and stiffness matrices of every other element are calculated as,

$$[m_c] = \frac{G_n^2 \gamma IL}{6} \begin{bmatrix} 2 & 1 \\ 1 & 2 \end{bmatrix} \quad (33)$$

$$[m_L] = \frac{G_n^2 \gamma IL}{2} \begin{bmatrix} 1 & 0 \\ 0 & 1 \end{bmatrix} \quad (34)$$

$$[k] = \frac{G_n^2 GJ}{L} \begin{bmatrix} 1 & -1 \\ -1 & 1 \end{bmatrix} \quad (35)$$

System Inertia and Stiffness Matrix

Several processes are involved in arriving at a final set of equations of motion for a system based on Finite Element modeling. So far we have considered processes at the element level for generating element matrices. The element matrices are assembled into the system or global mass and stiffness matrices by a method commonly referred to as the "direct stiffness" method.

The "direct stiffness" method for assembling the system matrices is based on the fact that work and energy are scalar quantities so that, for example, the total strain energy of a structure is the sum of the strain energy contributions of all of its elements. In addition, the element displacements referred to global axes can be simply identified with the appropriate system displacements.

The method of assembly of the element matrices into the system or global matrices is as follows:

The end nodes of each shaft element are referred to by node number 1 and 2. Each of these elements is connected to other elements sharing common nodes. Thus, each element is connected to two global nodes that are labeled from one to the total number of global nodes. The components of the element matrix are added to the global matrix in the rows and columns that correspond to the global node numbers of the ends of the element. For example, if the ends of an element correspond to the global node 4

and 9, then the (1,1) component of the element matrix is added to (4,4) component of the global matrix, (1,2) component is added to (4,9), (2,1) component is added to (9,4) and (2,2) component is added to (9,9) component of the global matrix. This procedure is applied to both the stiffness and mass element matrices in order to form the global matrices.

The differential equation assuming a lumped parameter mass matrix for a straight-line model can be written as

$$\left(\frac{I_1}{2}\right)\ddot{\theta}_1 + K_1[\theta_1 - \theta_2] = 0 \quad (36)$$

$$\left(\frac{I_{n-1} + I_n}{2}\right)\ddot{\theta}_n + K_n[\theta_n - \theta_{n+1}] + K_{n-1}[\theta_n - \theta_{n-1}] = 0, n=2,3,..N-1 \quad (37)$$

$$\left(\frac{I_N}{2}\right)\ddot{\theta}_N(t) + K_{N-1}[\theta_N(t) - \theta_{N-1}(t)] = 0 \quad (38)$$

which compares with the equation for a station using the lumped parameter model. However, there is no exact correspondence between the two equations because of the fact that lumped parameter equation is written after the station inertia's are lumped.

Solution Methods for the Eigenproblem [11]

The eigenvalues and eigenvectors, which are the undamped natural frequencies and mode shapes respectively, can be found from the system stiffness and mass matrices obtained above. The generalized eigenproblem associated with the above system is

$$K\phi = \lambda I\phi \quad (39)$$

where K and I are, respectively, the stiffness matrix and inertia matrix of the Finite Element assemblage. The eigenvalues λ_j and eigenvectors ϕ_j are the free vibration frequencies squared, and corresponding mode shape vectors, respectively. The stiffness matrix K has order n and is positive definite or positive semi-definite. The inertia matrix obtained in a consistent mass analysis is always positive definite, whereas a lumped inertia matrix is positive definite only if all diagonal elements are larger than zero, else it is positive semi-definite.

Several methods for solution of eigenproblems are available including vector iteration method, vector transformation method and polynomial iteration method. In each of these three groups there are several specific methods. In the present work, the vector transformation method of eigensolution based on the Generalized Jacobi's method is employed. A major advantage of this procedure is its simplicity and stability. Also, the transformation of the generalized eigenproblem to the standard form is avoided when using this method.

However, the Jacobi solution method solves simultaneously for all eigenvalues and corresponding eigenvectors. In torsional vibration analysis, we are interested in only the first few natural frequencies, and the use of this method can be very inefficient, in particular when the order of K and I is large, as compared to the Polynomial Transfer Matrix method.

For the rotor system that is free-free at the ends, the stiffness matrix is not positive definite. In order for the eigensolution based on Jacobi's method to work, it is

required that both the stiffness and inertia matrix are positive definite. In order to solve this problem, a procedure called shifting is used. In the solution, $K\phi = \lambda I\phi$, a shift ρ on K is performed by calculating

$$\hat{K} = K + \rho I \quad (40)$$

The transformed eigenproblem is then

$$\hat{K}\psi = \mu I\psi \quad (41)$$

To identify how the eigenvalues and eigenvectors of Eq. (37) are related to Eq. (38), the latter is re-written in the form

$$K\psi = \delta I\psi \quad (42)$$

where $\delta = \rho - \mu$. However, Eq. (39) is, in fact, the eigenproblem $K\phi = \lambda I\phi$. Since the solution of this problem is unique, we have

$$\lambda_i = \mu_i - \rho; \quad \phi_i = \psi_i \quad (43)$$

As an example to demonstrate the procedure of shifting, a simple two-element system is modeled. The nodal inertias are assumed to be 1 in·lb·s² attached at each node whereas the element stiffness is assumed to be 1 lb·in/rad. The assembled system inertia and stiffness matrix is given by

$$I = \begin{bmatrix} 1 & 0 & 0 \\ 0 & 1 & 0 \\ 0 & 0 & 1 \end{bmatrix} \quad K = \begin{bmatrix} 1 & -1 & 0 \\ -1 & 2 & -1 \\ 0 & -1 & 1 \end{bmatrix}$$

The computed eigenvalues for this system are

$$\lambda = [0 \quad 1 \quad 3]$$

and the eigenvectors are

$$\Phi = \begin{bmatrix} 0.577 & -0.707 & 0.408 \\ 0.577 & 0 & -0.816 \\ 0.577 & 0.707 & 0.408 \end{bmatrix}$$

Applying a shift in the stiffness matrix as in Eq. (37), where $\rho = 10$, the transformed stiffness matrix is

$$\hat{K} = \begin{bmatrix} 11 & -1 & 0 \\ -1 & 12 & -1 \\ 0 & -1 & 11 \end{bmatrix}$$

which is positive definite. The calculated eigenvalues using the transformed stiffness matrix are

$$\mu = [10 \quad 11 \quad 13]$$

so the eigenvalues for the original system as calculated from Eq. (40) are

$$\mu - \rho = \lambda = [0 \quad 1 \quad 3]$$

Contrariety between Transfer Matrix and Finite Element Techniques

The first difference between the two techniques in question lies in the way in which the equations of motion are derived for each technique. While the Transfer Matrix technique relies on expressing the state variables like torques and angular displacements at a station in the rotor model in terms of the variables of the previous station, the Finite Element method is based on the formulation of shape functions and the principle of virtual work. Hence, the latter can be readily applied to non-linear elements of higher order, and would yield consistent mass formulation. In the Transfer Matrix method, an

application specific, highly optimized algorithm takes complete benefit of the imposed shortcomings in modeling for numerically solving the equations; however, typically only single line models are allowed. The Finite Element method, on the other hand, uses general-purpose sparse matrix solving algorithms that permit models of any complexity, even multi-line models.

In practice, however, often the Transfer Matrix and Finite Element models are identical, leading to similar results. It is easy to see that the size of the matrices needed for the Finite Element method would be much greater than that of the matrices used by the Transfer Matrix technique. Although the Transfer Matrix algorithm runs multiply faster than the Finite Element one, its usage is often limited to simpler models, mostly single-line. Contrary to this, the Finite Element algorithm, though slower, may be applied to a wide variety of rotordynamic problems. In the present scenario of continually computational power, the longer computational time taken by the Finite Element methods may soon be offset.

TIME-TRANSIENT ANALYSIS

In recent times, the use of synchronous motors has been continually increasing considering the fact that they are highly economical to use as compared to other driving equipment. The rising cost of power has led to a revival in the use of synchronous motors despite the fact that synchronous motors are a major cause for exciting torsional vibration in turbomachinery. The latter leads to inherent problems in synchronous motor driven turbomachinery that require analysis, in lieu of which high stresses and fatigue failures may occur over time in weak shaft members. Synchronous motor startups are often highly detrimental to their driven members due to their high torque fluctuation and must be thoroughly analyzed in order to avoid premature failures. The designer must perform sufficient analysis to enable him to predict the torque and stress variation over time in the machine elements during startup. This information can then be used per the designer's discretion for designing a reliable member that can withstand the torque and stress fluctuation for a reasonable length of time [23].

The transient torque and stress history can be predicted by numerically integrating the equations of motion for a discrete mass-elastic shaft model, leading to determination of the angular displacements at each time-step. With the introduction of damping into the torsional equations of motion, the latter become coupled and, hence, difficult to solve. The modal method is then used to reduce the number of degrees of freedom of the system and uncouple the equations of motion even with damping. This implementation of modal coordinates to transform the equations of motion can bring

about a useful simulation of the transient angular displacements after numerical integration of the equations [36], besides saving a lot on computation time. Proportional damping can be used for drive trains that have an extremely small amount of damping. In such cases, the coupled modal equations of motion are uncoupled by assuming the damping matrix to be proportional to the inertia or stiffness matrix. This, in effect, means that the modal cross-coupled damping terms are neglected. However, drive trains having couplings with a high value of localized damping (e.g. Holset couplings) cannot be analyzed using this method since the damping matrix in such cases cannot be assumed proportional. Such systems then need to be analyzed by solving the coupled equations of motion using physical coordinates rather than modal coordinates to account for the "point" damping at the couplings.

There are several techniques to perform a transient analysis on a rotor model, viz. numerical integration that generates a time-marching solution with a miniscule time step, Duhamel's integration that uses the "impulse response" functions of the rotor system, and the harmonic balance technique that uses the Fast Fourier Transform (FFT) chiefly for steady state responses. Of these, the numerical integration technique is the most common and will be discussed in this chapter. The major classes of numerical integration methods are as follows:

- (a) Methods yielding implicit or explicit solution of the dynamic equations of equilibrium
- (b) Single step or multi step methods
- (c) Conditionally or unconditionally stable methods

- (d) Component mode synthesis, which is a technique that is used to reduce the order of the system, subsequently expediting the calculation.

Starting a Synchronous Motor [1]

Synchronous motors are like induction motors in that they both have stator windings that produce a rotating magnetic field. Unlike an induction motor, the synchronous motor is excited by an external DC source and, therefore, requires slip rings and brushes to provide current to the rotor. In the synchronous motor, the rotor locks into step with the rotating magnetic field and rotates at synchronous speed. If the synchronous motor is loaded to the point where the rotor is pulled out of step with the rotating magnetic field, no torque is developed, and the motor will stop. A synchronous motor is not self-starting because torque is only developed when running at synchronous speed; therefore, the motor needs some type of device to bring the rotor to synchronous speed. Synchronous motors use a wound rotor, which contains coils of wire placed in the rotor slots. Slip rings and brushes are used to supply current to the rotor.

A synchronous motor may be started by a DC motor on a common shaft. When the motor is brought to synchronous speed, AC current is applied to the stator windings. The DC motor now acts as a DC generator and supplies DC field excitation to the rotor of the synchronous motor. The load may now be placed on the synchronous motor. Synchronous motors are more often started by means of a squirrel-cage winding embedded in the face of the rotor poles. The motor is then started as an induction motor and brought to 95% of synchronous speed, at which time direct current is applied, and

the motor begins to pull into synchronism. The torque required to pull the motor into synchronism is called the “pull-in torque”.

The asymmetry of a synchronous motor during startup process produces pulsating electromagnetic torques, which may be as high in magnitude as the average accelerating torque. In an induction motor, the rotor is symmetrical and the flux linkage is independent of the rotor position relative to the stator field, whereas in a synchronous motor, the flux linkage (and thus, torque) between rotor and stator varies depending upon whether the rotor poles are in phase with the stator field or have a phase difference of 90°. During sub-synchronous operation as in the case of motor startup, this produces torque modulation at a varying frequency. These undesirable transient pulsating torques may cause fatigue failures in the shafts of the system. During startup, the electromagnetic torque of a synchronous motor can be written as

$$T_m = T_a + T_p \quad (44)$$

where, T_a is the accelerating unidirectional average motor torque,

and, T_p is the pulsating component of motor torque due to magnetic saliency

When the synchronous motor is started as an induction machine without field excitation, the frequency of the pulsating component of torque varies as twice the slip frequency of the motor ω_s

$$\omega_s = f [1 - (\omega_m / \omega_{sync})] \quad (45)$$

$$\omega_e = 2\omega_s = 2f [1 - (\omega_m / \omega_{sync})] \quad (46)$$

Thus, the excitation frequency ω_e decreases linearly from twice line frequency at standstill to zero when the motor reaches synchronous speed. Considering that the line frequency is 60 Hz in the United States, the excitations begin at a frequency of 120 Hz which linearly decreases to zero as the motor reaches synchronism. It should, thus, be well noted here that a torsional natural frequency that is located below twice the line frequency will create resonance when the motor speed passes through or is close to the “encounter” speed. The motor “encounter” speeds in rpm at which one can expect the torsional natural frequency ω_i to be stimulated by the twice line frequency excitation can be written as follows:

$$\omega_{res} = 60 \cdot \omega_{syn} \left(1 - \frac{\omega_i}{2f} \right) \quad (47)$$

Modeling and Analysis

A mass-elastic model created for smaller equivalent systems with relatively fewer degrees of freedom is typically used with the damping information and the forcing and loading torques to generate a time-transient history of the instantaneous torques produced in each shaft element during the startup process. As explained earlier, this is performed by numerical integration of equations of motion for every inertia, at each time step, with respect to time. The motor is considered at rest initially with the assumption that the electromagnetic torque is suddenly applied. As each inertia of the system responds to the unbalanced torque, the system accelerates. At every time step, instantaneous values of average torque, pulsating torque, rotational speed, etc. are calculated and recorded and

the integration proceeds. Thus, the motor startup is mathematically simulated and the torques in each shaft are calculated at each time step. It should be recognized that it is advisable to choose the time step for numerical integration to get accurate results for the highest torsional natural frequency of interest.

However, for much larger systems, this method may often be tedious in the sense it involves longer computational times and the demand for greater computational power for performing the analyses faster. Heretofore, this was a major concern in analysis of larger systems. Employing modal coordinates for larger systems can greatly reduce the number of degrees of freedom and hence, significantly cut down on the required computational time and resources. This is a viable option to integration using physical coordinates, provided that the damping can be approximated as proportional.

Run-up Calculations

A preliminary run-up analysis is helpful to determine the total time for the synchronous motor driven system to reach synchronism, and hence, predict the length of time the numerical integration must proceed. The pulsating component of the motor torque does not contribute to the acceleration of the system, and hence, only the average drive and load torques are considered while performing the preliminary run-up calculations. The equation governing the motion for the rotor system for the run-up analysis can be written as:

$$\sum T = I\alpha \quad (48)$$

where, α is the angular acceleration of the drive train, rad/s^2 .

One can numerically integrate this equation with the modified Euler's method, and determine the angular acceleration and angular velocity at each time step. The time taken for the angular velocity to reach the operating speed is considered the run-up time.

Transient Calculations

Once the run-up time has been calculated, the modal information with the drive torques, the pulsating torque and load torques is used to perform the transient analysis. The modal information embodies the eigenvalues and eigenvectors calculated using the Transfer Matrix method described in the previous chapter. Additionally, damping information must be included in the form of modal damping.

The rotor system behaves per the second order spring-inertia-damper equation of motion:

$$[I]\{\ddot{\theta}\} + [C]\{\dot{\theta}\} + [K]\{\theta\} = \{F(t, \dot{\theta})\} \quad (49)$$

The number of equations represented by Eq. (49) may be reduced by modal decomposition by substitution of variables:

$$\theta(x, t) = \sum \phi_{jm}(x) q_j(t) \quad (50)$$

In matrix form, this may be written as

$$\{\theta\} = [P_m]\{q\} \quad (51)$$

with $[P_m]$ being the modal matrix whose columns are the mode shapes that are normalized with respect to the inertia matrix.

The equations of motion then become

$$[I][P_m]\{\ddot{q}\} + [C][P_m]\{\dot{q}\} + [K][P_m]\{q\} = \{F(t, \dot{\theta})\} \quad (52)$$

Pre-multiplying both sides of the Eq. (52) by the transpose of the modal matrix yields

$$[P_m]^T [I][P_m]\{\ddot{q}\} + [P_m]^T [C][P_m]\{\dot{q}\} + [P_m]^T [K][P_m]\{q\} = [P_m]^T \{T(t, \dot{\theta})\} \quad (53)$$

This reduces to the uncoupled set of equations

$$[I_{den}]\{\ddot{q}\} + [C_m]\{\dot{q}\} + [K_m]\{q\} = [P]^T \{T(t, \dot{\theta})\} \quad (54)$$

The values of the modal damping factors ζ_i are usually found experimentally and generally range from 2% to 4%, but other values may also be possible. The modal damping factors may be determined by performing a damped analysis for determination of damped frequencies and damped mode shapes described briefly later in this section. Since inexactitude of the modal damping factor would greatly affect the resultant stresses, a careful analysis of the rotor system to decide upon an accurate set of factors is required. After citing many references, Corbo et al. [16] conclude that the minimum amount of damping that could be expected for a typical geared machine consisting of a motor, gearbox, and a compressor is 2% of the critical value. They recommend the use of this value in absence of actual test data as they deem it to be conservative for such a machine. However, they also caution the reader on the use of this generic damping ratio by observing that common misinterpretations might yield incorrect damping coefficients for individual shaft elements.

After the modal damping matrix has been defined, various methods can be used to perform numerical integration of the Eq. (54) to yield a time history of the modal

coordinates. For the purpose of accomplishing the above, the second order equation can be reduced to first order by substituting

$$\{\dot{q}\} = \{v\} \quad (55)$$

Thus, Eq. (54) then becomes

$$\begin{Bmatrix} \dot{q} \\ \dot{v} \end{Bmatrix} = \begin{bmatrix} 0 & [\text{Iden}] \\ -[K_m] & -[C_m] \end{bmatrix} \begin{Bmatrix} q \\ v \end{Bmatrix} + \begin{Bmatrix} 0 \\ \{T\} \end{Bmatrix} \quad (56)$$

If the system is linearized to eliminate external torques, the damped frequencies and damped mode shapes can be determined by writing Eq. (56) as

$$\begin{Bmatrix} \dot{q} \\ \dot{v} \end{Bmatrix} = \begin{bmatrix} 0 & [\text{Iden}] \\ -[K_m] & -[C_m] \end{bmatrix} \begin{Bmatrix} q \\ v \end{Bmatrix} \quad (57)$$

Assuming a solution of the form,

$$\{q\} = \{\psi\}e^{\lambda t} \quad (58)$$

where $\{\psi\}$ and λ are in complex form, we get

$$\{\dot{q}\} = \lambda\{\psi\}e^{\lambda t} \quad (59)$$

$$\{\dot{v}\} = \lambda\{\phi\}e^{\lambda t} \quad (60)$$

where $\{\phi\} = \lambda\{\psi\}$. Therefore, the modal damped equations of motion are transformed to

$$\lambda \begin{Bmatrix} \{\psi\} \\ \{\phi\} \end{Bmatrix} = \begin{bmatrix} 0 & [\text{Iden}] \\ -[K_m] & -[C_m] \end{bmatrix} \begin{Bmatrix} \{\psi\} \\ \{\phi\} \end{Bmatrix} \quad (61)$$

Equation (61) is an eigen-problem that can be solved by an iterative computer method like the QR algorithm to calculate the damped natural frequencies and mode

shapes. Finally, the vector of the generalized coordinates $\{q\}$ is transformed back to the physical coordinates $\{\theta\}$ using the reverse transformation $\{q\} = [P_m]^T \{\theta\}$.

One can also integrate Eq. (56) using the modified Euler method, fourth-order Runge Kutta method, and similar techniques to obtain a time-transient history of the modal coordinates. Then by applying the reverse transformation $\{q\} = [P_m]^T \{\theta\}$, the time transient history of the physical angular velocity and the physical angular displacement for each station can be determined. Once this is done, the torque is calculated using its proportionality to the difference between the calculated angular displacements and velocities (with damping) of the adjacent stations.

$$T = K(\theta_2 - \theta_1) = K\Delta\theta \quad (62)$$

The stiffness K of the element is determined by the shear modulus and the geometry of the element. The maximum shear stress is also calculated from basic torque equation:

$$\frac{T}{J} = \frac{G\Delta\theta}{L} = \frac{S}{r} \quad (63)$$

where, T = torque applied to the shaft ends, in-lb

J = polar area moment of inertia of the shaft cross-section, in⁴

G = shear modulus of the shaft material, psi

$\Delta\theta$ = difference in angular displacements between the shaft ends, rad

r = radius at which the shear stress S is calculated, in

L = length of the shaft element under consideration, in

Hence, we get the maximum shear stress for a shaft element as

$$S = \frac{Gd_o \Delta \theta}{2L} = \frac{Td_o}{2J} \quad (64)$$

Here, the maximum radius of the shaft element is considered since the maximum shear stress occurs on the outermost edge of the shaft.

Integration of the Torque Vector

Special consideration needs to be given when integrating using modal coordinates if the forcing torque frequency is a function of running speed. Illustrating this is the torque model for a synchronous motor, in which many a time, a frequency-dependent motor torque may be expressed as

$$T_m = T_a + T_p \sin(\omega_e t + \Phi) \quad (65)$$

The frequency of the pulsating vector generating the oscillating torque must be integrated with respect to time to determine its correct angular position $\beta = \omega_e t$ within the sinusoidal relation.

$$\beta = \int \omega_e dt \quad (66)$$

In case of a synchronous motor, the analytical solution is given by [1]:

$$\beta = 4\pi f \left(t - \frac{\theta_t}{\omega_{syn}} \right) \quad (67)$$

For a non-synchronous motor, β is determined by the trapezoidal technique as explained in Orsey et al. [24]:

$$\beta_{i+1} = \beta_i + \left[\frac{\omega_{e_i} + \omega_{e_{i+1}}}{2} \right] \Delta t \quad (68)$$

Types of Forcing Torque

The software used for the present study, *XLTRC-TORSION*, can handle four different types of torsional forcing function inputs: synchronous motor input, arbitrary pulsating sinusoidal torque input, average torque input, and time dependent torque input. With these four options, or combinations of these options, nearly all input torsional forcing functions can be modeled. *XLTRC-TORSION* can handle as many input forcing functions as needed. These input forcing functions may be applied at any station in the drive train, and more than a single input may be attached to the same station.

Below is a brief description of each type of forcing function that can be input into *XLTRC-TORSION*:

(a) Synchronous Motor Torque Input Option:

The synchronous motor torque option is used for analysis of synchronous motor driven systems. This option requires the input of torque values for speeds below and up to the synchronous operating speed. The input torque for this option may be expressed as a summation of an average torque and a pulsating torque as in Eq. (65). The pulsating torque is modeled as a sine wave (pulsating torque is zero at time zero). In order to define the model with a cosine curve, a phase shift Φ may be entered as input.

Two types of torque should be entered for each rpm as shown in Fig. 5: the average drive torque and the amplitude of the pulsating torque. The torque values should

be entered as a percentage of full load torque, and the program interpolates for unknown values.

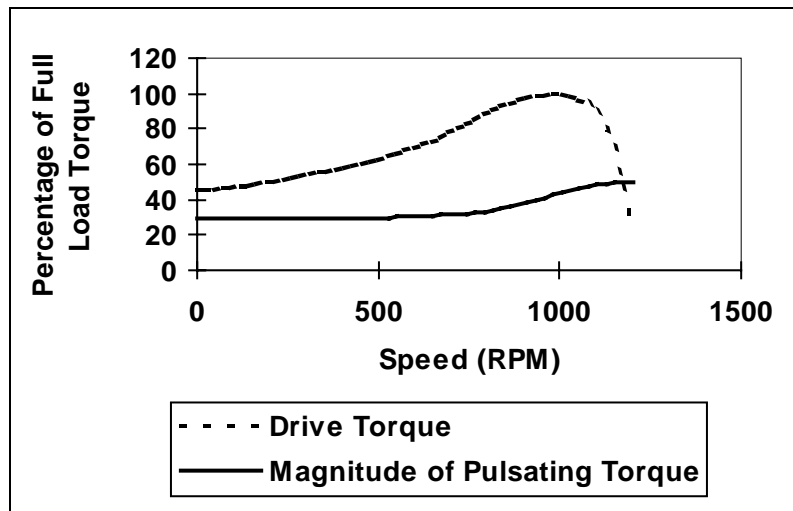


Fig. 5 Synchronous motor torque input

(b) Arbitrary Pulsating Frequency Torque Input Option:

In case of synchronous motors, the pulsating component of the torque oscillates at a frequency equal to twice the slip frequency of the motor, thereby, posing a linear variation with rotor velocity as illustrated by Fig. 6. However, in several cases, rotors may have pulsating input torques that are some function of the running speed, not necessarily linear. This may be simulated using the speed dependent pulsating torque input option. If this option is used, Eq. (68) is used to integrate the sine function. The

input for this option is the similar to the synchronous motor torque input option with the additional input of the frequency of the pulsating torque for each rotor speed.

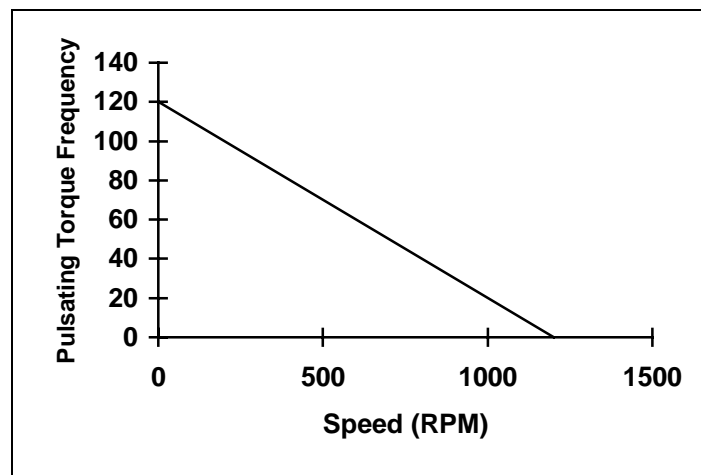


Fig. 6 Pulsating frequency of a synchronous machine

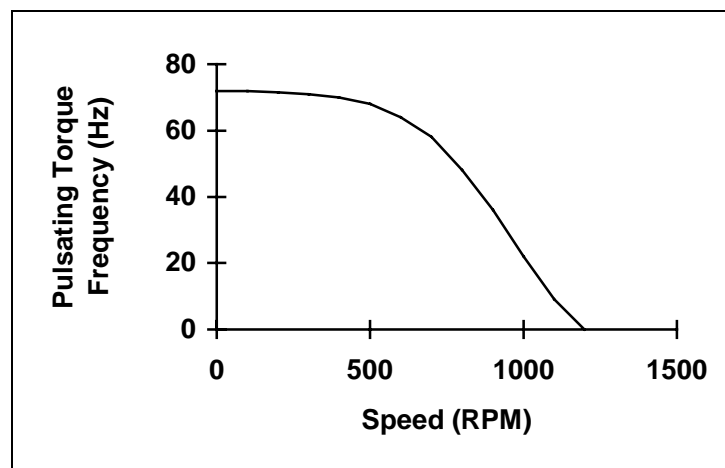


Fig. 7 Arbitrary frequency as a function of rotor speed

(c) Input Torque without a Pulsating Component Option:

Torques with no pulsating component (Fig. 7) may be entered using this input option. In this case, the only data that needs to be input is the average torque as a function of rotor speed. This option is helpful while defining a non-harmonic load torque as a function of the running speed, e.g. compressor load torque with respect to speed, pump load torque-speed curve.

(d) Torque as a Function of Time:

If the transient variation of the forcing torque is known as shown in Fig. 8, this generic option may be used to define the torque acting on the system. The program internally uses these input values directly, as the integration progresses through time, to find the torque that corresponds to the current time. If an intermediate time step lies between two entered time values, the program interpolates for the unknown torque at that time step. It is mandatory that one enters definite torque-time values till the run up speed is reached, otherwise the program fails.

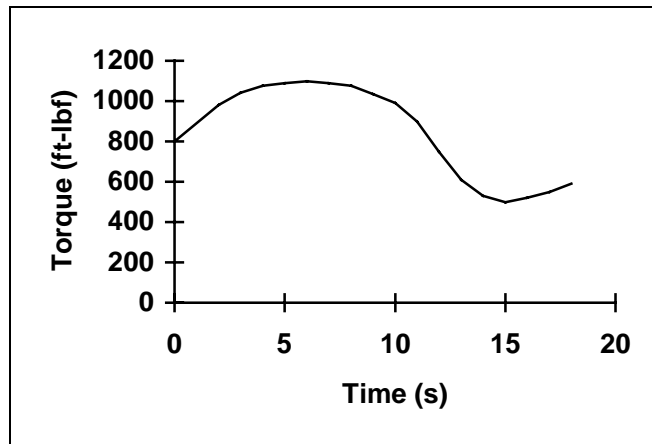


Fig. 8 Torque as an arbitrary function of time

Campbell Diagrams

Torsional interference diagrams or Campbell diagrams, as they are commonly known, are extensively used in the design of rotating machinery. They help in deciding and checking the operating speeds of the machine and the forcing function frequencies that need to be moved away from the natural frequencies of the system in order to avoid resonance. The known excitation frequencies are plotted on the abscissa, and natural frequencies (lateral or torsional) and excitation frequencies are plotted on the ordinate axis. Figure 9 illustrates this relation with the aid of a Campbell diagram that shows how the excitation frequency passes through the natural frequencies during startup.

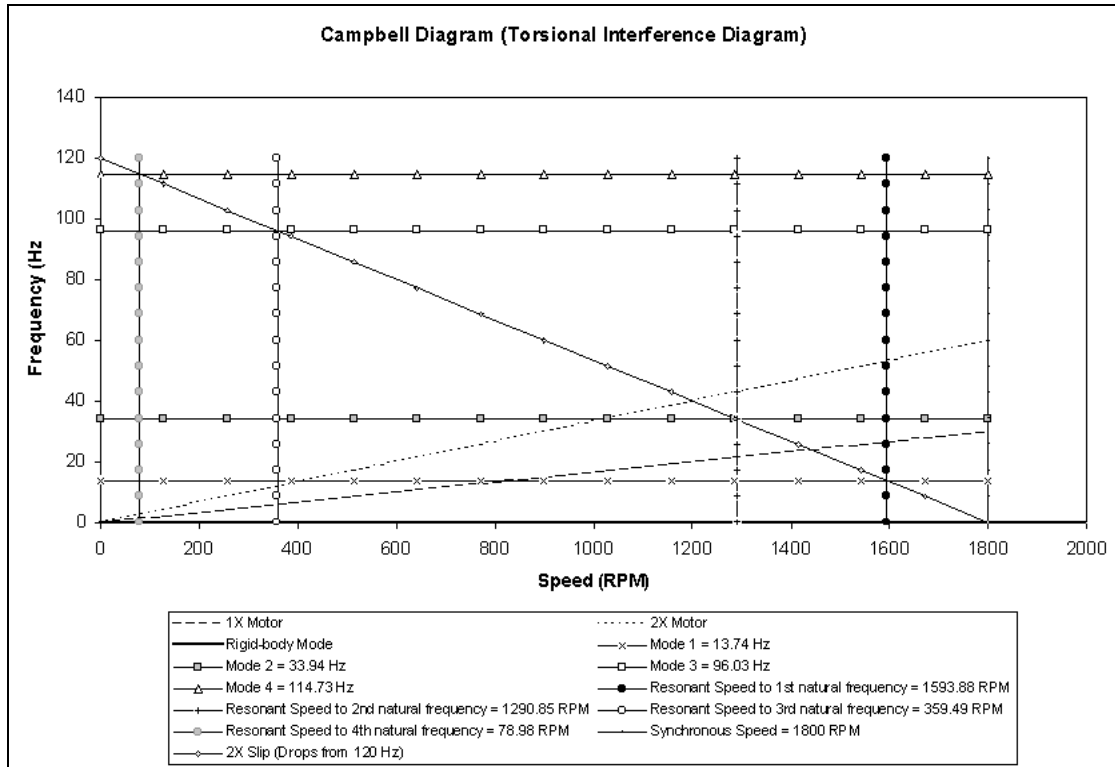


Fig. 9 Torsional interference diagram (Campbell diagram)

If a "salient pole" synchronous motor is used to drive a machine, an excitation frequency that is equal to twice the line frequency reduced proportionately by the slip ratio would be a predominant forcing function frequency [1]. The motor slip ratio is given by:

$$S_R = \frac{N_S - N_M}{N_S} \quad (69)$$

where, N_S = synchronous speed, rpm

N_M = motor speed (varies during the startup), rpm

Thus, the excitation frequency would be:

$$\omega_e = 4\pi L_f \left(\frac{N_s - N_M}{N_s} \right) \text{ rad/s} \quad (70)$$

where, L_f = line frequency = 60 Hz in the United States.

Driving Torque Definition for Use in Transient Analyses

A study was conducted as a part of the directed studies course under the supervision of Dr. John Vance to determine the appropriate definition of driving torque to be used in transient analysis of drive trains driven by a synchronous motor. The two definitions that needed to be compared were (i) definition of driving torque as a function of the excitation frequency, and (ii) definition of driving torque as a function of the angular position of the motor inertia. A simple case study of an air compressor train modeled as a five-disk rotor was considered and recommendations were made based on the results obtained from the subsequent analysis using both the definitions of driving torque.

As discussed earlier, under the starting conditions, the synchronous motor electromagnetic torque can be considered to be a sum of its average and pulsating components. Thus, the generic definition of the driving torque of a synchronous motor may be stated as [1]:

$$T_1(t) = T_{avg} + T_{pul} \quad (71)$$

In this equation, the pulsating torque T_{pul} can be defined in two different ways. One definition assumes the pulsating torque to be a direct function of the excitation frequency ω_e , defined as [1]:

$$\omega_e = 4\pi L_f S_R \quad (72)$$

where S_R is the motor slip ratio defined as $S_R = \frac{N_s - N_m}{N_s}$ (73)

Hence, the first definition of pulsating torque can be written as

$$T_{pul} = T_{osc} \cos(\omega_e t) \quad (74)$$

Thus, the definition of the driving torque of a synchronous motor during startup may be written as

$$T_1(t) = T_{avg} + T_{osc} \cos \left[4\pi L_f \left(1 - \frac{N_m}{N_s} \right) \cdot t \right] \quad (75)$$

However, the pulsating torque component T_{pul} may also be stated as being a function of the instantaneous angular position $\alpha(t)$ of the rotating torque vector T_o that generates the oscillating torque, i.e.

$$T_{pul} = T_{osc} \cos[\alpha(t)] \quad (76)$$

In Eq. (76), the instantaneous value of $\alpha(t)$ is given by [1]

$$\begin{aligned} \alpha(t) &= \int_0^t \omega_e dt = 4\pi L_f \int_0^t \left(1 - \frac{N_m}{N_s} \right) dt \\ \therefore \alpha(t) &= 4\pi L_f \left(t - \frac{\theta_1}{\Omega_s} \right) \end{aligned} \quad (77)$$

Thus, the other definition of the driving torque of a synchronous motor during startup may be stated as

$$T_1(t) = T_{avg} + T_{osc} \cos \left[4\pi L_f \left(t - \frac{\theta_1}{\Omega_s} \right) \right] \quad (78)$$

The study was used to determine the appropriate definition of driving torque (Eq. (75) or Eq. (78)), and make necessary recommendations based on the results.

Case Study of a Five-Disk Rotor

A “dummy” air compressor train shown in Fig. 10 was considered, which had been modeled as having five lumped inertias/disks and assumed values as shown in Fig. 11. The motor, which was modeled as inertia 1, had a synchronous speed of 1800 rpm.

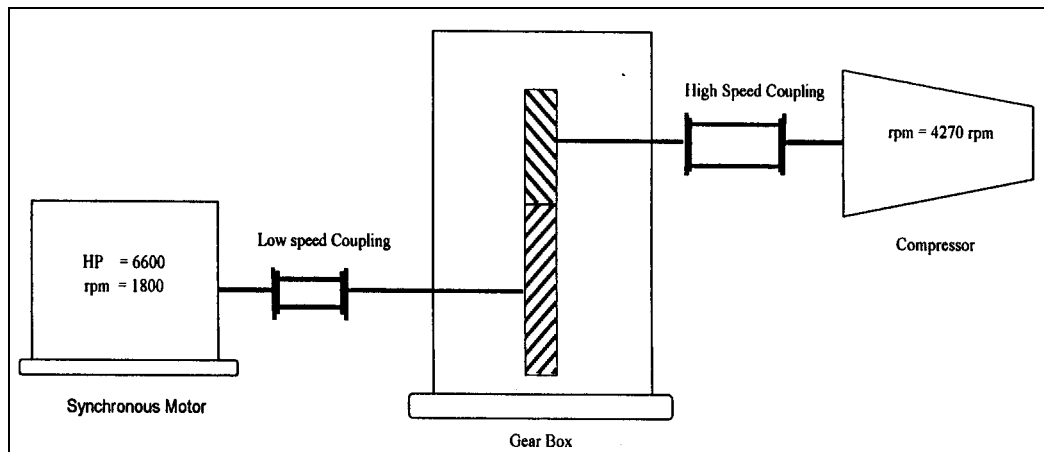


Fig. 10 “Dummy” air compressor train under study, with assumed values

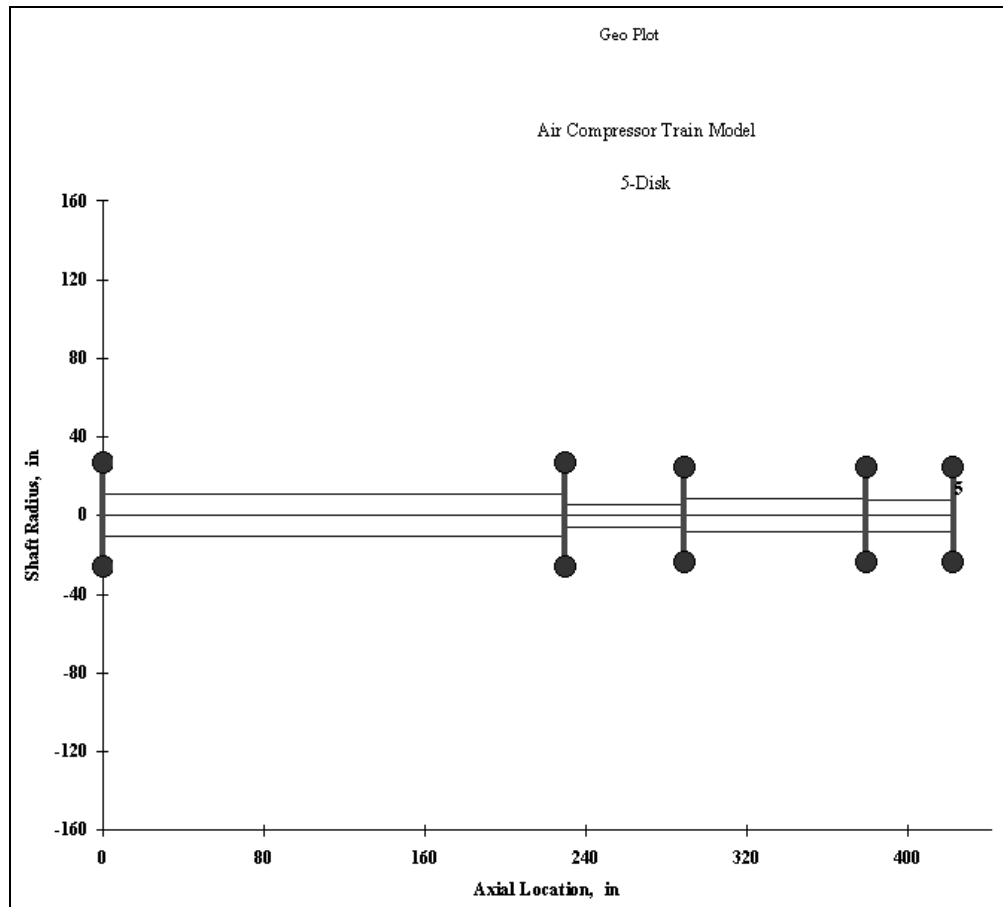


Fig. 11 Geometry plot of a five-disk train

The first four undamped natural frequencies of the system were calculated as 13.94 Hz, 33.96 Hz, 96.08 Hz and 114.8 Hz (excluding the zero frequency rigid-body mode). Only the first four natural frequencies needed to be considered as they lay below 2X-line frequency (120 Hz). The Campbell diagram showing the calculated natural frequencies, the slip frequency and the motor speeds at which pulsation was expected is

shown in Fig. 12. The corresponding encounter speeds were calculated as 78.98 rpm, 359.49 rpm, 1290.85 rpm and 1593.88 rpm.

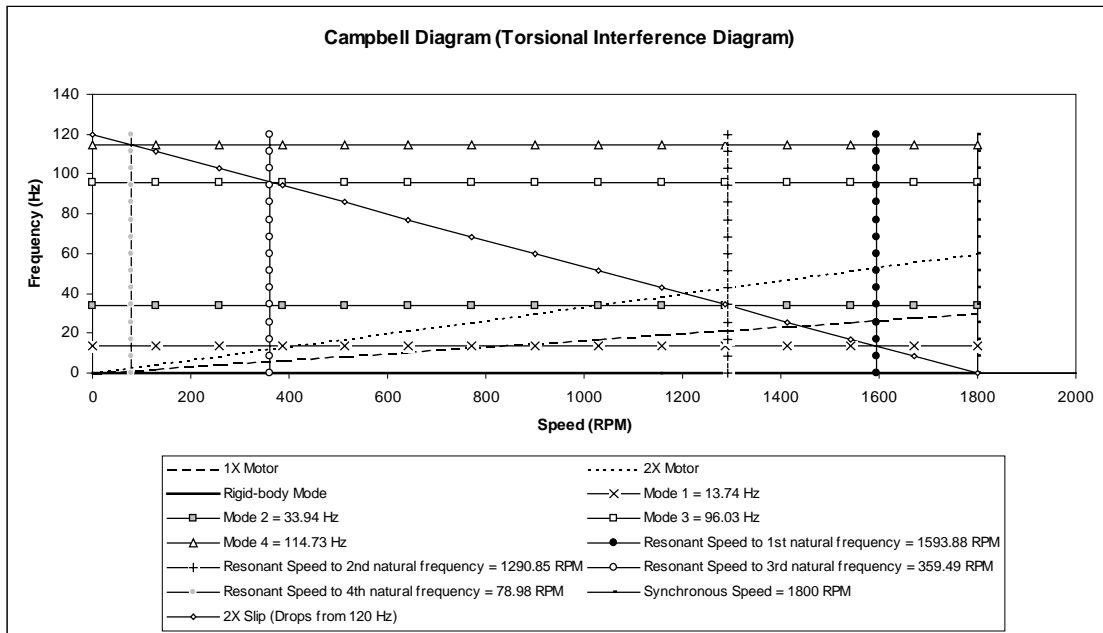


Fig. 12 Campbell diagram

The run-up plot of the motor is shown in Fig. 13. This plot indicates that the motor would reach its synchronous speed of 1800 rpm in 26.95 seconds. This graph may also be used to determine the motor speed reached at a particular time instant of interest.

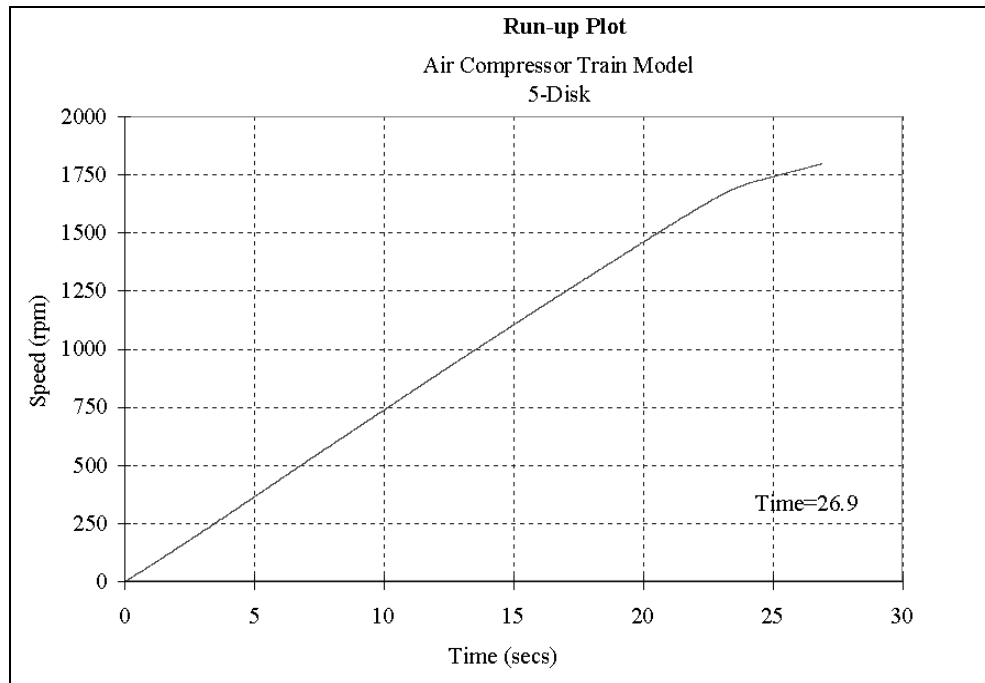


Fig. 13 Run-up plot of the motor

First, the transient torque plot for the motor inertia obtained by using the relation for driving torque stated in Eq. (78) shown in Fig. 14 was considered. Some salient characteristics could be stated by evaluating this torque plot:

- Transient response to the initial torque pulsation remains till the motor speed reaches about 150 rpm.
- Resonant response is predicted around 17.8 seconds, which corresponds to a motor speed of 1300 rpm. This value matches 1290.85 rpm as predicted by the Campbell diagram.

- Large resonant response is predicted around 22 seconds, which corresponds to a motor speed of 1600 rpm. This speed matches 1593.88 rpm as predicted by the Campbell diagram.

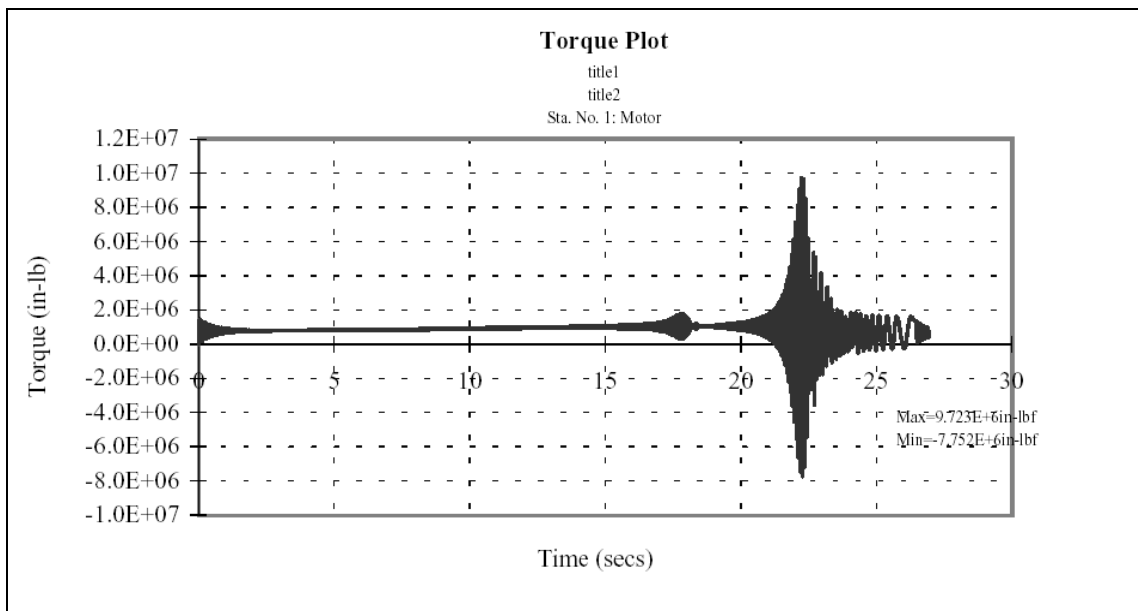


Fig. 14 Torque plot using definition of driving torque in Eq. (78), with no damping considered

The torque plot obtained using the driving torque definition in Eq. (75) is shown in Fig. 15. A careful evaluation brings the following characteristics to the fore:

- Transient response to the initial torque pulsation is seen till the motor speed reaches about 200 rpm.
- Resonant response is predicted around 7.5 seconds corresponding to 600 rpm. The motor torque shows very large pulsation, which lasts till the motor speed reaches about 825 rpm (1X motor frequency intersects the first natural frequency around this period on the Campbell diagram).
- Resonant response is predicted around 23 seconds corresponding to 1625 rpm. The motor torque again shows large fluctuations, which last till the synchronous speed of 1800 rpm is reached. This poorly matches 1593.88 rpm, as predicted by the Campbell diagram.
- The maximum torque predicted in this case is almost one order of magnitude less than that predicted in the previous case.

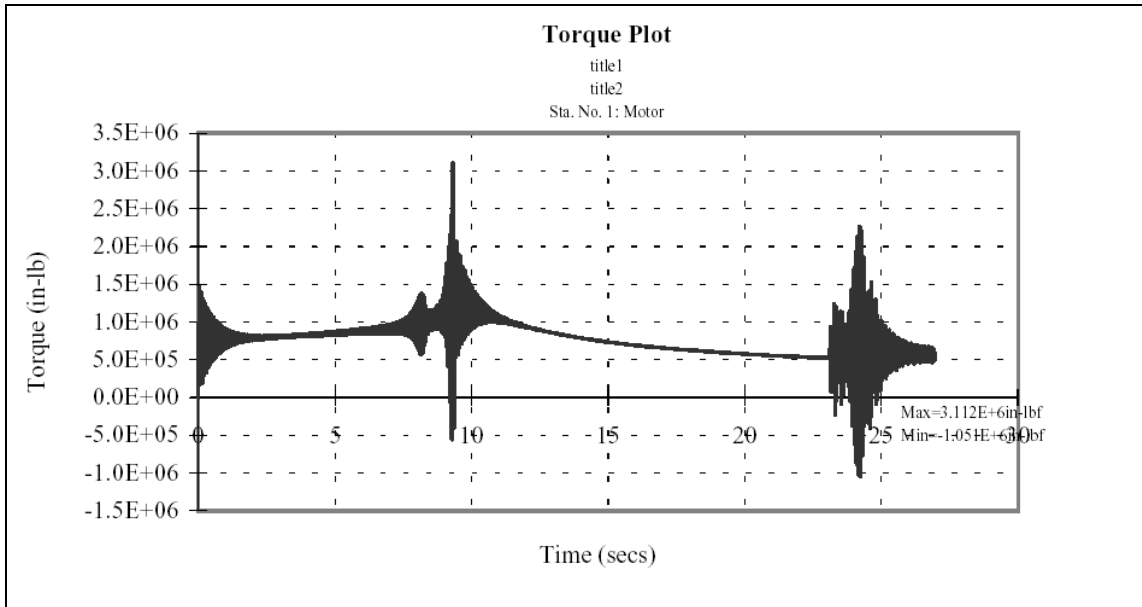


Fig. 15 Torque plot using definition of driving torque in Eq. (75), with no damping considered

Comparison of results of the above two cases showed that the resonant speeds predicted by using Eq. (78) for driving torque were much closer in agreement with those predicted by the Campbell diagram, only if the resonant speeds corresponding to 2X slip frequency were considered. However, a closer look at Fig. 15 reveals that pulsation around the region where 1X motor frequency intersects the natural frequency line, though substantial, was absent in Fig. 14.

Now, in order to verify our results with damping, the following dummy values were used for incorporating damping into our model:

- Motor HP = 6600
- Overall bearing HP loss = 2%

- Overall shaft damping = 2%

The Campbell diagram and the run-up plot of the motor remain unchanged. The torque plots obtained by using Eq. (78) and Eq. (75) as definitions of driving torque are shown in Figures 16 and 17 respectively.

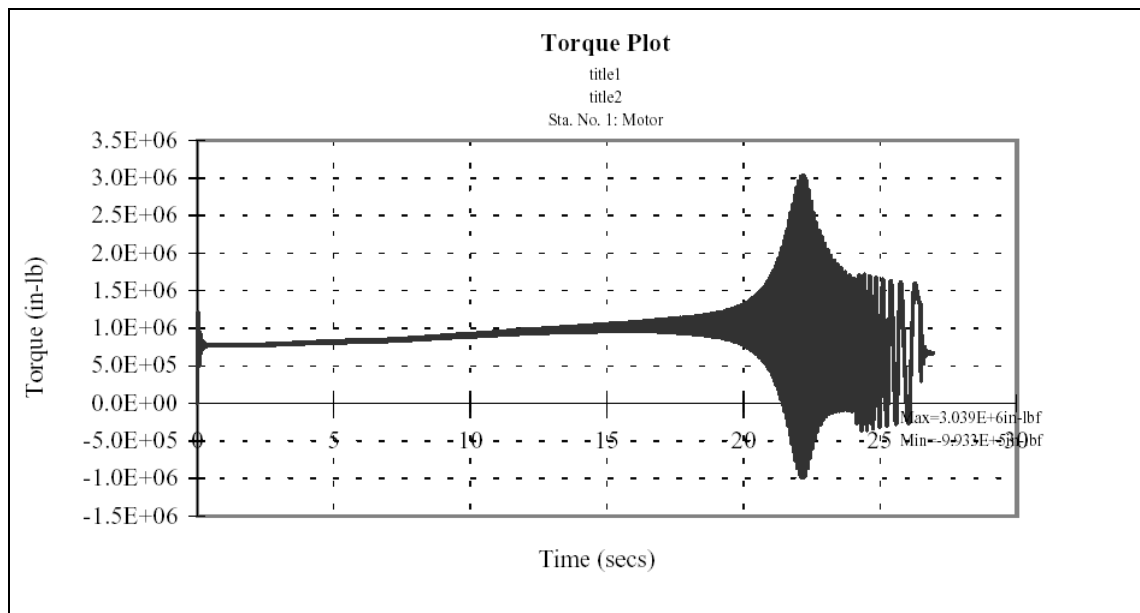


Fig. 16 Torque plot using definition of driving torque in Eq. (78), and considering damping

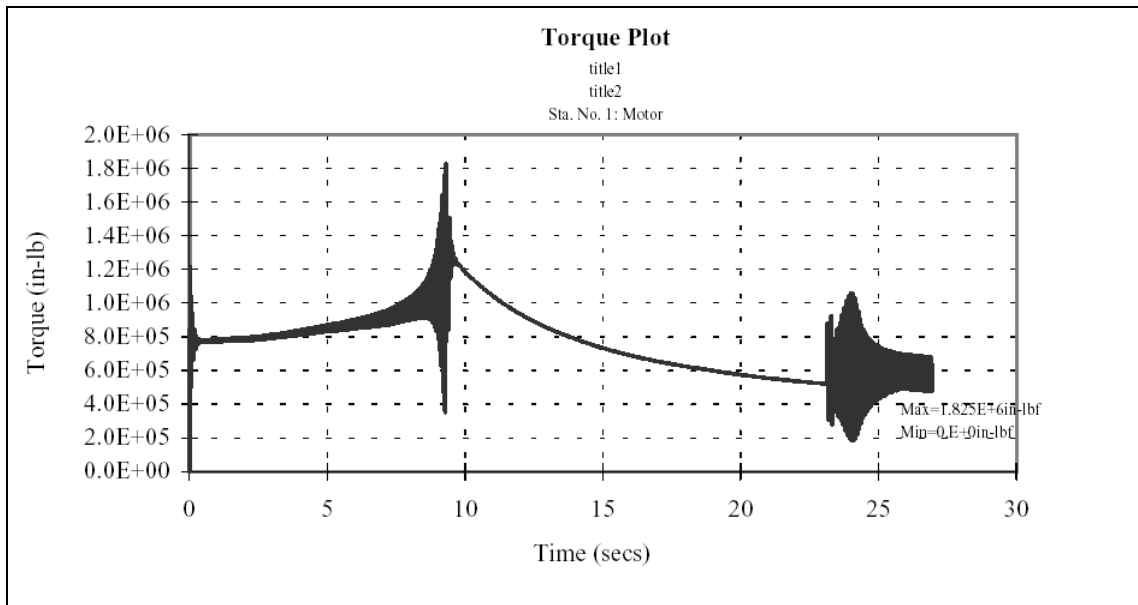


Fig. 17 Torque plot using definition of driving torque in Eq. (75), and considering damping

The following characteristics were noted by comparing the torque values and resonant speeds in Figures 16 and 17:

- Predicted response to the initial pulsation lasts for a slightly longer time if driving torque definition in Eq. (75) is used, as opposed to the definition in Eq. (78).
- The maximum predicted torque is much lower when Eq. (75) is used, than when Eq. (78) is used.
- An additional response is predicted around 8.5 seconds when Eq. (75) is used. This happens at a motor speed of around 600 rpm, as seen from Fig. 17. Again, this corresponds to the 1X motor frequency intersecting the first natural frequency line.

- Large response is predicted around 22 seconds (1600 rpm) with Eq. (78), and 24 seconds (1700 rpm) with Eq. (75). Again, the maximum torque values predicted during this period are much lower when Eq. (75) is used.
- The torque values do not become negative when Eq. (75) is used (Fig. 17), but during some portion of the plot in Fig. 16, where Eq. (78) is used, the torque values become negative.

The observations made above confirmed that pulsation around the intersection of the first natural frequency and 1X motor frequency was absent in Fig. 16, though results of Fig. 16 gave a better correlation with the Campbell diagram, when compared with Fig. 17, where Eq. (75) had been used. The torque values during the pulsation around 22 seconds were also much lower when Eq. (75) was used for defining driving torque.

Analysis Summary

The driving torque definition that considers the instantaneous angular position of the motor inertia, i.e. Eq. (78), gives better correlation with the Campbell diagram when compared with Eq. (75), which considers the driving torque as a direct function of the excitation frequency (ω). However, an additional pulsation, corresponding to the intersection of 1X motor frequency line with the first natural frequency line on the Campbell diagram, with torque values lower yet substantial, is completely missed by the driving torque definition in Eq. (78), but appears when Eq. (75) is used. There is no reason to believe that any 1X excitation actually exists, if the excitation is from motor slip (Eq. (69)). Hence, it may be recommended that the Eq. (78) should be used for the

definition of driving torque for transient analysis and predicting the number of machine startups (or for designing the shaft diameter for a predetermined number of startups), with a higher factor of safety.

$$T_1(t) = T_{avg} + T_{osc} \cos \left[4\pi L_f \left(t - \frac{\theta_1}{\Omega_s} \right) \right] \quad (79)$$

A factor of safety of 1.35 has been recommended by Corbo et al. [15], whereas some other references specify a highly conservative factor of safety of 2.0. However, a factor of safety in the range 1.7 to 1.8 may be safely adopted for design as a compromise between being too conservative and avoiding the risk of premature machine failures.

CUMULATIVE FATIGUE ASSESSMENT AND PREDICTING NUMBER OF STARTS

Unless properly analyzed and designed, machines employing synchronous motors face the grave threat of significantly shortened lives due to failures. This is due to the fact that synchronous motors present large fluctuating torques during machine startup. The resultant torsional stresses on the shaft can be greater than the endurance limit of the material of the shaft. With the shaft elements of the machines being subject to such high stresses, it is essential to determine the number of startups the machine can survive. *XLTRC-TORSION* incorporates the capability of predicting the life of a machine using cumulative fatigue analysis.

Traditionally, in order to calculate the number of startups for a machine, either the stress-life theory or strain-life theory has been used, the former having been used more often than the latter. The present study, however, uses the strain-life approach described in [15] as the stress-life approach yields highly conservative results, which are often unwarranted. The stress-life approach using the $S-N$ curve is based on the assumption that life of a machine component depends upon the level of stress carried, whereas the strain-life theory advocates that strain is the governing factor instead of stress.

From elementary elasticity, the total strain on a part is the sum of the elastic and plastic strains, both being related linearly to the life N on a log-log graph. In the High Cycle Fatigue (HCF) regime, the elastic strain dominates the total strain, whereas in the

Low Cycle Fatigue (LCF) regime, the plastic strain dominates. Shigley and Mischke [17] assert that the partition between HCF and LCF regions may be made at the point where both the plastic and elastic strains are equal.

It has been categorically stated in [15] that the traditional safety factor of 2.0 is overly conservative, and hence, a lower value may safely be prescribed for the same. Corbo et al. [15] claim that their method produces acceptable results, concomitantly being conservative.

After the transient response analysis as detailed in the previous chapters has been performed on the rotor model, the data on variation of torque with respect to time for different stations is available. The method used for determining the maximum and minimum torques during each torque cycle and counting the number of such torque cycles can be briefly explained as follows:

The maximum torque during the motor startup is determined from the results of the transient analysis. Then the torque troughs immediately preceding and following the peak are determined. The lower of these two values is then selected. For example, if the trough after the peak is lower, this trough is paired with the peak. Then all other torque crests are paired with the troughs just following them.

One should run the code for prediction of fatigue life on a number of stations which may be considered “weak” by judgement due to there being abrupt diametrical steps, key-ways, etc., at or near the stations. The maximum and minimum torques obtained earlier are converted into shear stress for each station under consideration using the basic equation [15]:

$$\tau = T \times \frac{R}{J} \quad (80)$$

J for a shaft section may be determined as follows:

$$J = \frac{\pi}{32} d^4 \text{ for a solid shaft with diameter } d, \text{ and} \quad (81)$$

$$J = \frac{\pi}{32} (d_o^4 - d_i^4) \text{ for a hollow shaft with } d_i \text{ and } d_o \text{ as inner and outer diameters}$$

Once the maximum and minimum values of shear stress are determined, one should proceed to determine the cyclic shear stress as [15]:

$$\tau_{cyclic} = 0.5 \times (\tau_{max} - \tau_{min}) \quad (82)$$

The Coffin-Manson equation that governs the strain-life approach gives the value of true strain $\epsilon(N)$ corresponding to a life of N cycles [15]:

$$\epsilon(N) = \left(\frac{\sigma_f'}{E} \right) \times N^b + \epsilon_f' \times N^c \quad (83)$$

The values of true stress at fracture during tensile test σ_f' , true strain at fracture during tensile test ϵ_f' , elastic strain component b , and plastic strain component c and the modulus of elasticity E for various steels can be obtained from [18]. *XLTRC-TORSION* has the feature for accepting these values as input if one does not prefer the values being plugged in by the software that uses saved tables taken from [18]. Values and equations for determination of the various design factors have also been stored in *XLTRC-Torsion* using applicable equations, charts and tables from [15-19, 25, 26, 29-31, 33, 35].

The value of true stress $S(N)$ corresponding to a life of N cycles can be obtained by just multiplying $\varepsilon(N)$ with the modulus of elasticity E . Using this value, the allowable shear stress for a life of N cycles may be determined as follows [15]:

$$\tau(N) = \frac{S(N) \times FSh \times ka(N) \times kb(N)}{kfs(N) \times SF} \quad (84)$$

The values of the shear factor (F_{sh}) and factor of safety (SF) have been taken as 0.577 (from Von-Mises theory) and 1.35 respectively as suggested in [15]. The value of $ka(N)$ may be determined using Eq. (85) [15]:

$$ka(N) = \frac{10^{bka}}{N^{mka}} \quad (85)$$

where,

$$mka = \frac{\log \left[\frac{ka(1000)}{ka(10^6)} \right]}{3.0} \quad (86)$$

$$bka = \log \left\{ \frac{[ka(1000)]^2}{ka(10^6)} \right\}$$

The value of $ka(10^6)$ can be determined from Eq. (87) [25]. The values of a and b to be put into this equation are also provided in [25] for various surface finish methods.

$$ka(10^6) = a \times UTS^b \quad (87)$$

The value of $ka(1000)$ in Eq. (86) is taken as 1.0.

The value of $kb(N)$ in Eq. (84) may be calculated as follows [15]:

$$kb(N) = \frac{10^{bkb}}{N^{mkb}} \quad (88)$$

where,

$$mkb = \frac{\log \left[\frac{kb(1000)}{kb(10^6)} \right]}{3.0} \quad (89)$$

$$bkb = \log \left\{ \frac{[kb(1000)]^2}{kb(10^6)} \right\}$$

The value of $kb(10^6)$ for a shaft of diameter d is calculated from the following empirical relationships:

Corbo et al [15]: $kb(10^6) = \left(\frac{d}{0.3} \right)^{-0.1133}$, for $0.11" \leq d < 2"$ or $d > 10"$ (90)

Shigley & Mischke [17]: $kb(10^6) = 0.859 - 0.02125d$, for $2" < d \leq 10"$

The value of $kb(1000)$ in Eq. (89) is taken as 1.0.

The value of $kfs(N)$ to be inserted into Eq. (84) is computed as [15]:

$$kfs(N) = \frac{10^{bkf}}{N^{mkf}} \quad (91)$$

where,

$$mkf = \frac{\log \left[\frac{kfs(1000)}{kfs(10^6)} \right]}{3.0} \quad (92)$$

$$bkf = \log \left\{ \frac{[kfs(1000)]^2}{kfs(10^6)} \right\}$$

The value of $kfs(10^6)$ for a shaft of diameter d is computed from [17]:

$$kfs(10^6) = 1 + q(ks - 1) \quad (93)$$

where, notch sensitivity q is obtained from the notch sensitivity curves [19]. The value of kts is obtained from the following equation [26], for a stepped shaft that changes from a greater diameter D to smaller diameter d , with a fillet radius r at the step:

$$kts = 0.78 + 0.2 \left(\frac{D}{d} \right)^{-10} + \left(\frac{r}{d} \right)^{-0.46} \sqrt{\frac{0.002 - 0.125 \left(\frac{D}{d} \right)^2 + 0.123 \left(\frac{D}{d} \right)^4}{1 - 2.75 \left(\frac{D}{d} \right)^2 + 2.55 \left(\frac{D}{d} \right)^4}} \quad (94)$$

The value of $kfs(1000)$ in the Eq. (92) is obtained from $kfs(10^6)$ as follows [15]:

$$kfs(1000) = [kfs(10^6)]^{0.5} \quad (95)$$

Once the values for all the parameters in Eq. (84) have been determined, the τ - N graph can be plotted on a log-log scale. Conventionally, the value of τ corresponding to $N=1E+06$ cycles is the shear endurance limit. The shear endurance limit is compared with the cyclic shear stress values (τ_{cyclic}) determined earlier. Only those cycles having τ_{cyclic} greater than the shear endurance limit are taken into further consideration. The number of allowable cycles (N_j) for each such value of τ_{cyclic} is obtained from Eq. (84). These values would be less than 10^6 as only those τ_{cyclic} greater than the shear endurance limit are considered. One can then use methods like the bisection method, the Newton-Raphson method to determine the number of cycles from τ_{cyclic} values.

The allowable number of starts (n) for the machine can finally be calculated from the calculated N_j using [15]:

$$n = \frac{0.5}{\sum \left(\frac{1}{N_j} \right)} \quad (96)$$

This procedure outlined in [15] emphasizes the need for selecting shaft elements with smaller diameters when compared with the whole rotor, sections with known high stress concentration or keyways, and determining the τ - N curve for each such shaft element of interest in order to perform life calculations. The minimum such obtained life would be the number of startups that the machine can survive.

VALIDATION OF CODE-GENERATED RESULTS WITH ANALYSIS AND TEST DATA

In order to verify the accuracy and reliability of the code, validation of the results of the code with experimental data was necessary. Hence, data for an air compressor driven by a 66,000 HP synchronous motor was requested from the industry. This data was made available in the form of Microsoft Excel sheets containing graphs from actual transient tests obtained by conducting strain gage tests. Additional information regarding the model has been obtained from Corbo et al. [15, 16].

66,000 HP Air Compressor Train

Details regarding the air compressor train under study are given in Fig. 18.

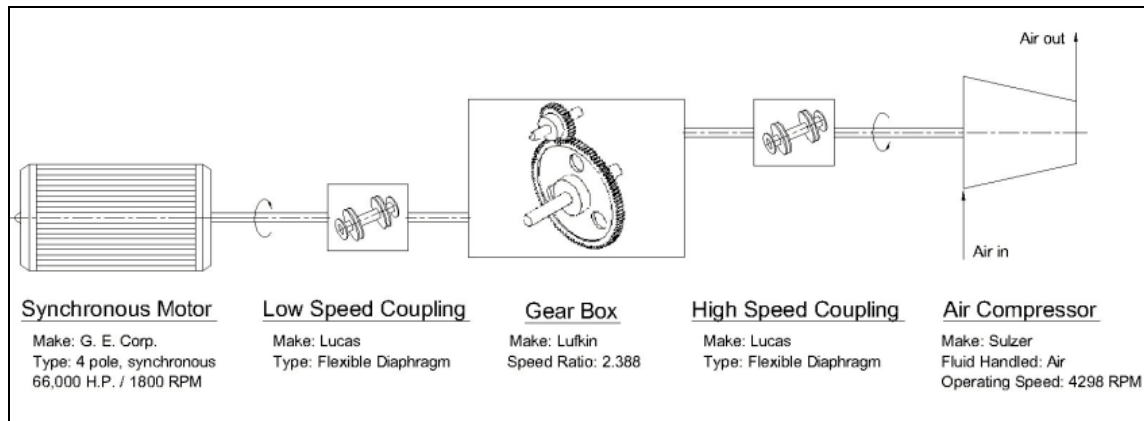


Fig. 18 Air Compressor Train – Schematic

Compressor:

Make: Sulzer

Fluid Handled: Air

Operating Speed: 4298 RPM

Motor:

Make: General Electric Corporation

Type: Four-pole, synchronous

HP: 66000

Synchronous Speed: 1800 RPM

Gearbox:

Make: Lufkin

Gear ratio: 2.388

Couplings (Motor shaft/Compressor shaft):

Make: Lucas

Type: Flexible diaphragm

Motorshaft coupling (Low-speed) torsional stiffness: 479.98E+6 lb-in/rad

Compressor shaft coupling (High-speed) torsional stiffness: 241.88E+6 lb-in/rad

Analytical Model of the Drive Train

Data required for preparing an analytical model of the air compressor (Tables 1 to 4) was available from earlier reports [27, 28] presented to the Turbomachinery Research Consortium (TRC) at Texas A&M University, College Station, TX. In all, four models were made for the air compressor train – two for verification by the Transfer Matrix method and two for verification by the Finite Element method. Each of these groups had models of the drive train utilizing five inertias and seventy-four inertias. The five inertia model was a simplified equivalent of the more detailed seventy-four inertia model and was created in order to corroborate results with the model created by Corbo et al. [16], who had used the five inertia model in order to be compatible with the limitations of their transient response program. The five significant inertias included in the five inertia model (Fig. 19) were: the motor rotor, the low speed coupling hub, the gear mesh (gear and pinion), the high speed coupling hub and the air compressor rotor. The seventy-four inertia model (Fig. 20), however, was more detailed and included changes in shaft diameter and a segregation of the above inertias into smaller inertias per significant changes in geometry. The shafts were assumed to behave as torsional springs.

Table 1 Geometric data for the five inertia, Transfer Matrix model

INPUT TABLE OF BEAM AND STATION DEFINITIONS, MAX. TWO BEAM PER STATION ALLOWED									
<i>Station</i>	<i>Length</i>	<i>OD</i>	<i>ID</i>	<i>Weight Density</i>	<i>Shear Modulus</i>	<i>Added Ip</i>	<i>Gear Ratio</i>	<i>Torsional Stiffness</i>	
<i>#</i>	<i>in</i>	<i>in</i>	<i>in</i>	<i>lb/in³</i>	<i>psi</i>	<i>lb-in²</i>		<i>lb-in/rad</i>	
1	230.000	21.069	0.000	0.000	1.15E+07	1.30E+07	1.00	9.67E+08	Motor Rotor
2	59.055	11.619	0.000	0.000	1.15E+07	1.03E+06	1.00	3.48E+08	LS Coupling hub
3	90.500	16.303	0.000	0.000	1.15E+07	8.34E+06	1.00	8.81E+08	Gear Mesh
4	43.307	15.743	0.000	0.000	1.15E+07	2.87E+06	1.00	1.60E+09	HS Coupling hub
5	0.000	0.000	0.000	0.000	1.15E+07	2.68E+07	1.00	0.00E+00	Comp. Rotor

Table 2 Geometric data for the seventy-four inertia, Transfer Matrix model

INPUT TABLE OF BEAM AND STATION DEFINITIONS, MAX. TWO BEAM PER STATION ALLOWED									
<i>Station</i>	<i>Length</i>	<i>OD</i>	<i>ID</i>	<i>Weight Density</i>	<i>Shear Modulus</i>	<i>Added Ip</i>	<i>Gear Ratio</i>	<i>Torsional Stiffness</i>	
#	in	in	in	lb/in ³	psi	lb-in ²		lb-in/rad	
1	3.000	2.000	0.000	0.283	1.15E+07	0.00E+00	1.00	0.00E+00	End of motor sh
2	1.000	3.000	0.000	0.283	1.15E+07	0.00E+00	1.00	0.00E+00	
3	17.000	4.000	0.000	0.283	1.15E+07	0.00E+00	1.00	0.00E+00	
4	0.500	4.800	0.000	0.283	1.15E+07	0.00E+00	1.00	0.00E+00	
5	0.500	5.600	0.000	0.283	1.15E+07	0.00E+00	1.00	0.00E+00	
6	3.300	5.600	0.000	0.283	1.15E+07	2.30E+04	1.00	0.00E+00	Exciter
7	0.200	5.800	0.000	0.283	1.15E+07	0.00E+00	1.00	0.00E+00	
8	0.800	8.300	0.000	0.283	1.15E+07	0.00E+00	1.00	0.00E+00	
9	3.600	5.300	0.000	0.283	1.15E+07	0.00E+00	1.00	0.00E+00	
10	0.900	8.300	0.000	0.283	1.15E+07	0.00E+00	1.00	0.00E+00	
11	0.800	8.300	0.000	0.283	1.15E+07	0.00E+00	1.00	0.00E+00	
12	1.400	8.400	0.000	0.283	1.15E+07	0.00E+00	1.00	0.00E+00	
13	4.422	10.827	0.000	0.283	1.15E+07	0.00E+00	1.00	0.00E+00	
14	4.842	12.790	0.000	0.283	1.15E+07	0.00E+00	1.00	0.00E+00	
15	5.236	9.829	0.000	0.283	1.15E+07	0.00E+00	1.00	0.00E+00	
16	5.236	9.829	0.000	0.283	1.15E+07	0.00E+00	1.00	0.00E+00	
17	6.772	12.790	0.000	0.283	1.15E+07	0.00E+00	1.00	0.00E+00	
18	17.130	17.717	0.000	0.283	1.15E+07	0.00E+00	1.00	0.00E+00	
19	12.362	21.654	0.000	0.283	1.15E+07	0.00E+00	1.00	0.00E+00	
20	15.899	43.306	0.000	0.283	1.15E+07	0.00E+00	1.00	0.00E+00	
21	25.601	43.306	0.000	0.283	1.15E+07	2.35E+06	1.00	0.00E+00	Motor rotor
22	25.601	43.306	0.000	0.283	1.15E+07	0.00E+00	1.00	0.00E+00	
23	15.899	43.306	0.000	0.283	1.15E+07	2.35E+06	1.00	0.00E+00	Motor rotor
24	12.362	21.654	0.000	0.283	1.15E+07	0.00E+00	1.00	0.00E+00	
25	13.630	17.717	0.000	0.283	1.15E+07	0.00E+00	1.00	0.00E+00	
26	6.693	13.971	0.000	0.283	1.15E+07	0.00E+00	1.00	0.00E+00	
27	5.315	13.170	0.000	0.283	1.15E+07	0.00E+00	1.00	0.00E+00	
28	5.315	13.170	0.000	0.283	1.15E+07	0.00E+00	1.00	0.00E+00	
29	4.764	13.971	0.000	0.283	1.15E+07	0.00E+00	1.00	0.00E+00	
30	7.421	13.800	0.000	0.283	1.15E+07	0.00E+00	1.00	0.00E+00	
31	2.500	22.000	0.000	0.283	1.15E+07	0.00E+00	1.00	0.00E+00	
32	59.055	12.585	0.000	0.000	1.15E+07	9.94E+04	1.00	4.79E+08	Coupling Hub
33	1.500	20.500	0.000	0.283	1.15E+07	9.94E+04	1.00	0.00E+00	Coupling Hub
34	9.500	12.000	0.000	0.283	1.15E+07	0.00E+00	1.00	0.00E+00	Beg. Of gear sha
35	16.000	14.000	0.000	0.283	1.15E+07	0.00E+00	1.00	0.00E+00	
36	5.833	20.000	0.000	0.283	1.15E+07	0.00E+00	1.00	0.00E+00	
37	17.500	22.434	0.000	0.283	1.15E+07	1.41E+06	2.39	0.00E+00	Gear+Pinion
38	16.875	10.250	0.000	0.283	1.15E+07	0.00E+00	2.39	0.00E+00	
39	2.500	10.000	0.000	0.283	1.15E+07	0.00E+00	2.39	0.00E+00	
40	6.375	9.500	0.000	0.283	1.15E+07	0.00E+00	2.39	0.00E+00	
41	1.250	18.000	0.000	0.283	1.15E+07	0.00E+00	2.39	0.00E+00	End of pinion sh
42	43.307	9.817	0.000	0.000	1.15E+07	2.70E+04	2.39	2.42E+08	Coupling Hub
43	1.260	9.646	0.000	3.313	1.15E+07	2.70E+04	2.39	0.00E+00	Coupling Hub

Table 2 Continued

INPUT TABLE OF BEAM AND STATION DEFINITIONS, MAX. TWO BEAM PER STATION ALLOWED								
<i>Station</i>	<i>Length</i>	<i>OD</i>	<i>ID</i>	<i>Weight Density</i>	<i>Shear Modulus</i>	<i>Added Ip</i>	<i>Gear Ratio</i>	<i>Torsional Stiffness</i>
<i>#</i>	<i>in</i>	<i>in</i>	<i>in</i>	<i>lb/in³</i>	<i>psi</i>	<i>lb-in²</i>		<i>lb-in/rad</i>
44	8.583	9.843	0.000	0.283	1.15E+07	0.00E+00	2.39	0.00E+00
45	12.047	9.843	0.000	0.283	1.15E+07	0.00E+00	2.39	0.00E+00
46	5.315	12.399	0.000	0.451	1.15E+07	0.00E+00	2.39	0.00E+00
47	10.394	17.815	0.000	0.329	1.15E+07	0.00E+00	2.39	0.00E+00
48	16.043	18.408	0.000	0.283	1.15E+07	4.28E+05	2.39	0.00E+00
49	3.602	18.504	0.000	0.283	1.15E+07	0.00E+00	2.39	0.00E+00
50	17.677	18.491	0.000	0.283	1.15E+07	3.35E+05	2.39	0.00E+00
51	4.921	17.688	0.000	0.292	1.15E+07	2.41E+05	2.39	0.00E+00
52	5.433	15.992	0.000	0.284	1.15E+07	0.00E+00	2.39	0.00E+00
53	12.953	17.979	0.000	0.349	1.15E+07	0.00E+00	2.39	0.00E+00
54	4.429	19.447	0.000	0.298	1.15E+07	4.18E+05	2.39	0.00E+00
55	7.736	15.881	0.000	0.289	1.15E+07	0.00E+00	2.39	0.00E+00
56	8.583	18.042	0.000	0.284	1.15E+07	0.00E+00	2.39	0.00E+00
57	18.287	21.411	0.000	0.294	1.15E+07	0.00E+00	2.39	0.00E+00
58	5.138	23.228	0.000	0.283	1.15E+07	0.00E+00	2.39	0.00E+00
59	8.169	21.977	0.000	0.295	1.15E+07	9.51E+05	2.39	0.00E+00
60	15.650	19.213	0.000	0.283	1.15E+07	0.00E+00	2.39	0.00E+00
61	13.662	19.230	0.000	0.305	1.15E+07	0.00E+00	2.39	0.00E+00
62	14.882	20.176	0.000	0.611	1.15E+07	0.00E+00	2.39	0.00E+00
63	10.059	18.465	0.000	0.283	1.15E+07	8.25E+04	2.39	0.00E+00
64	10.059	17.165	0.000	0.332	1.15E+07	1.79E+06	2.39	0.00E+00
65	14.705	16.377	0.000	0.284	1.15E+07	0.00E+00	2.39	0.00E+00
66	14.764	15.473	0.000	0.287	1.15E+07	0.00E+00	2.39	0.00E+00
67	7.421	13.641	0.000	0.431	1.15E+07	0.00E+00	2.39	0.00E+00
68	12.008	9.843	0.000	0.283	1.15E+07	0.00E+00	2.39	0.00E+00
69	0.591	9.843	0.000	0.283	1.15E+07	0.00E+00	2.39	0.00E+00
70	8.858	6.890	0.000	0.283	1.15E+07	0.00E+00	2.39	0.00E+00
71	8.130	6.890	0.000	2.250	1.15E+07	0.00E+00	2.39	0.00E+00
72	2.840	6.890	0.000	0.283	1.15E+07	0.00E+00	2.39	0.00E+00
73	1.378	7.898	0.000	0.489	1.15E+07	0.00E+00	2.39	0.00E+00
74	0.000	0.000	0.000	0.283	1.15E+07	0.00E+00	2.39	0.00E+00

Beg of compress

Table 3 Geometric data for the five inertia, Finite Element model

INPUT TABLE (CONICAL ELEMENTS)											
Shaft element	Global Node		Length in	OD left in	ID left in	OD right in	ID right in	Weight Density lb/in ³	Shear Modulus psi	Gear Ratio	Element Stiffness in-lb
	Node 1	Node 2									
1	1	2	230.000	21.069	0.000	21.069	0.000	0.000	1.15E+07	1.000	9.67E+08
2	2	3	59.055	11.619	0.000	11.619	0.000	0.000	1.15E+07	1.000	3.48E+08
3	3	4	90.500	16.303	0.000	16.303	0.000	0.000	1.15E+07	1.000	8.81E+08
4	4	5	43.307	15.743	0.000	15.743	0.000	0.000	1.15E+07	1.000	1.60E+09

ADDED INERTIAS		
Node #	Added Inertia lb-in ²	Gear Ratio of node
1	1.30E+07	1.00 Motor Rotor
2	1.03E+06	1.00 LS Coupling hub
3	8.34E+06	1.00 Gear Mesh
4	2.87E+06	1.00 HS Coupling hub
5	2.68E+07	1.00 <u>Comp. Rotor</u>

Table 4 Geometric data for the seventy-four inertia, Finite Element model

INPUT TABLE (CONICAL ELEMENTS)											
Shaft element #	Global Node		Length	OD left	ID left	OD right	ID right	Weight Density	Shear Modulus	Gear Ratio	Element Stiffness
	Node 1	Node 2	in	in	in	in	in	lb/in ³	psi		in-lb
1	1	2	3.000	2.000	0.000	2.000	0.000	0.283	1.15E+07	1.000	0.00E+00
2	2	3	1.000	3.000	0.000	3.000	0.000	0.283	1.15E+07	1.000	0.00E+00
3	3	4	17.000	4.000	0.000	4.000	0.000	0.283	1.15E+07	1.000	0.00E+00
4	4	5	0.500	4.800	0.000	4.800	0.000	0.283	1.15E+07	1.000	0.00E+00
5	5	6	0.500	5.600	0.000	5.600	0.000	0.283	1.15E+07	1.000	0.00E+00
6	6	7	3.300	5.600	0.000	5.600	0.000	0.283	1.15E+07	1.00	0.00E+00
7	7	8	0.200	5.800	0.000	5.800	0.000	0.283	1.15E+07	1.00	0.00E+00
8	8	9	0.800	8.300	0.000	8.300	0.000	0.283	1.15E+07	1.000	0.00E+00
9	9	10	3.600	5.300	0.000	5.300	0.000	0.283	1.15E+07	1.00	0.00E+00
10	10	11	0.900	8.300	0.000	8.300	0.000	0.283	1.15E+07	1.00	0.00E+00
11	11	12	0.800	8.300	0.000	8.300	0.000	0.283	1.15E+07	1.00	0.00E+00
12	12	13	1.400	8.400	0.000	8.400	0.000	0.283	1.15E+07	1.00	0.00E+00
13	13	14	4.422	10.827	0.000	10.827	0.000	0.283	1.15E+07	1.00	0.00E+00
14	14	15	4.842	12.790	0.000	12.790	0.000	0.283	1.15E+07	1.00	0.00E+00
15	15	16	5.236	9.829	0.000	9.829	0.000	0.283	1.15E+07	1.00	0.00E+00
16	16	17	5.236	9.829	0.000	9.829	0.000	0.283	1.15E+07	1.00	0.00E+00
17	17	18	6.772	12.790	0.000	12.790	0.000	0.283	1.15E+07	1.00	0.00E+00
18	18	19	17.130	17.717	0.000	17.717	0.000	0.283	1.15E+07	1.00	0.00E+00
19	19	20	12.362	21.654	0.000	21.654	0.000	0.283	1.15E+07	1.00	0.00E+00
20	20	21	15.899	43.306	0.000	43.306	0.000	0.283	1.15E+07	1.00	0.00E+00
21	21	22	25.601	43.306	0.000	43.306	0.000	0.283	1.15E+07	1.00	0.00E+00
22	22	23	25.601	43.306	0.000	43.306	0.000	0.283	1.15E+07	1.00	0.00E+00
23	23	24	15.899	43.306	0.000	43.306	0.000	0.283	1.15E+07	1.00	0.00E+00
24	24	25	12.362	21.654	0.000	21.654	0.000	0.283	1.15E+07	1.00	0.00E+00
25	25	26	13.630	17.717	0.000	17.717	0.000	0.283	1.15E+07	1.00	0.00E+00
26	26	27	6.693	13.971	0.000	13.971	0.000	0.283	1.15E+07	1.00	0.00E+00
27	27	28	5.315	13.170	0.000	13.170	0.000	0.283	1.15E+07	1.00	0.00E+00
28	28	29	5.315	13.170	0.000	13.170	0.000	0.283	1.15E+07	1.00	0.00E+00
29	29	30	4.764	13.971	0.000	13.971	0.000	0.283	1.15E+07	1.00	0.00E+00
30	30	31	7.421	13.800	0.000	13.800	0.000	0.283	1.15E+07	1.00	0.00E+00
31	31	32	2.500	22.000	0.000	22.000	0.000	0.283	1.15E+07	1.00	0.00E+00
32	32	33	59.055	12.581	0.000	12.581	0.000	0.000	1.15E+07	1.00	4.79E+08
33	33	34	1.500	20.500	0.000	20.500	0.000	0.283	1.15E+07	1.00	0.00E+00
34	34	35	9.500	12.000	0.000	12.000	0.000	0.283	1.15E+07	1.00	0.00E+00
35	35	36	16.000	14.000	0.000	14.000	0.000	0.283	1.15E+07	1.00	0.00E+00
36	36	37	5.833	20.000	0.000	20.000	0.000	0.283	1.15E+07	1.00	0.00E+00
37	37	38	17.500	22.434	0.000	22.434	0.000	0.283	1.15E+07	2.39	0.00E+00
38	38	39	16.875	10.250	0.000	10.250	0.000	0.283	1.15E+07	2.39	0.00E+00
39	39	40	2.500	10.000	0.000	10.000	0.000	0.283	1.15E+07	2.39	0.00E+00
40	40	41	6.375	9.500	0.000	9.500	0.000	0.283	1.15E+07	2.39	0.00E+00
41	41	42	1.250	18.000	0.000	18.000	0.000	0.283	1.15E+07	2.39	0.00E+00
42	42	43	43.307	9.814	0.000	9.814	0.000	0.000	1.15E+07	2.39	2.42E+08
43	43	44	1.260	9.646	0.000	9.646	0.000	3.313	1.15E+07	2.39	0.00E+00

Table 4 Continued

INPUT TABLE (CONICAL ELEMENTS)												
Shaft element #	Global Node		Length	OD left	ID left	OD right	ID right	Weight Density	Shear Modulus	Gear Ratio	Element Stiffness	
	Node 1	Node 2	in	in	in	in	in	lb/in ³	psi		in-lb	
44	44	44	45	8.583	9.843	0.000	9.843	0.000	0.283	1.15E+07	2.39	0.00E+00
45	45	45	46	12.047	9.843	0.000	9.843	0.000	0.283	1.15E+07	2.39	0.00E+00
46	46	46	47	5.315	12.399	0.000	12.399	0.000	0.451	1.15E+07	2.39	0.00E+00
47	47	47	48	10.394	17.815	0.000	17.815	0.000	0.329	1.15E+07	2.39	0.00E+00
48	48	48	49	16.043	18.408	0.000	18.408	0.000	0.283	1.15E+07	2.39	0.00E+00
49	49	49	50	3.602	18.504	0.000	18.504	0.000	0.283	1.15E+07	2.39	0.00E+00
50	50	50	51	17.677	18.491	0.000	18.491	0.000	0.283	1.15E+07	2.39	0.00E+00
51	51	51	52	4.921	17.688	0.000	17.688	0.000	0.292	1.15E+07	2.39	0.00E+00
52	52	52	53	5.433	15.992	0.000	15.992	0.000	0.284	1.15E+07	2.39	0.00E+00
53	53	53	54	12.953	17.979	0.000	17.979	0.000	0.349	1.15E+07	2.39	0.00E+00
54	54	54	55	4.429	19.447	0.000	19.447	0.000	0.298	1.15E+07	2.39	0.00E+00
55	55	55	56	7.736	15.881	0.000	15.881	0.000	0.289	1.15E+07	2.39	0.00E+00
56	56	56	57	8.583	18.042	0.000	18.042	0.000	0.284	1.15E+07	2.39	0.00E+00
57	57	57	58	18.287	21.411	0.000	21.411	0.000	0.294	1.15E+07	2.39	0.00E+00
58	58	58	59	5.138	23.228	0.000	23.228	0.000	0.283	1.15E+07	2.39	0.00E+00
59	59	59	60	8.169	21.977	0.000	21.977	0.000	0.295	1.15E+07	2.39	0.00E+00
60	60	60	61	15.650	19.213	0.000	19.213	0.000	0.283	1.15E+07	2.39	0.00E+00
61	61	61	62	13.662	19.230	0.000	19.230	0.000	0.305	1.15E+07	2.39	0.00E+00
62	62	62	63	14.882	20.176	0.000	20.176	0.000	0.611	1.15E+07	2.39	0.00E+00
63	63	63	64	10.059	18.465	0.000	18.465	0.000	0.283	1.15E+07	2.39	0.00E+00
64	64	64	65	10.059	17.165	0.000	17.165	0.000	0.332	1.15E+07	2.39	0.00E+00
65	65	65	66	14.705	16.377	0.000	16.377	0.000	0.284	1.15E+07	2.39	0.00E+00
66	66	66	67	14.764	15.473	0.000	15.473	0.000	0.287	1.15E+07	2.39	0.00E+00
67	67	67	68	7.421	13.641	0.000	13.641	0.000	0.431	1.15E+07	2.39	0.00E+00
68	68	68	69	12.008	9.843	0.000	9.843	0.000	0.283	1.15E+07	2.39	0.00E+00
69	69	69	70	0.591	9.843	0.000	9.843	0.000	0.283	1.15E+07	2.39	0.00E+00
70	70	70	71	8.858	6.890	0.000	6.890	0.000	0.283	1.15E+07	2.39	0.00E+00
71	71	71	72	8.130	6.890	0.000	6.890	0.000	2.250	1.15E+07	2.39	0.00E+00
72	72	72	73	2.840	6.890	0.000	6.890	0.000	0.283	1.15E+07	2.39	0.00E+00
73	73	73	74	1.378	7.898	0.000	7.898	0.000	0.489	1.15E+07	2.39	0.00E+00

Table 4 Continued

ADDED INERTIAS		
Node #	Added Inertia lb-in²	Gear Ratio of node
ai_node	aip	ai_gr
1	0.00E+00	1.00
2	0.00E+00	1.00
3	0.00E+00	1.00
4	0.00E+00	1.00
5	0.00E+00	1.00
6	2.30E+04	1.00
7	0	1.00
8	0	1.00
9	0.00	1
10	0.00	1
11	0	1.00
12	0	1.00
13	0	1.00
14	0	1.00
15	0	1.00
16	0	1.00
17	0	1.00
18	0	1.00
19	0	1.00
20	0	1.00
21	2353800	1.00
22	0	1.00
23	2353800	1.00
24	0	1.00
25	0	1.00
26	0	1.00
27	0	1.00
28	0	1.00
29	0	1.00
30	0	1.00
31	0	1.00
32	99398	1.00
33	99398	1.00
34	0	1.00
35	0	1.00
36	0	1.00
37	1411042	2.39
38	0	2.39
39	0	2.39
40	0	2.39
41	0	2.39
42	27027	2.39
43	27027	2.39

Table 4 Continued

ADDED INERTIAS		
Node #	Added Inertia lb-in²	Gear Ratio of node
44	0	2.39
45	0	2.39
46	0	2.39
47	0	2.39
48	427598	2.39
49	0	2.39
50	335463	2.39
51	240671	2.39
52	0	2.39
53	0	2.39
54	418022	2.39
55	0	2.39
56	0	2.39
57	0	2.39
58	0	2.39
59	951066	2.39
60	0	2.39
61	0	2.39
62	0	2.39
63	82525	2.39
64	1787700	2.39
65	0	2.39
66	0	2.39
67	0	2.39
68	0	2.39
69	0	2.39
70	0	2.39
71	0	2.39
72	0	2.39
73	0	2.39
74	0	2.39

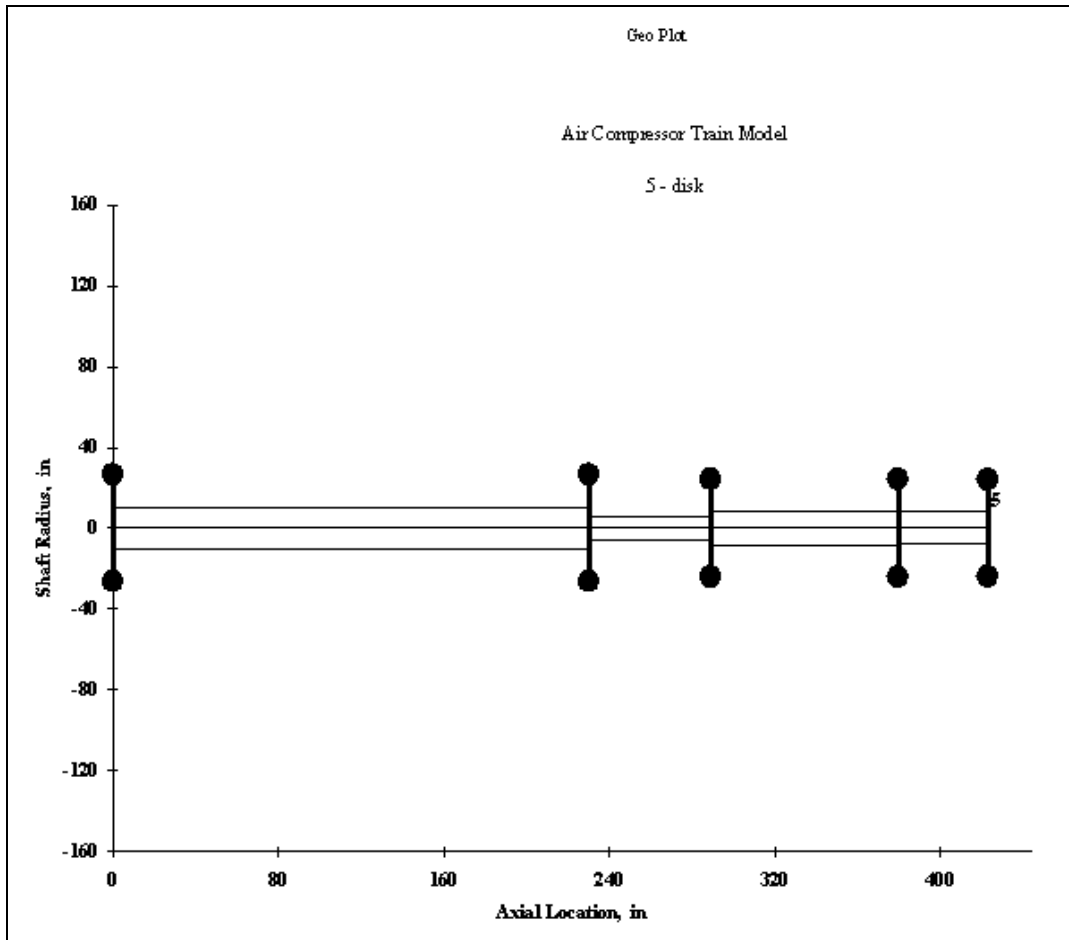


Fig. 19 Five inertia model of the air compressor train

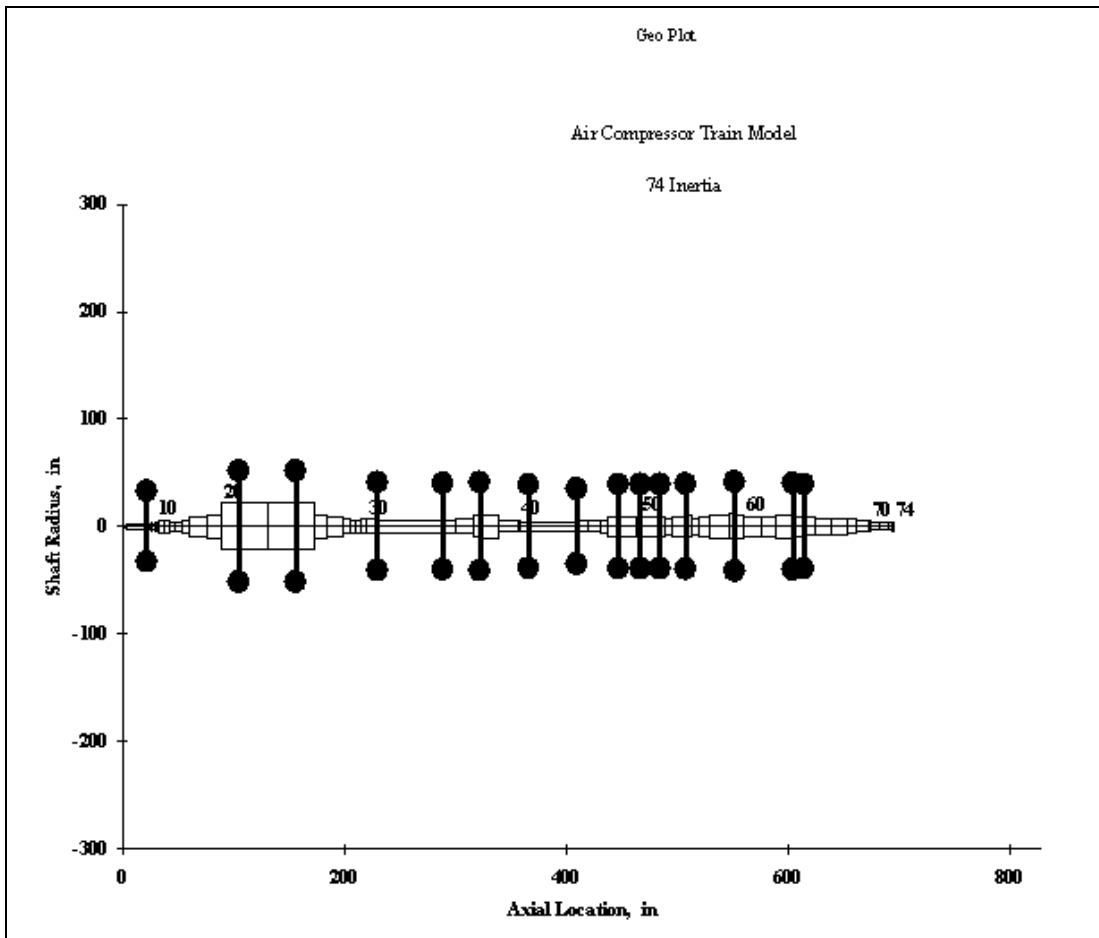


Fig. 20 Seventy-four inertia model of the air compressor train

Undamped Torsional Natural Frequency Calculation

An undamped torsional natural frequency analysis was run using the five inertia model in the Transfer Matrix module. This analysis helped to determine the approximate ranges where the torsional natural frequencies of the drive train would lie. One would hope that an undamped natural frequency analysis of a more detailed model would reveal the system natural frequencies close to the ones calculated using the equivalent model.

Undamped torsional natural frequency analysis was run on the seventy-four inertia model in the Transfer Matrix module and also on the Finite Element versions of the five and seventy-four inertia models in the Finite Element module. Table 5 shows the calculated and measured torsional natural frequencies of the system.

Table 5 Comparison of undamped torsional natural frequency results

Mode	<i>XLTRC-Torsion</i> Transfer Matrix Module		<i>XLTRC-Torsion</i> Finite Element Module		Corbo et al. [15, 16]	<i>Experimental</i> (Approx.)
	5 Inertia	74 Inertia	5 Inertia	74 Inertia		
I	13.74	13.97	13.41	13.98	14.00	13.00
II	33.94	33.68	33.95	33.78	34.00	37.00
III	96.03	111.87	96.04	111.94	111.90	119.93
IV	114.73	206.39	114.74	206.69	115.3	N/A

Information regarding the torsional natural frequencies of the third mode from experimental measurements was not directly available. It was calculated from the available torque-time graph (Fig. 21) at the place where a distinct pulsation was observed near start, since that would be the point where the 2X line frequency corresponds to the third natural frequency. The corresponding graph of motor startup was used to find the actual speed reached at the time when the heavy pulsation was observed. Then, Eq. (97), which was derived from Eq. (47), was used to calculate the corresponding torsional natural frequency.

$$N_{NatFreq} = \left(1 - \frac{NatFreq_{Hz}}{2 * 60}\right) * 1800$$

$$\therefore NatFreq_{Hz} = \left(1 - \frac{N_{NatFreq}}{1800}\right) * 120 \quad (97)$$

where,

$NatFreq_{Hz}$ = Torsional natural frequency in Hz

$N_{NatFreq}$ = Resonant speed corresponding to the torsional natural frequency

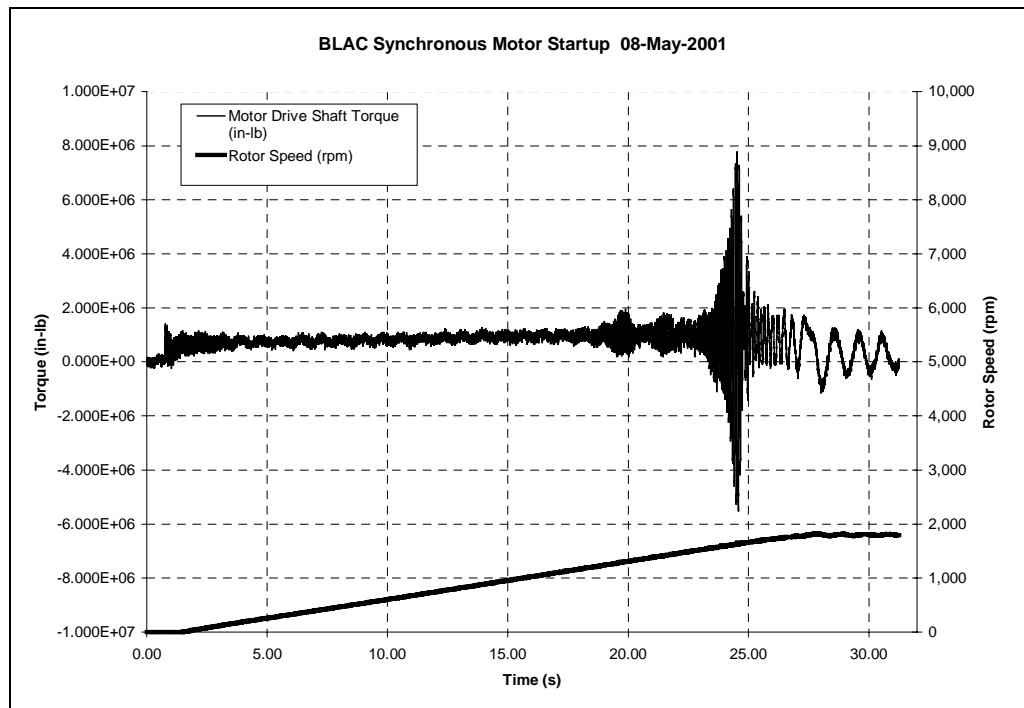


Fig. 21 Run-up and transient torque graphs plotted using data from experiments

The first three natural frequencies were calculated at 23.3 s (1635 RPM), 18.5 s (1250 RPM) and 1.5 s (1 RPM). Pulsation seen at other places on the graph was not appreciable enough to determine higher modes.

It can be seen that undamped torsional frequency analysis on all the four models gave good results for the first two modes. The actual third mode was under-predicted by all the four models. Both Transfer Matrix and Finite Element methods applied to the seventy-four inertia model gave results closer (within 6.7%) to the actual third mode obtained from experiments. The results for the third mode obtained for the five inertia model using both the methods under-predicted the third mode by a large amount. The fourth mode could not be detected from the experimental data and hence no comparison would be justified.

Campbell Diagrams

Using the results of the undamped torsional natural frequency analysis, Campbell diagrams for the four models were plotted. They appear similar for the five inertia model using results from the Transfer Matrix and Finite Element modules since their calculated natural frequencies were fairly close. They show four resonant speeds corresponding to their natural frequencies since all the four modes lie below the twice line frequency excitation (120 Hz), which in turn decreases linearly until it becomes zero at synchronous speed. However, the seventy-four inertia model analyzed in both the Transfer Matrix and Finite Element modules estimated the fourth mode higher than 120 Hz and, hence, have only three resonant speeds where the dropping twice line frequency

line intersects with the horizontal natural frequency lines. Figure 22 shows the Campbell diagram from Corbo et al. [15], while Figures 23 to 26 show Campbell diagrams for the four models.

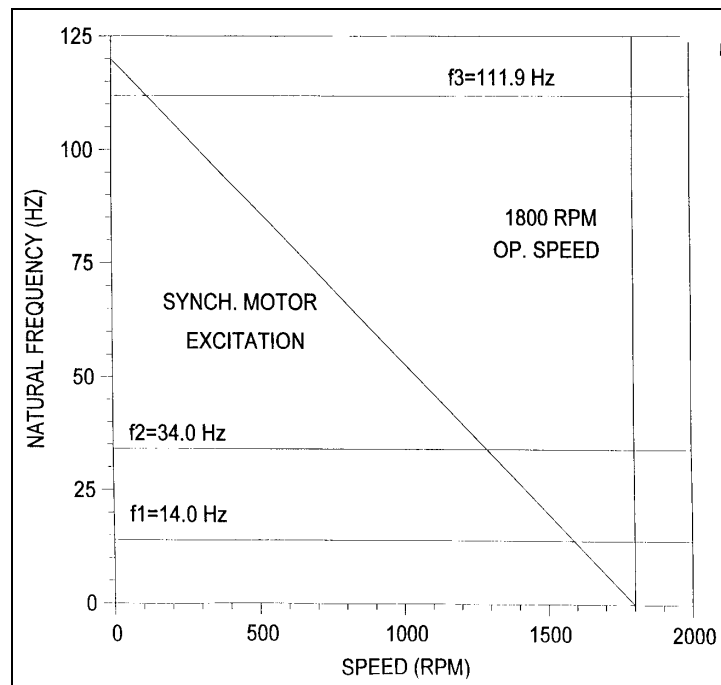


Fig. 22 Campbell diagram from Corbo et al. [15]

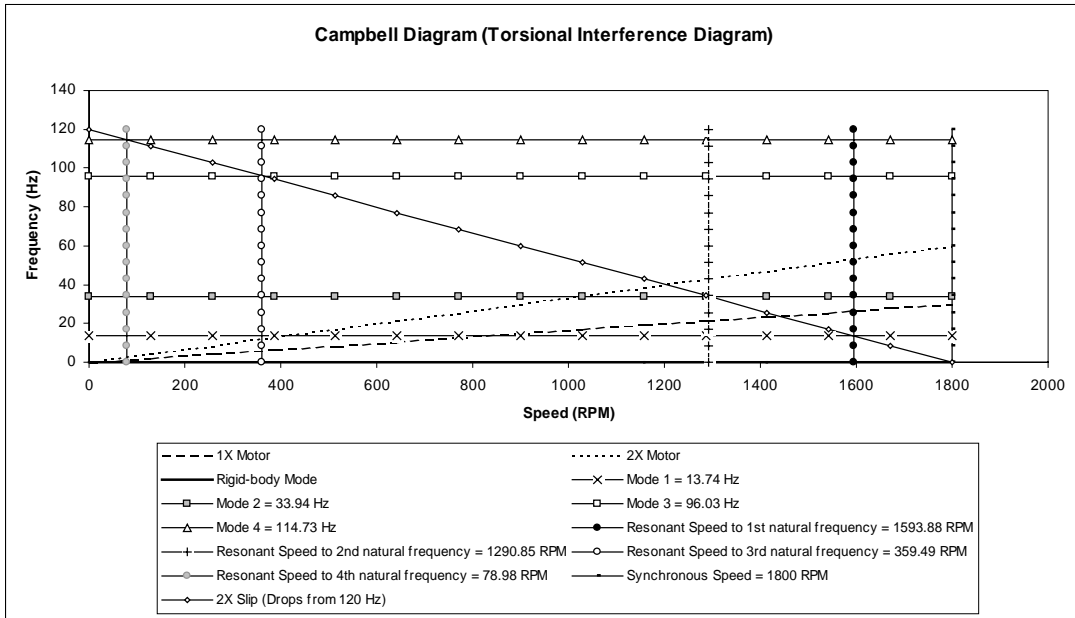


Fig. 23 Campbell diagram for the five inertia model using Transfer Matrix method

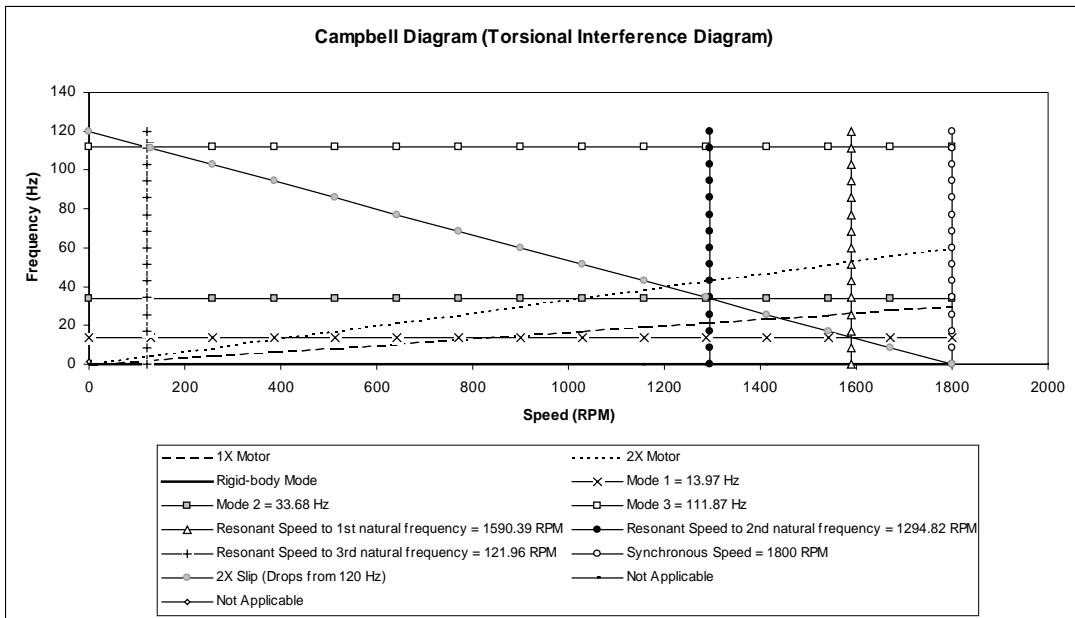


Fig. 24 Campbell diagram for the seventy-four inertia model using Transfer Matrix method

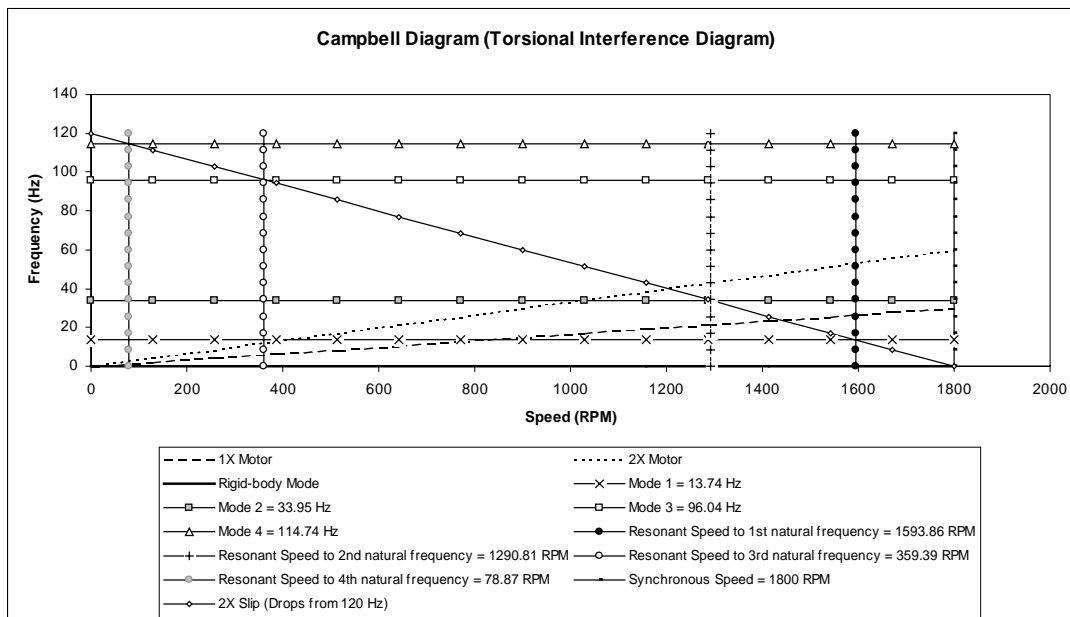


Fig. 25 Campbell diagram for the five inertia model using Finite Element method

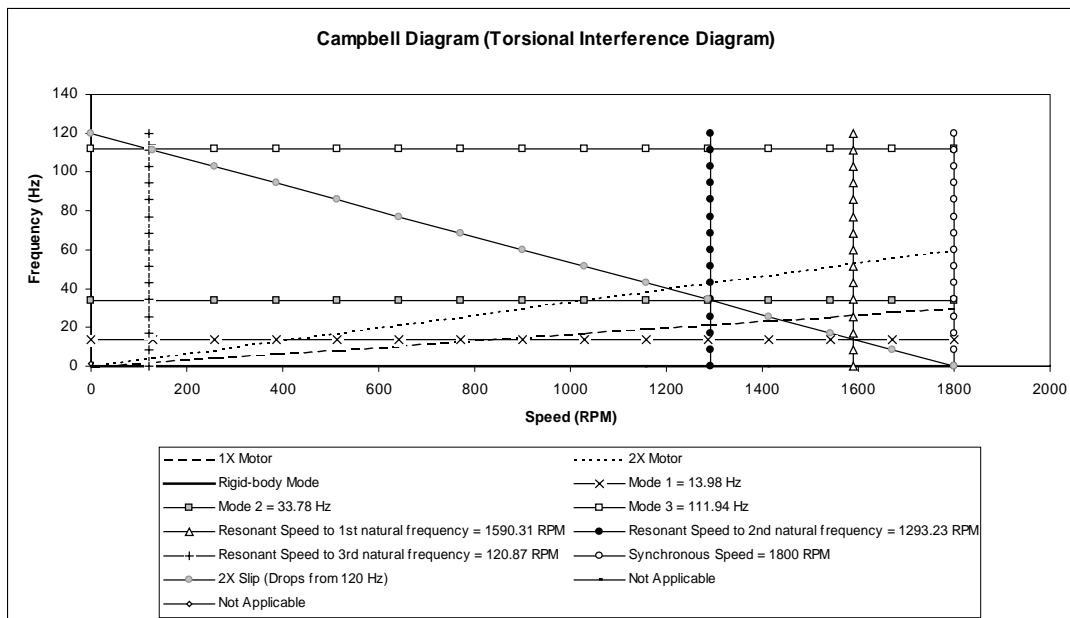


Fig. 26 Campbell diagram for the seventy-four inertia model using Finite Element method

Mode Shapes

The first four mode shapes calculated for all the four models are depicted in Figures 27 to 30. It is clear that mode shapes for the first two modes for all the four models corroborate well with each other and with the mode shapes calculated by Corbo et al. [15]. It should be noted that though mode shapes for the third mode look similar for all the models, they occur at different frequencies. Since the fourth mode eigenvalues for the five inertia models are mutually closer, they show similar mode shapes, as is also true for the seventy-four inertia models. Mode shapes calculated by Corbo et al. [15] are shown in Figures 31 and 32 for ease of comparison with the mode shapes generated for the four models being discussed.

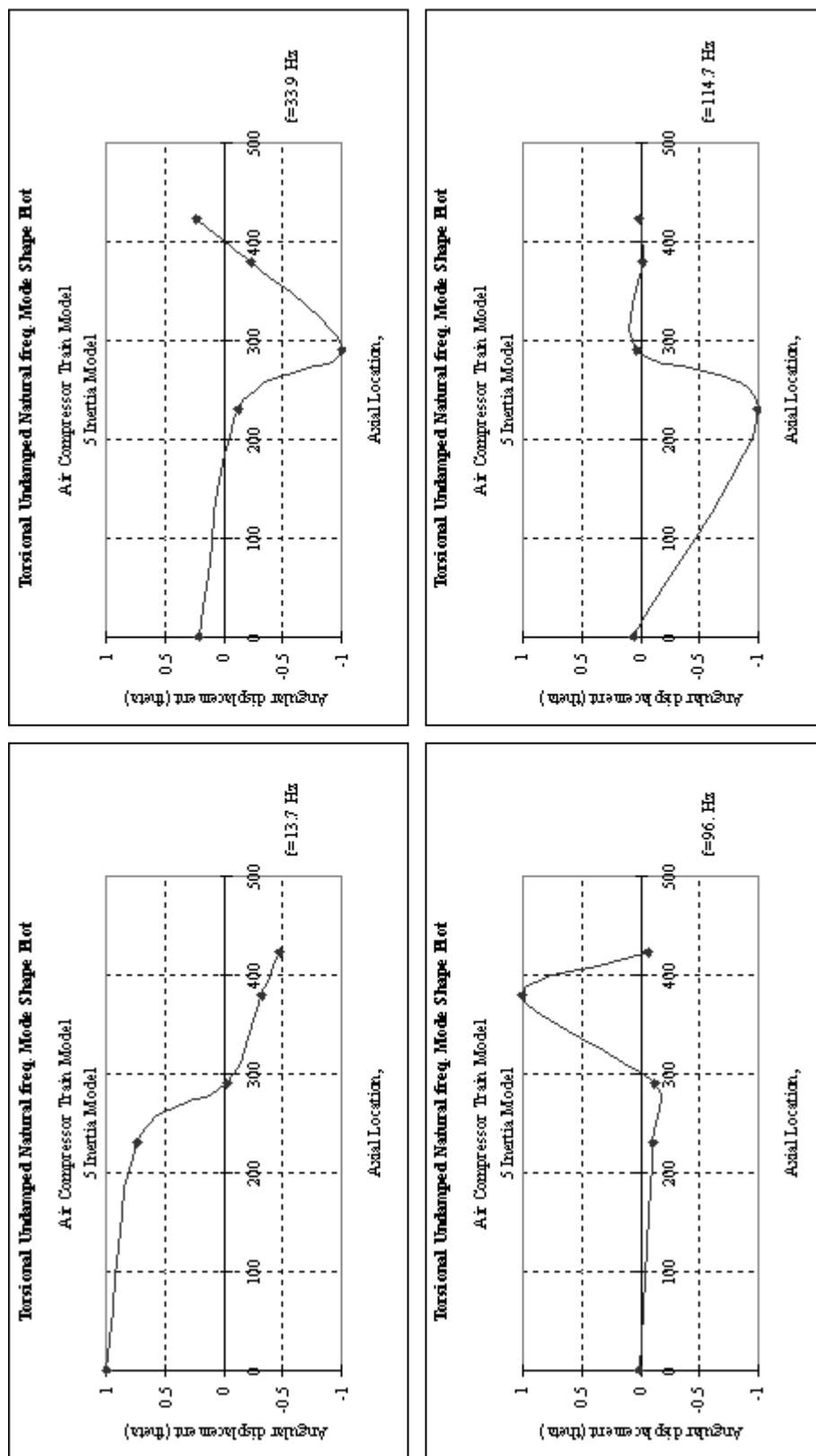


Fig. 27 Mode shapes for the five inertia model using Transfer Matrix method

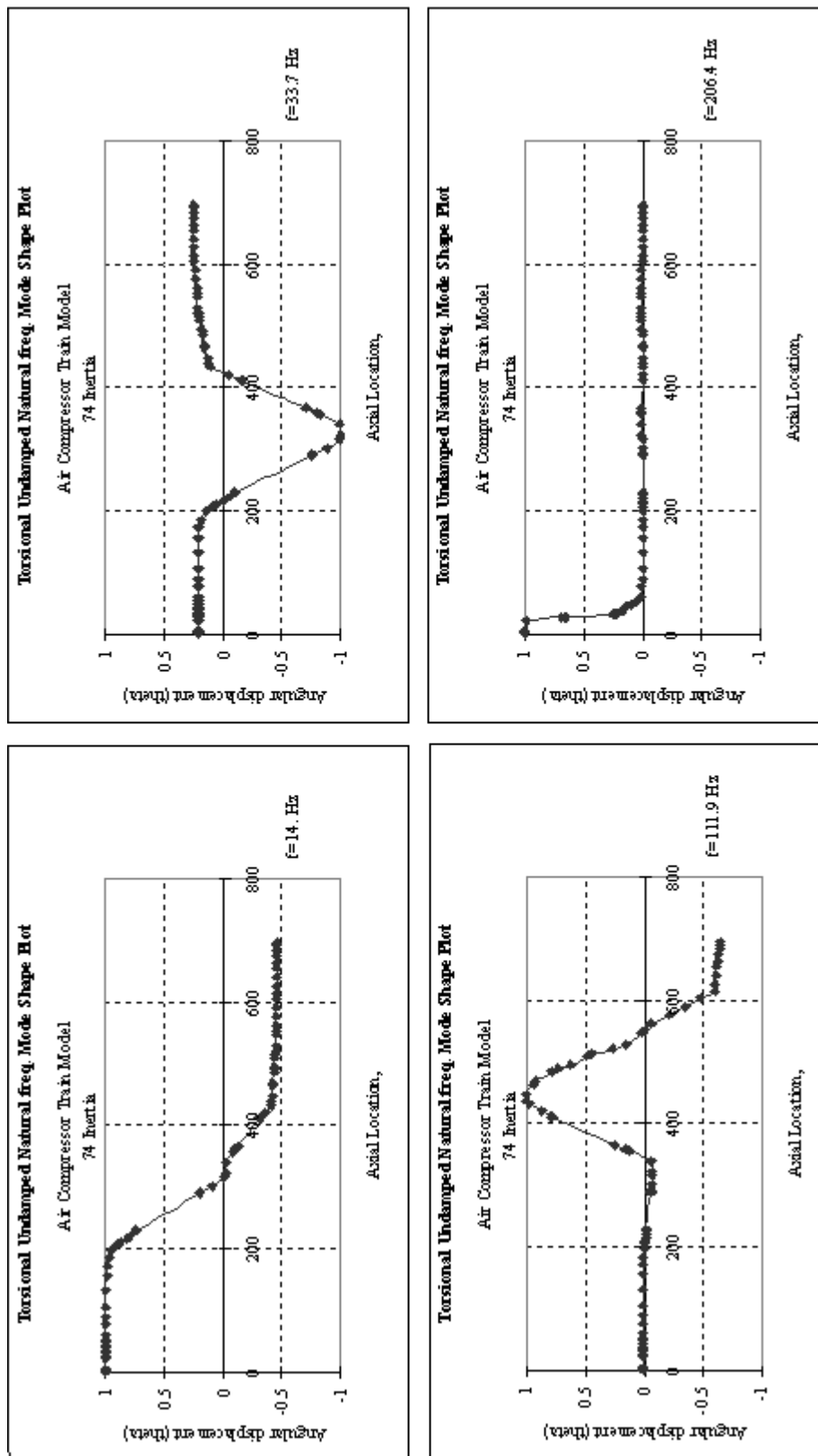


Fig. 28 Mode shapes for the seventy-four inertia model using Transfer Matrix method

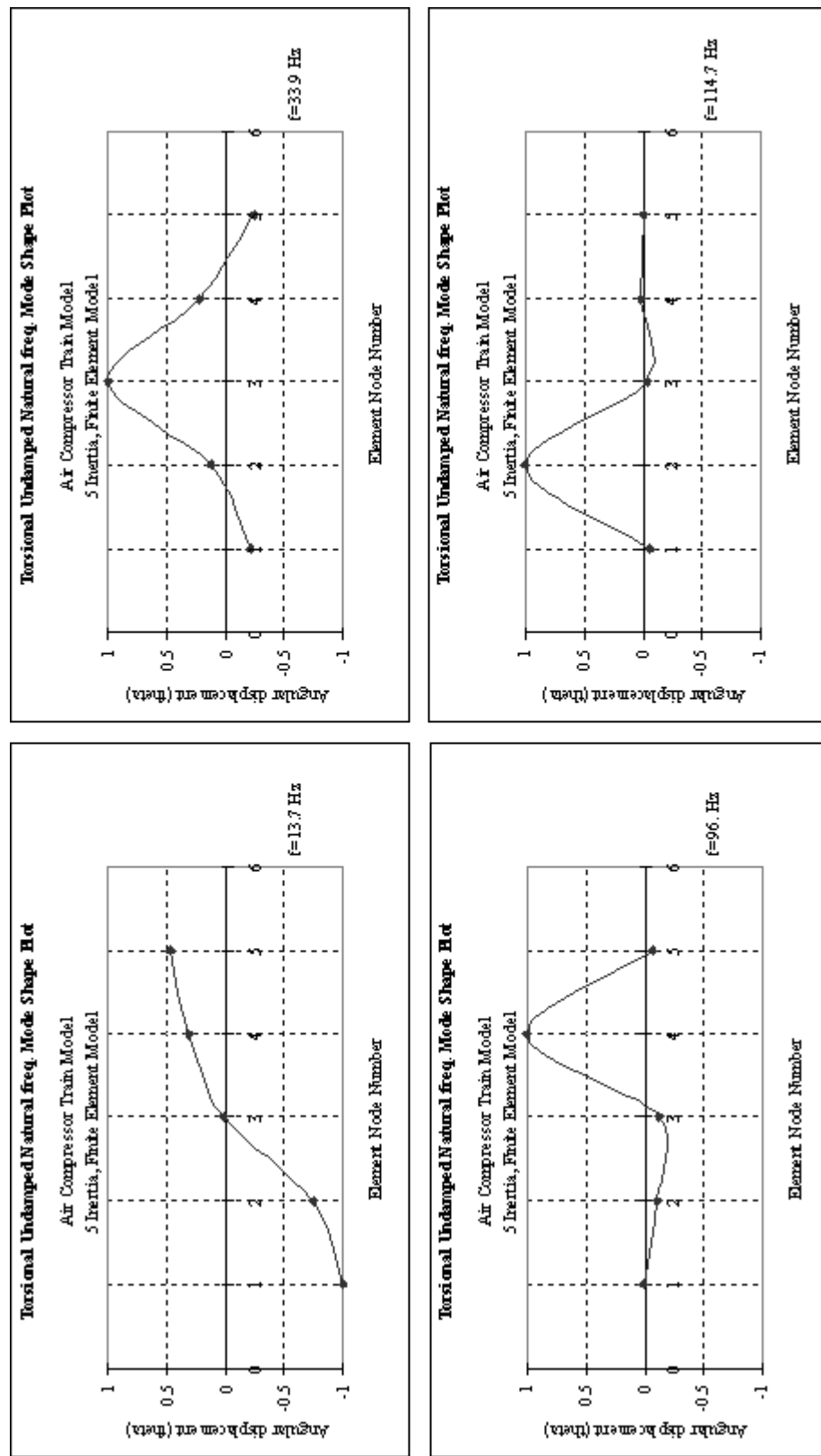


Fig. 29 Mode shapes for the five inertia model using Finite Element method

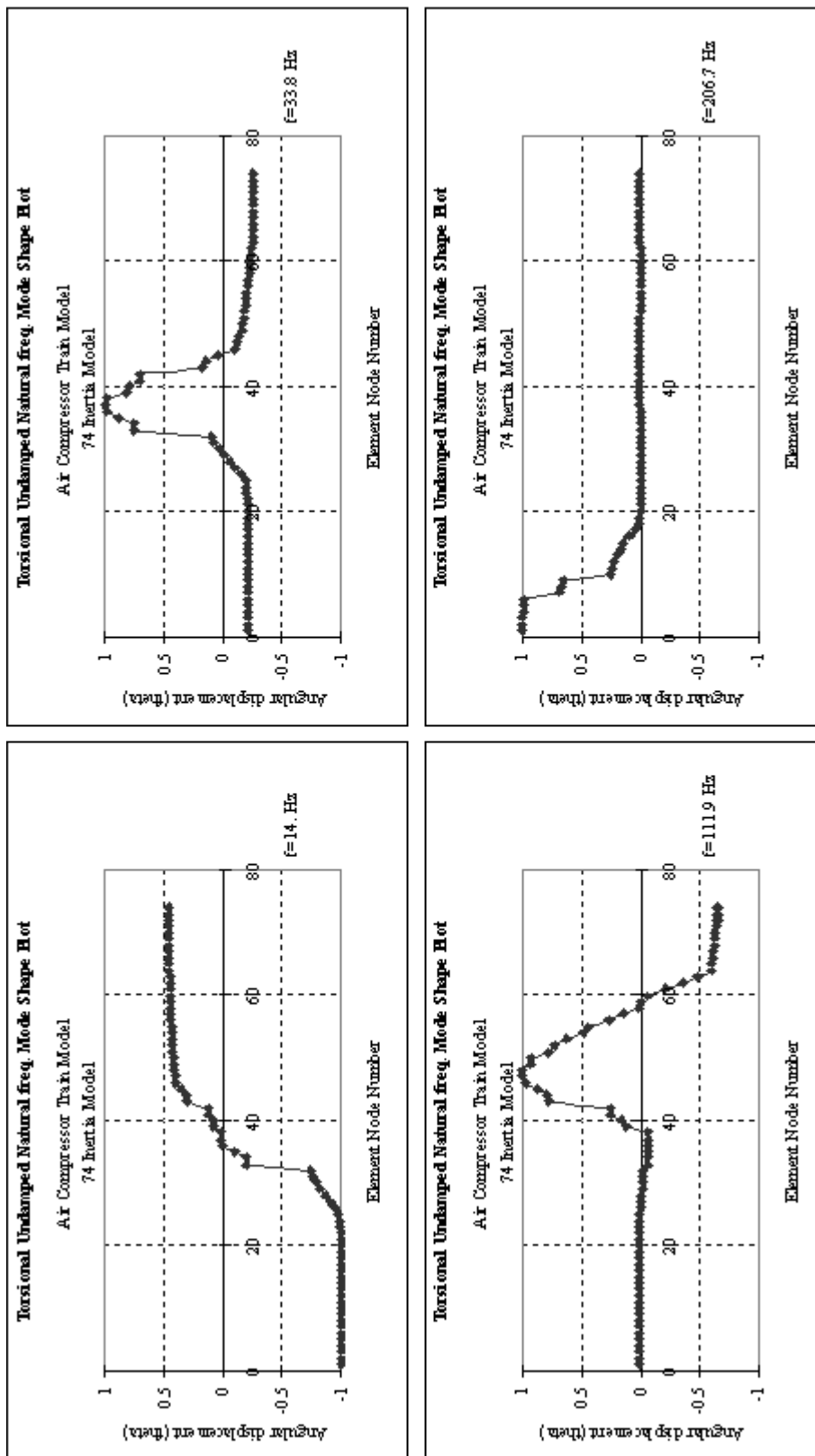


Fig. 30 Mode shapes for the seventy-four inertia model using Finite Element method

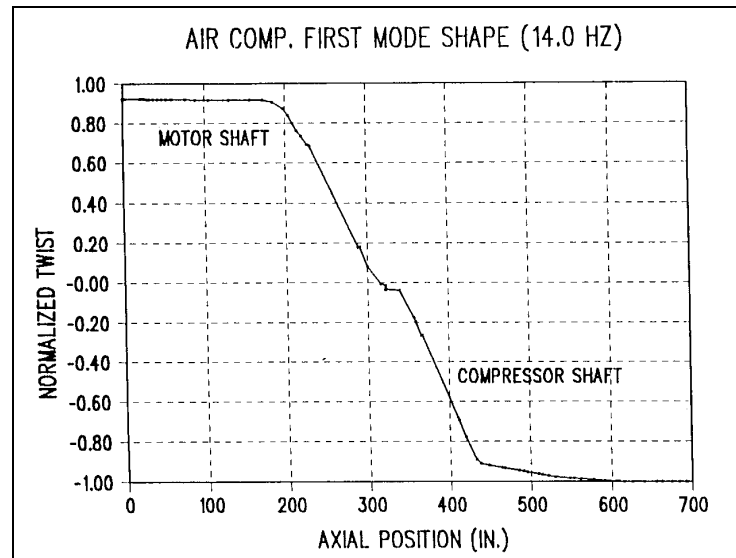


Fig. 31 Mode Shape for first mode (14.00 Hz) from Corbo et al. [15]

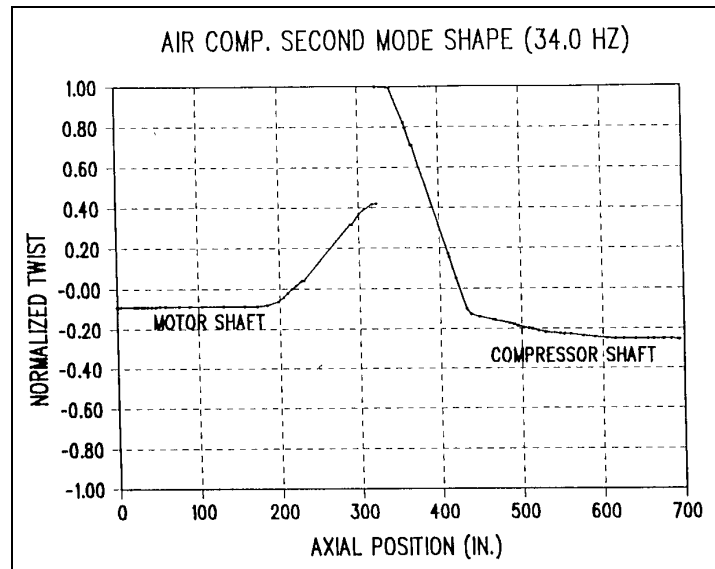


Fig. 32 Mode Shape for second mode (34.00 Hz) from Corbo et al. [15]

Transient Analysis Results

Corbo et al. [16] have used the five inertia model for performing transient analysis on the system in order to be compatible with the limitations of the transient analysis program they employed. Hence, transient analysis was performed using both the five inertia Transfer Matrix and Finite Element models described earlier besides the seventy-four inertia models in order to give a better picture of conformance of results.

Transient analysis was performed on the four models using the 'Transient Analysis' subroutine in both the Transfer Matrix and Finite Element modules of *XLTRC-TORSION*. Using the yardstick given by Corbo et al. [16], a generic damping ratio of 0.02 was employed, besides neglecting gear backlash effects. The motor and compressor (load) characteristic curves used for the analysis were taken as shown in Figures 33 and 34, while the input data for transient analysis is presented in Tables 6 to 9. Note that the compressor was started with the valve closed, and hence, 100% full load torque does not appear on the compressor (load) torque curve. If the compressor had been started with its valve open, the full load torque would have been reached around the synchronous speed of the motor.

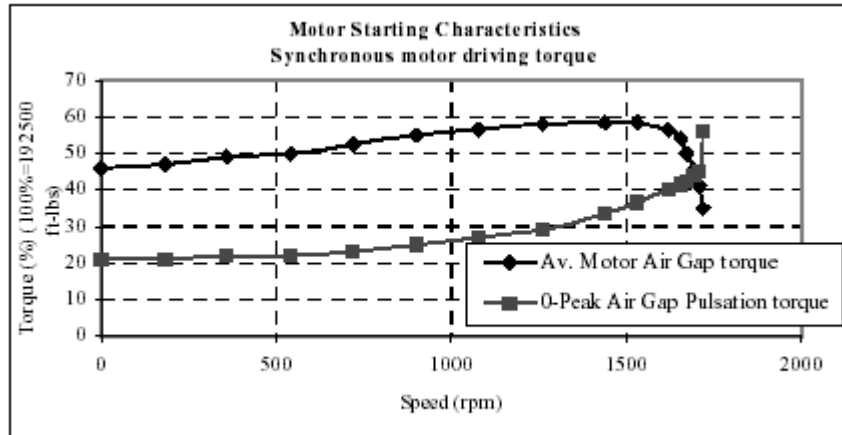


Fig. 33 Motor torque characteristic curve

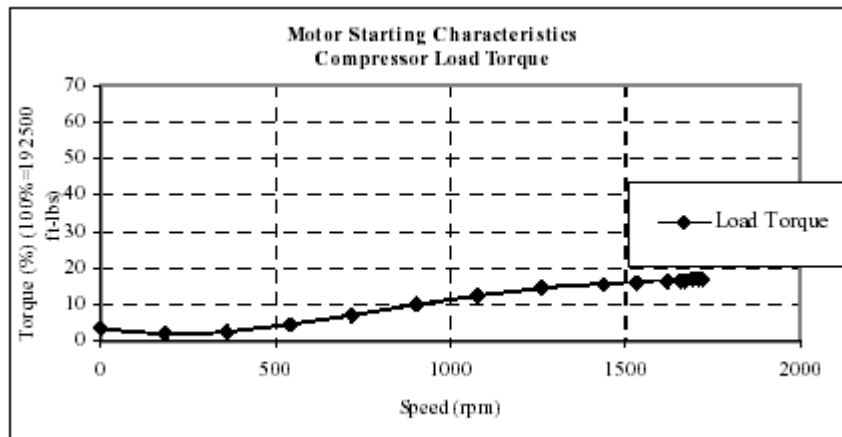


Fig. 34 Compressor (load) torque characteristic curve

Table 6 Transient analysis input data for the five inertia, Transfer Matrix model

Trans					
<i>Synchronous speed</i>	1800	rpm	<i>Output station</i>	<i>Titles to be placed on plots</i>	
<i>Line frequency</i>	60	Hz		1	
<i>Initial angular velocity</i>	0	rpm			
<i>No of modes for modal analysis</i>	3	inc. rigid body			
<i>Modal Damping ratio, zeta</i>	0.02	for all modes			
<i>No of torque sources</i>	2	-			
<i>Input torque options</i>	<i>Station number of torque input</i>	<i>Number of torque values</i>	<i>Speed ratio</i>	<i>full load torque</i>	<i>phase shift</i>
				<i>in-lb</i>	<i>deg</i>
1	1	16	1	2310000	0
3	5	16	1	-2310000	0
Add/delete to have as many rows as there are 'No. of torque sources'					
<---1. Synchronous motor drive torque (option 1)					
<--- 2. Compressor Load torque (option 3)					
<i>Speed</i>	<i>Average Drive/ Load torque</i>	<i>Pulsating torque</i>	<i>freq of motor pulsating torque</i>	<i>time</i>	<i>torque</i>
<i>rpm</i>	<i>% of FLT</i>	<i>% of FLT</i>	<i>Hz</i>	<i>sec</i>	<i>in-lb</i>
0	46.0	21.0			
180	47.0	21.0			
360	49.0	22.0			
540	50.0	22.0			
720	52.5	23.0			
900	55.0	25.0			
1080	56.5	27.0			
1260	58.0	29.0			
1440	58.5	33.5			
1530	58.5	36.5			
1620	56.5	40.0			
1656	54.0	41.5			
1674	50.0	42.5			
1692	45.5	44.0			
1710	41.0	45.0			
1721	35.0	56.0			
0	3.5				
180	2.1				
360	2.7				
540	4.6				
720	7.2				
900	10.0				
1080	12.5				
1260	14.5				
1440	15.5				
1530	16.0				
1620	16.5				
1656	16.5				
1674	16.5				
1692	17.0				
1710	17.0				
1721	17.0				

Table 7 Transient analysis input data for the seventy-four inertia, Transfer Matrix model

<i>Trans</i>					
<i>Synchronous speed</i>	1800	rpm	<i>Output station</i>	<i>Titles to be placed on plots</i>	
<i>Line frequency</i>	60	Hz	27		
<i>Initial angular velocity</i>	0	rpm			
<i>No of modes for modal analysis</i>	3	inc. rigid body			
<i>Modal Damping ratio, zeta</i>	0.02	for all modes			
<i>No of torque sources</i>	2	-			

<i>Input torque options</i>	<i>Station number of torque input</i>	<i>Number of torque values</i>	<i>Speed ratio</i>	<i>full load torque</i>	<i>phase shift</i>
				<i>in-lb</i>	<i>deg</i>
1	21	16	1	2310000	0
3	58	16	1	-2310000	0

Add/delete to have as many rows as there are ' No. of torque sources'
 <---1. Synchronous motor drive torque (option 1)
 <--- 2. Compressor Load torque (option 3)

<i>Speed</i>	<i>Average Drive/ Load torque</i>	<i>Pulsating torque</i>	<i>freq of motor pulsating torque</i>	<i>time</i>	<i>torque</i>
<i>rpm</i>	<i>% of FLT</i>	<i>% of FLT</i>	<i>Hz</i>	<i>sec</i>	<i>in-lb</i>
0	46.0	21.0			
180	47.0	21.0			
360	49.0	22.0			
540	50.0	22.0			
720	52.5	23.0			
900	55.0	25.0			
1080	56.5	27.0			
1260	58.0	29.0			
1440	58.5	33.5			
1530	58.5	36.5			
1620	56.5	40.0			
1656	54.0	41.5			
1674	50.0	42.5			
1692	45.5	44.0			
1710	41.0	45.0			
1721	35.0	56.0			
0	3.5				
180	2.1				
360	2.7				
540	4.6				
720	7.2				
900	10.0				
1080	12.5				
1260	14.5				
1440	15.5				
1530	16.0				
1620	16.5				
1656	16.5				
1674	16.5				
1692	17.0				
1710	17.0				
1721	17.0				

Table 8 Transient analysis input data for the five inertia, Finite Element model

TRANSIENT (START UP) ANALYSIS INPUT SHEET					
<i>Synchronous speed</i>	1800	rpm	<i>Output Element #</i>	<i>Titles to be placed on plot</i>	
<i>Line frequency</i>	60	Hz	1		
<i>Initial angular velocity</i>	0	rpm			
<i>No of modes for modal analysis</i>	3	inc. rigid body			
<i>Modal Damping ratio, zeta</i>	0.02	for all modes			
<i>No of Torque sources</i>	2				
<i>Input Torque options</i>	<i>Node number of torque input</i>	<i>Number of torque values</i>	<i>Speed ratio</i>	<i>full load torque in-lb</i>	<i>phase shift deg</i>
1	1	16	1	2310000	0
3	5	16	1	-2310000	0
<i>Speed rpm</i>	<i>Drive torque / Load torque % of FLT</i>	<i>Pulsating torque % of FLT</i>	<i>freq of motor pulsating torque Hz</i>	<i>time sec</i>	<i>torque in-lb</i>
0	46.0	21.0			
180	47.0	21.0			
360	49.0	22.0			
540	50.0	22.0			
720	52.5	23.0			
900	55.0	25.0			
1080	56.5	27.0			
1260	58.0	29.0			
1440	58.5	33.5			
1530	58.5	36.5			
1620	56.5	40.0			
1656	54.0	41.5			
1674	50.0	42.5			
1692	45.5	44.0			
1710	41.0	45.0			
1721	35.0	56.0			
0	3.5				
180	2.1				
360	2.7				
540	4.6				
720	7.2				
900	10.0				
1080	12.5				
1260	14.5				
1440	15.5				
1530	16.0				
1620	16.5				
1656	16.5				
1674	16.5				
1692	17.0				
1710	17.0				
1721	17.0				

Table 9 Transient analysis input data for the seventy-four inertia, Finite Element model

TRANSIENT (START UP) ANALYSIS INPUT SHEET					
<i>Synchronous speed</i>	1800	rpm	<i>Output Element #</i>	<i>Titles to be placed on plot</i>	
<i>Line frequency</i>	60	Hz	27	Motor Rotor	
<i>Initial angular velocity</i>	0	rpm			
<i>No of modes for modal analysis</i>	3	inc. rigid body			
<i>Modal Damping ratio, zeta</i>	0.02	for all modes			
<i>No of Torque sources</i>	2				
<i>Input Torque options</i>	<i>Node number of torque input</i>	<i>Number of torque values</i>	<i>Speed ratio</i>	<i>full load torque in-lb</i>	<i>phase shift deg</i>
1	21	16	1	2310000	0
3	58	16	1	-2310000	0
<i>Speed rpm</i>	<i>Drive torque / Load torque % of FLT</i>	<i>Pulsating torque % of FLT</i>	<i>freq of motor pulsating torque Hz</i>	<i>time sec</i>	<i>torque in-lb</i>
0	46.0	21.0			
180	47.0	21.0			
360	49.0	22.0			
540	50.0	22.0			
720	52.5	23.0			
900	55.0	25.0			
1080	56.5	27.0			
1260	58.0	29.0			
1440	58.5	33.5			
1530	58.5	36.5			
1620	56.5	40.0			
1656	54.0	41.5			
1674	50.0	42.5			
1692	45.5	44.0			
1710	41.0	45.0			
1721	35.0	56.0			
0	3.5				
180	2.1				
360	2.7				
540	4.6				
720	7.2				
900	10.0				
1080	12.5				
1260	14.5				
1440	15.5				
1530	16.0				
1620	16.5				
1656	16.5				
1674	16.5				
1692	17.0				
1710	17.0				
1721	17.0				

Note that the number of modal coordinates for transient analysis on all the four modal models was kept equal to three (inclusive of the rigid-body mode) to be able to compare the results with Corbo et al. [16]. The authors of [16] claim that the third natural frequency seldom takes part in synchronous motor responses, especially when its resonance point is at a very low speed. Hence, they have used two modes (three, if the rigid-body mode is also counted) for performing transient analysis on their simplified model with five inertias. Per [16], focusing the transient analysis for simulating the transient responses at the first two modes, while giving prime consideration to the fundamental mode, would be beneficial since they occur at much higher speeds during startup.

(a) Run-up analysis results

A preliminary run-up analysis performed on all the four models indicated that the synchronous speed of the motor would be reached around 27 seconds. This compares very well with the experimental results that discovered synchronous speed of 1800 RPM was reached around 28 seconds. Table 10 shows comparative evaluation of the calculated and measured run-up times.

Table 10 Comparison of estimated and actual run-up times

No.	Configuration	Run-up time (seconds)
1	Five inertia model, Transfer Matrix method	26.95
2	Seventy-four inertia model, Transfer Matrix method	26.89
3	Five inertia model, Finite Element method	27.74
4	Seventy-four inertia model, Finite Element method	26.86
5	Corbo et al. [15] (to 98% synchronous speed)	25.00
6	<i>Actual (measured)</i>	<i>28.00</i>

Figures 35 to 38 show the run-up curves for all the four models calculated using *XLTRC-Torsion*, while Fig. 39 shows the run-up curve plotted using data from experiments.

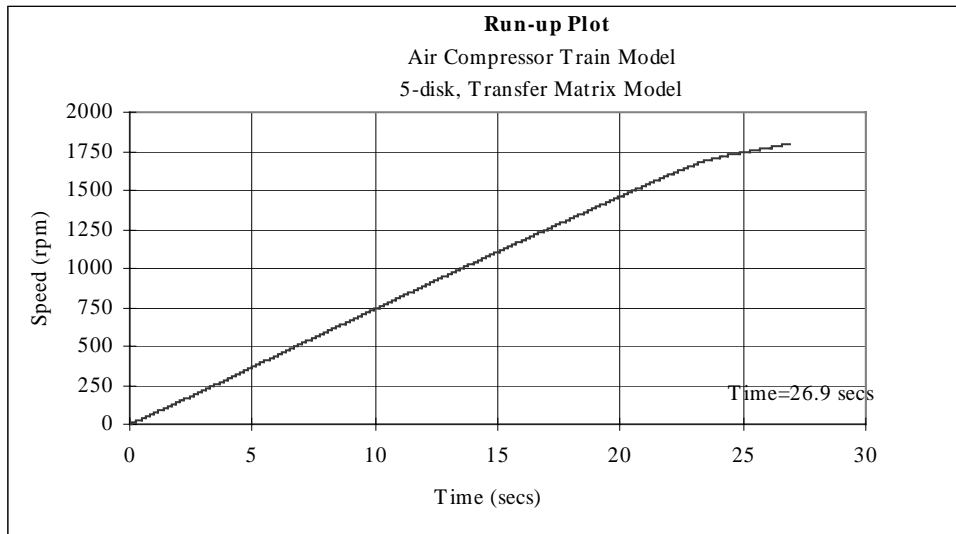


Fig. 35 Run-up curve for the five inertia, Transfer Matrix model

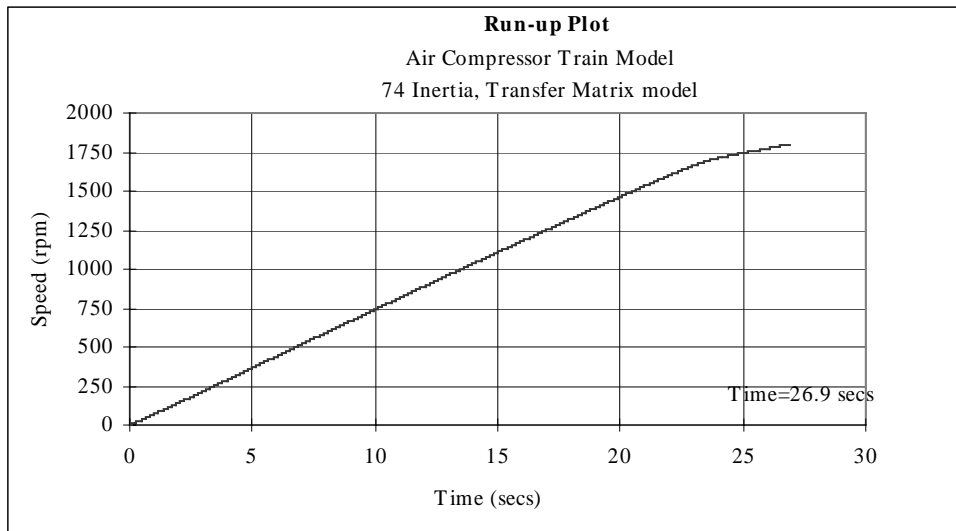


Fig. 36 Run-up curve for the seventy-four inertia, Transfer Matrix model

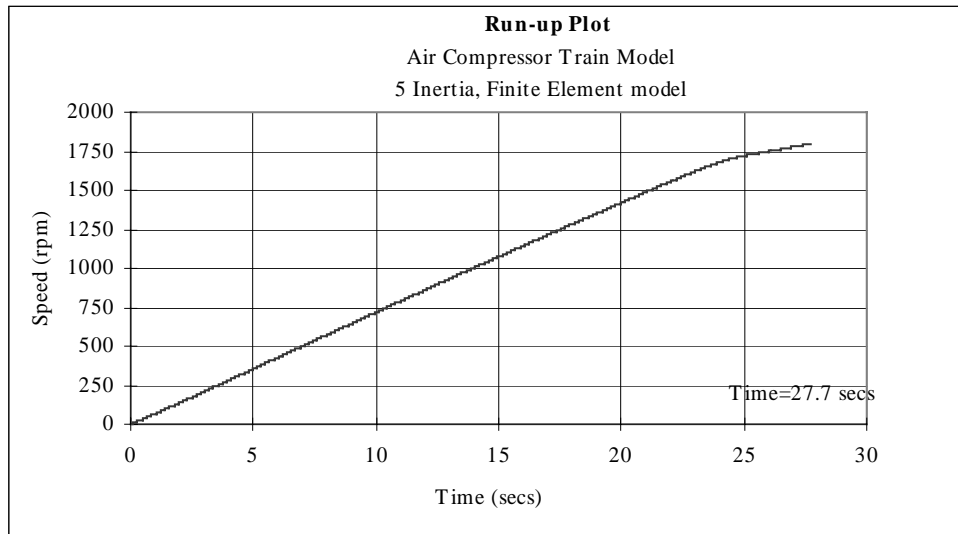


Fig. 37 Run-up curve for the five inertia, Finite Element model

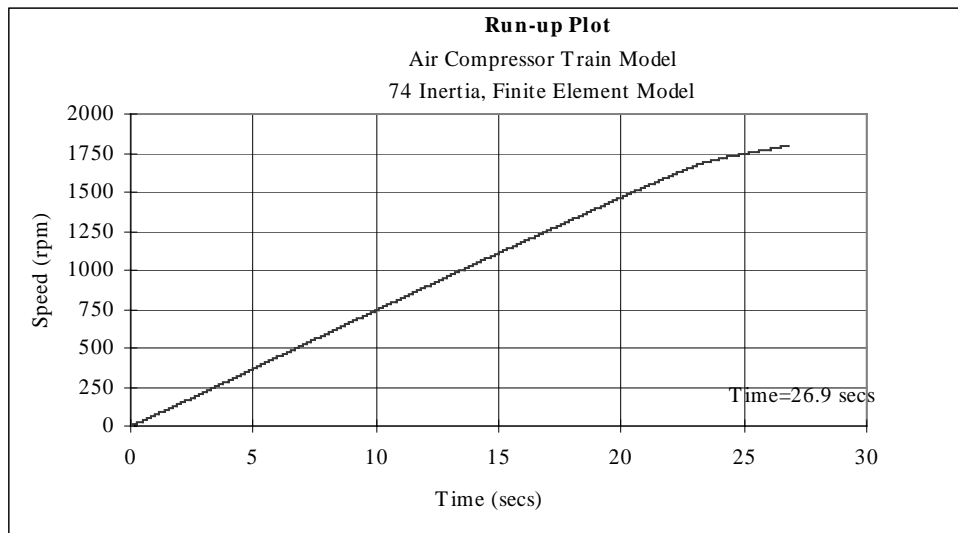


Fig. 38 Run-up curve for the seventy-four inertia, Finite Element model

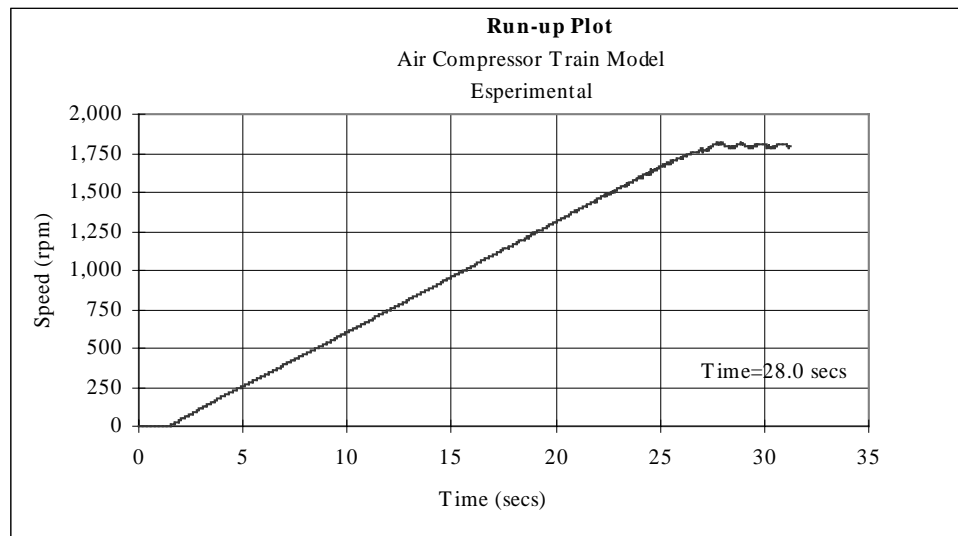


Fig. 39 Run-up curve plotted using data from experiments

(b) Transient torque analysis results

The graphs on the following pages show the results for the transient torque analysis on all the four models, besides showing the torque-time graph plotted using data from experiments. This treatise only incorporates results for the transient analysis on the motor rotor, as comparison data was available only for the motor rotor.

In the torque-time graph (Fig. 40) for the motor rotor (Station no. 1) of the five inertia, Transfer Matrix model, a significant response was observed at 21.9 s, when the motor speed reaches 1593 RPM (obtained from the run-up graph in Fig. 35) as expected. This correlates well with the intersection of the calculated first torsional natural frequency (13.74 Hz) line with the constantly dropping 2X slip frequency line on the Campbell diagram (Fig. 23). Maximum torque fluctuation on the graph was also seen

around this region with maximum and minimum torque values reaching $9.72\text{E}+06$ in·lb and $-7.75\text{E}+06$ in·lb respectively. Notable response was also seen at 17.64 s that corresponds to a motor speed of around 1290 RPM, which is the same as the predicted resonant speed to the second torsional natural frequency of 33.94 Hz. Though not very easy to demarcate, the region around 1 s (78 RPM) also shows an imperious response that corresponds with the resonant speed to the fourth torsional natural frequency of 114.73 Hz.

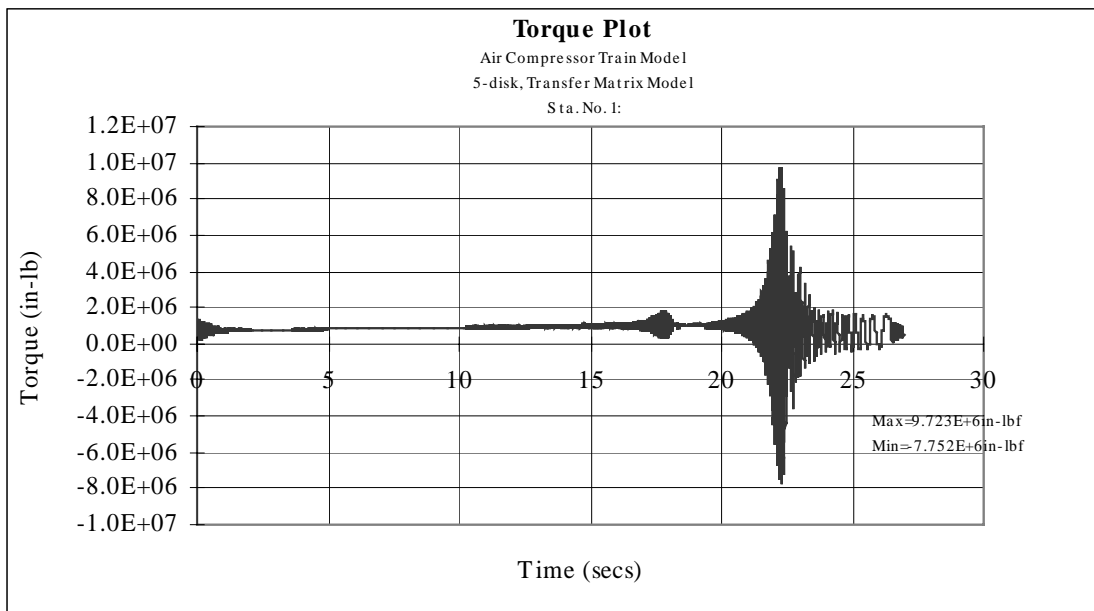


Fig. 40 Transient Torque plot for 5 inertia, Transfer Matrix model at Station No. 1 (Motor Rotor)

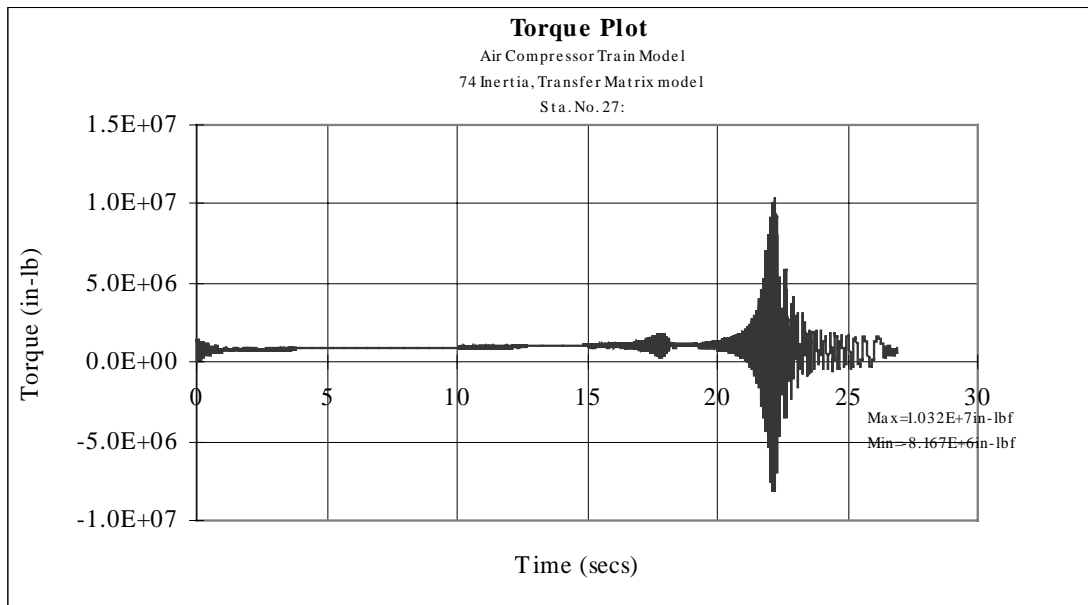


Fig. 41 Transient Torque plot for 74 inertia, Transfer Matrix model at Station No. 27 (Motor Rotor)

The torque-time graph (Fig. 41) for the motor rotor (Station no. 27) of the seventy-four inertia, Transfer Matrix model showed a significant response at 21.88 s (1590 RPM). This corresponds with the resonant speed to the first torsional eigenvalue of 13.97 Hz, thus showing good correlation with earlier predictions. Besides, this region showed the maximum fluctuation of torque values on the graph with maximum and minimum torque values of $1.03\text{E}+07$ in-lb and $-8.17\text{E}+06$ in-lb respectively. It was also easy to notice the conspicuous response at a motor speed of around 1294 RPM (17.64 s), which is also the predicted resonant speed to the second torsional natural frequency of 33.68 Hz. The region around 1.7 s (121 RPM) shows noticeable response that

corresponds with the resonant speed to the third torsional natural frequency of 111.87 Hz.

A significant response at 22.6 s (1593 RPM) was observed on the transient torque plot (Fig. 42) for the motor rotor (Node no. 1) of the five inertia, Finite Element model, which has a calculated first undamped torsional eigenvalue of 13.74 Hz. This region showed the maximum fluctuation of torque on the graph with a maximum torque of $9.44\text{E}+06$ in·lb and a minimum torque of $-7.47\text{E}+06$ in·lb. One can also notice the response at a motor speed of 1290 RPM (18.1 s), which is also the resonant speed to the second torsional natural frequency of 33.95 Hz, as predicted. The region around 1.2 s (79 RPM) also showed noticeable response that corresponds with the resonant speed to the fourth torsional natural frequency of 114.74 Hz.

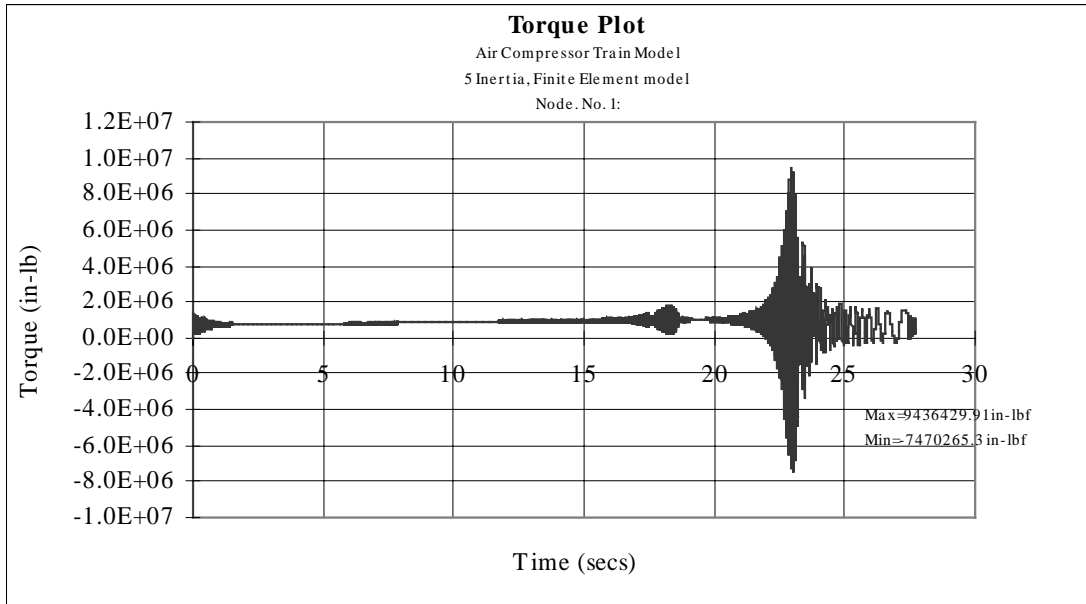


Fig. 42 Transient Torque plot for 5 inertia, Finite Element model at Node No. 1 (Motor Rotor)

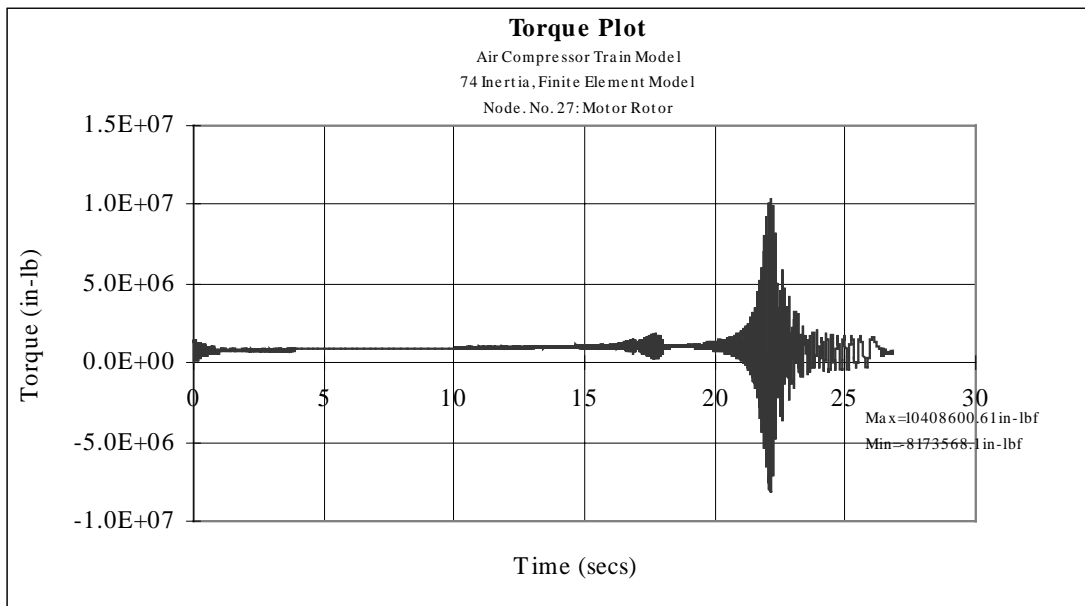


Fig. 43 Transient Torque plot for 74 inertia, Finite Element model at Node No. 27 (Motor Rotor)

The transient torque graph (Fig. 43) for the motor rotor (Node no. 27) of the seventy-four inertia, Finite Element model showed a significant response at 21.8 s, when the motor speed reaches 1590 RPM. This speed compares well with the resonant speed to the first torsional mode at 13.98 Hz. Maximum torque fluctuation on the graph was also seen in this region with a maximum torque of $1.04\text{E}+07$ in-lb and a minimum torque of $-8.17\text{E}+06$ in-lb. Significant response was also seen at the motor speed of 1293 RPM (at 17.6 s), which is also the resonant speed to the second torsional natural frequency of 33.78 Hz. The region around 1.7 s (118 RPM) shows notable response that closely corresponds to the resonant speed to the third torsional natural frequency of 111.94 Hz.

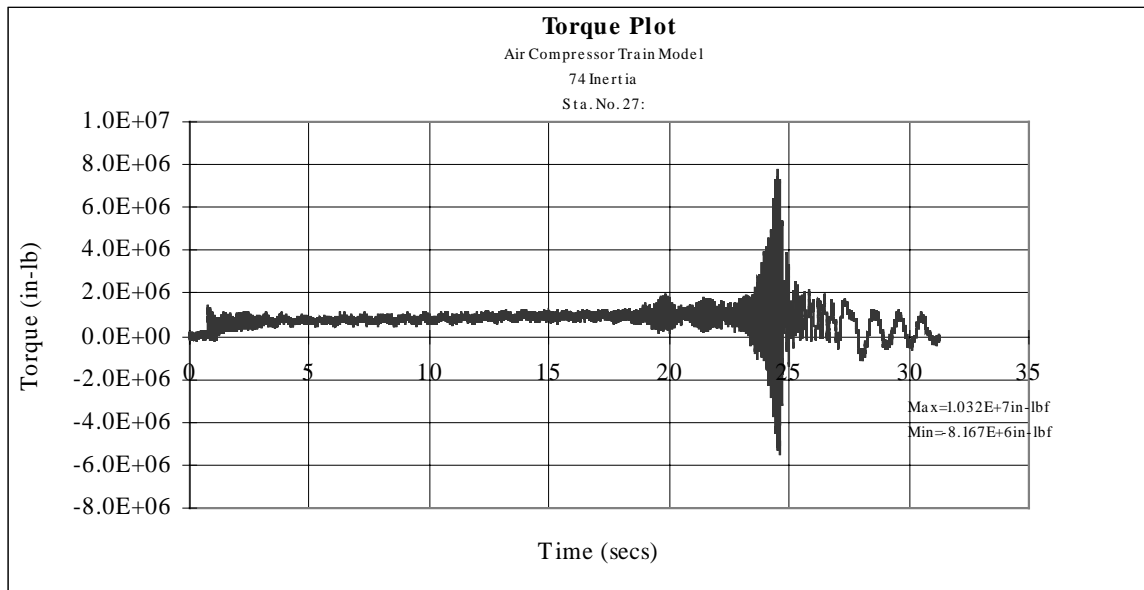


Fig. 44 Transient Torque plot for the 66,000 HP Air Compressor plotted using data from experiments

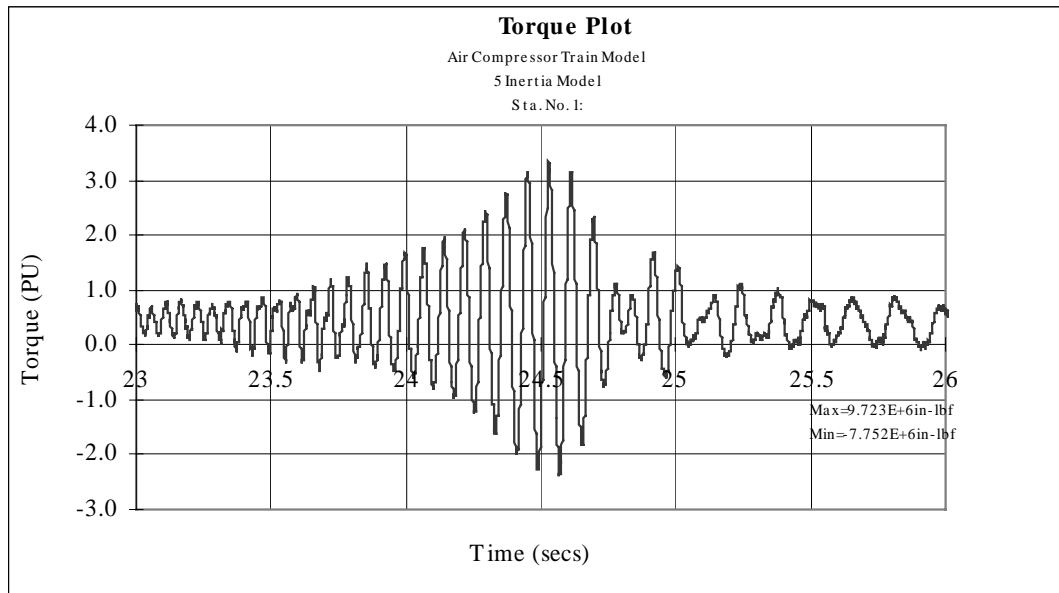


Fig. 45 A closer view of the Transient Torque plot for the 66,000 HP Air Compressor at resonant speed to the first torsional natural frequency plotted using data from experiments

Results for the transient torsional analysis could then be readily compared with the experimental results in Figures 44 and 45. The transient torque graph plotted using data from experiments showed a significant response at 23.3 s, when the motor speed reached 1635 RPM. Maximum torque fluctuation seen in this region lay between the maximum and minimum values of $7.72E+06$ in-lb and $-5.51E+06$ in-lb respectively. This region of high fluctuation occurred about 1.6 s later than that predicted by all the models, besides having lower values of the torque levels reached. Significant response was also seen at the motor speed of 1250 RPM (at 18.5 s), which is also the resonant

speed to the second torsional natural frequency of 37.00 Hz. The region around 1.7 s (118 RPM) showed notable response that closely corresponded with the resonant speed to the third torsional natural frequency of 111.94 Hz. Corbo et al. [16] predicted the resonant speed to the first torsional natural frequency to be occurring around 21.7 s (Fig. 50) at 1608 rpm, with maximum torque fluctuation between the approximate values of $1.11\text{E}+07$ in·lb and $-8.44\text{E}+06$ in·lb. They predicted the second mode resonant speed at 1256 rpm (17.2 s).

A better picture of conformance of the models can be had from the Figures 46 to 49, which “zoom in” on the response torque in the regions of highest torque fluctuation, which can be said to occur around the time when the motor speed coincides with the resonant speed. Since the torque results in Corbo et al. [16] as shown in Fig. 50 are provided in terms of “PU” (Per Unit, taking $1 \text{ PU} = 2.31\text{E}+06$ in·lb), other graphs were set so as to coalesce with those. It may be seen that, overall, the shapes of the predicted and actual torque curves look remarkably similar. Table 11 gives a summary of the transient torsional analysis results.

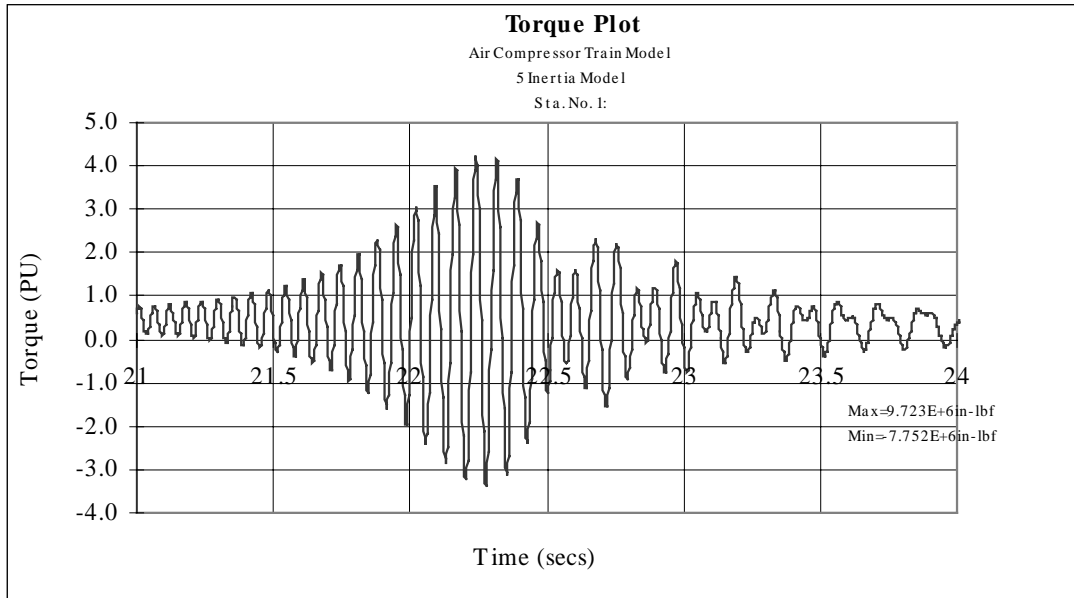


Fig. 46 A closer view of the Transient Torque plot for the 66,000 HP Air Compressor at resonant speed to the first torsional natural frequency predicted by the five inertia, Transfer Matrix model

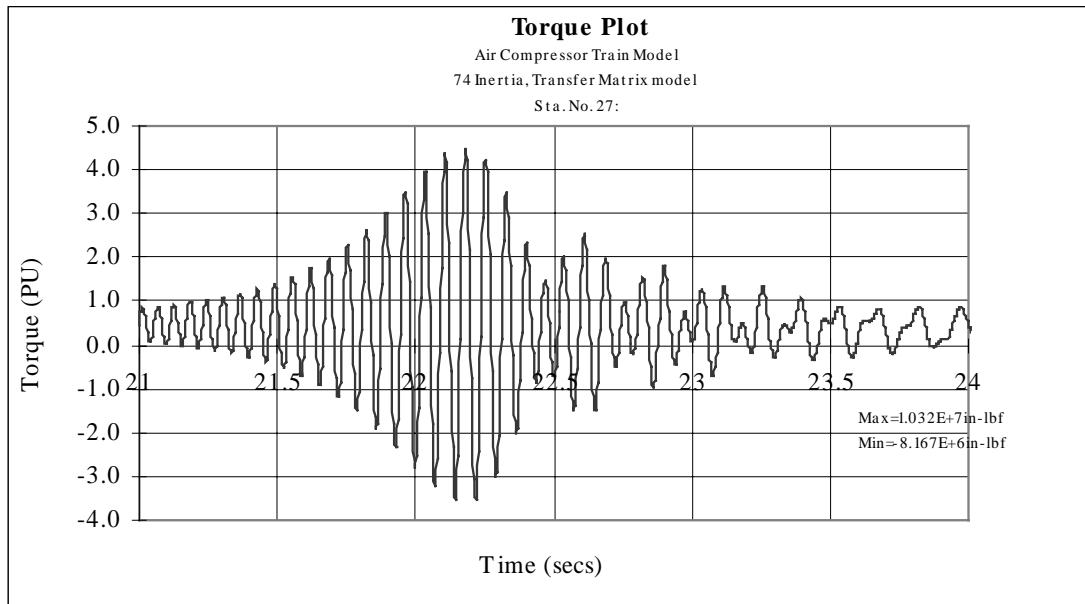


Fig. 47 A closer view of the Transient Torque plot for the 66,000 HP Air Compressor at resonant speed to the first torsional natural frequency predicted by the seventy-four inertia, Transfer Matrix model

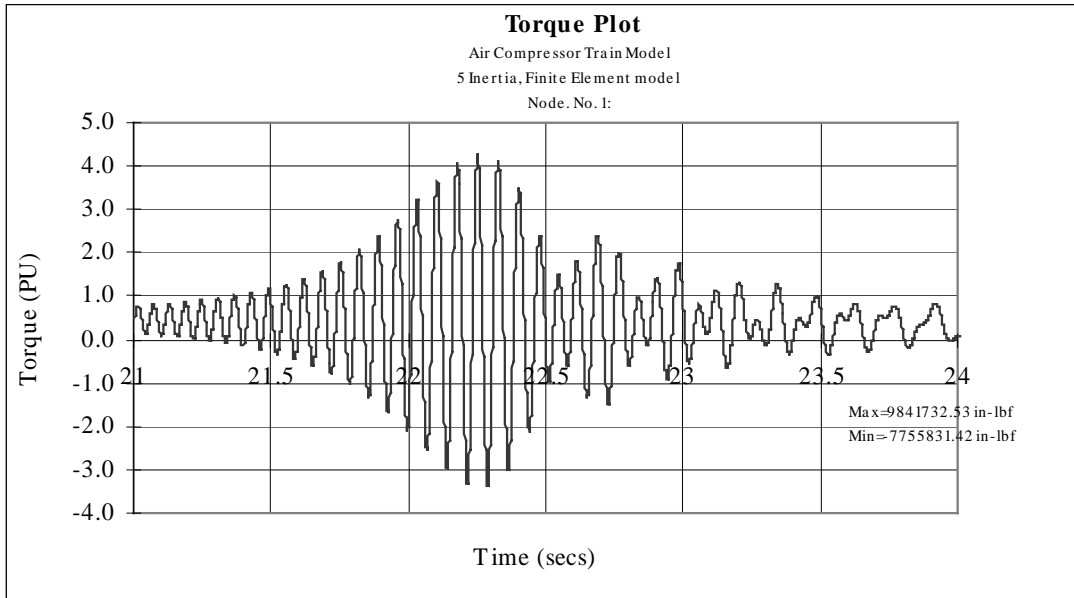


Fig. 48 A closer view of the Transient Torque plot for the 66,000 HP Air Compressor at resonant speed to the first torsional natural frequency predicted by the five inertia, Finite Element model

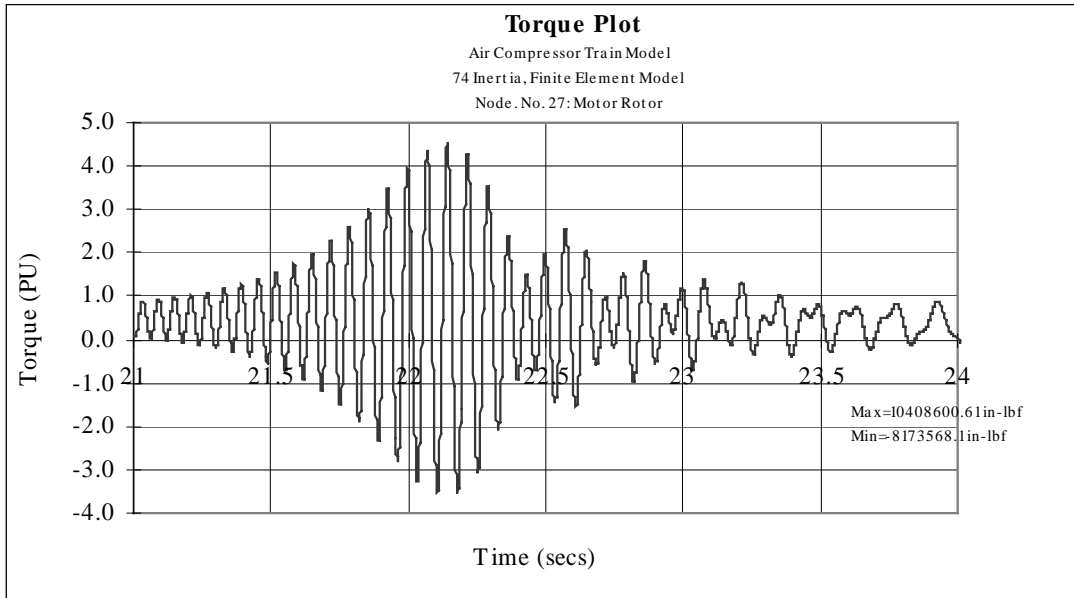


Fig. 49 A closer view of the Transient Torque plot for the 66,000 HP Air Compressor at resonant speed to the first torsional natural frequency predicted by the seventy-four inertia, Finite Element model

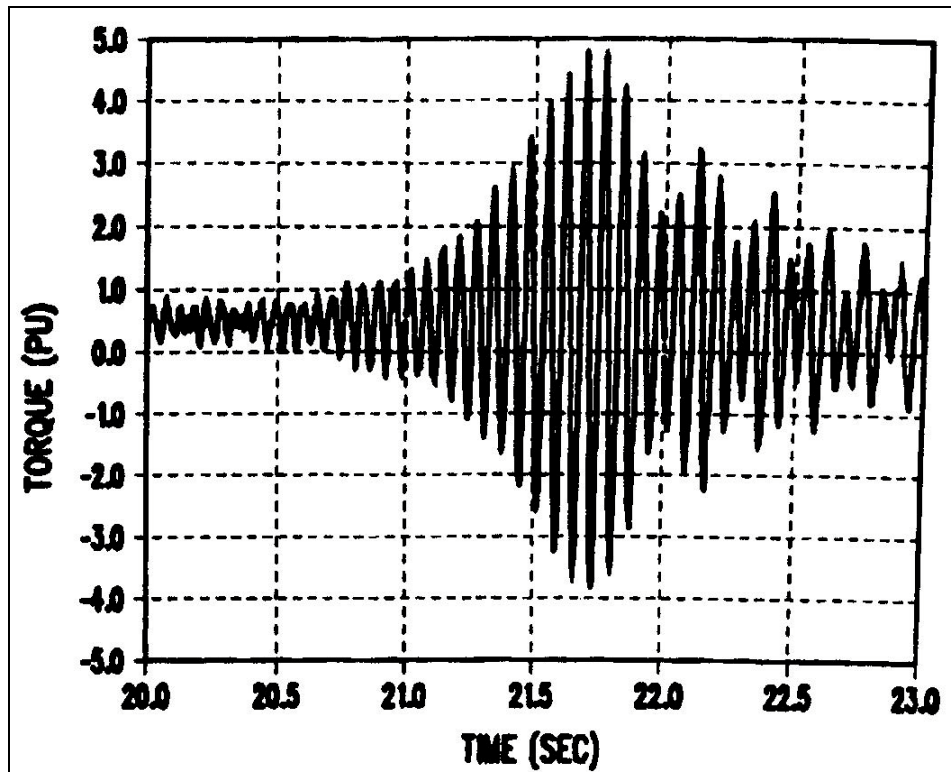


Fig. 50 A closer view of the Transient Torque plot for the 66,000 HP Air Compressor at resonant speed to the first torsional natural frequency predicted by Corbo et al. [16]

Table 11 Summary of results for the transient torque analyses

Criteria	5 Inertia TM	74 Inertia TM	5 Inertia FE	74 Inertia FE	Actual (Meas.)	Corbo et al. [15]
Max. Torque (in·lb)	9.72E+06	1.03E+07	9.44E+07	1.04E+07	7.72E+06	1.11E+07
Min. Torque (in·lb)	-7.75E+06	-8.17E+06	-7.47E+06	-8.17E+06	-5.51E+06	-8.44E+06
Resonant Speed to Mode I (RPM)	1593	1590	1593	1590	1635	1608
Time to reach Resonant Speed to Mode I (s)	21.90	21.88	22.60	21.80	23.30	21.70
Resonant Speed to Mode II (RPM)	1290	1294	1290	1293	1250	1256
Time to reach Resonant Speed to Mode II (s)	17.64	17.64	18.10	17.60	18.50	17.20

Cumulative Fatigue Analysis

As discussed earlier, cumulative fatigue damage analysis can be used to predict the number of starts a machine will survive. This is important especially in case of machines driven by synchronous motors, which are ample sources of contrite excitation. Cumulative fatigue analysis was performed on all the four models for the 66,000 HP air compressor as well as on the actual results from experiments at weak links in the system. The analysis was performed using the strain-life approach, since it is not overly conservative as compared to traditional methods, besides being concomitantly safe according to Corbo et al. [15].

Corbo et al. [16] had used the torque values that they had obtained from the transient analysis of the five inertia model to a station with a diameter of 13.17” that figured on their seventy-four inertia model. Their choice of this diameter was based on the fact that it was the “weak link” in the drive train based on geometry and stress concentration. While one may calculate torque values at a station using a simplified equivalent model, it is necessary to perform fatigue analysis using the “actual” diameter of the shaft. If simplification of the detailed model was accurate, one would obtain similar torque values at the “weak link” had the transient analysis been performed using the more detailed model. Since the motor rotor has an equivalent diameter of 21.069” in the five inertia model, this treatise also presents results for fatigue analysis using that diameter to confirm that using an equivalent diameter in place of an actual diameter in such cases may yield incorrect results of predicted life. As expected, the predicted

number of startups using the equivalent diameter of 21.069” looked dubiously high. Fatigue analysis was then performed using the actual diameter of 13.17” and values of design factors used by Corbo et al. [16] for direct comparison of results.

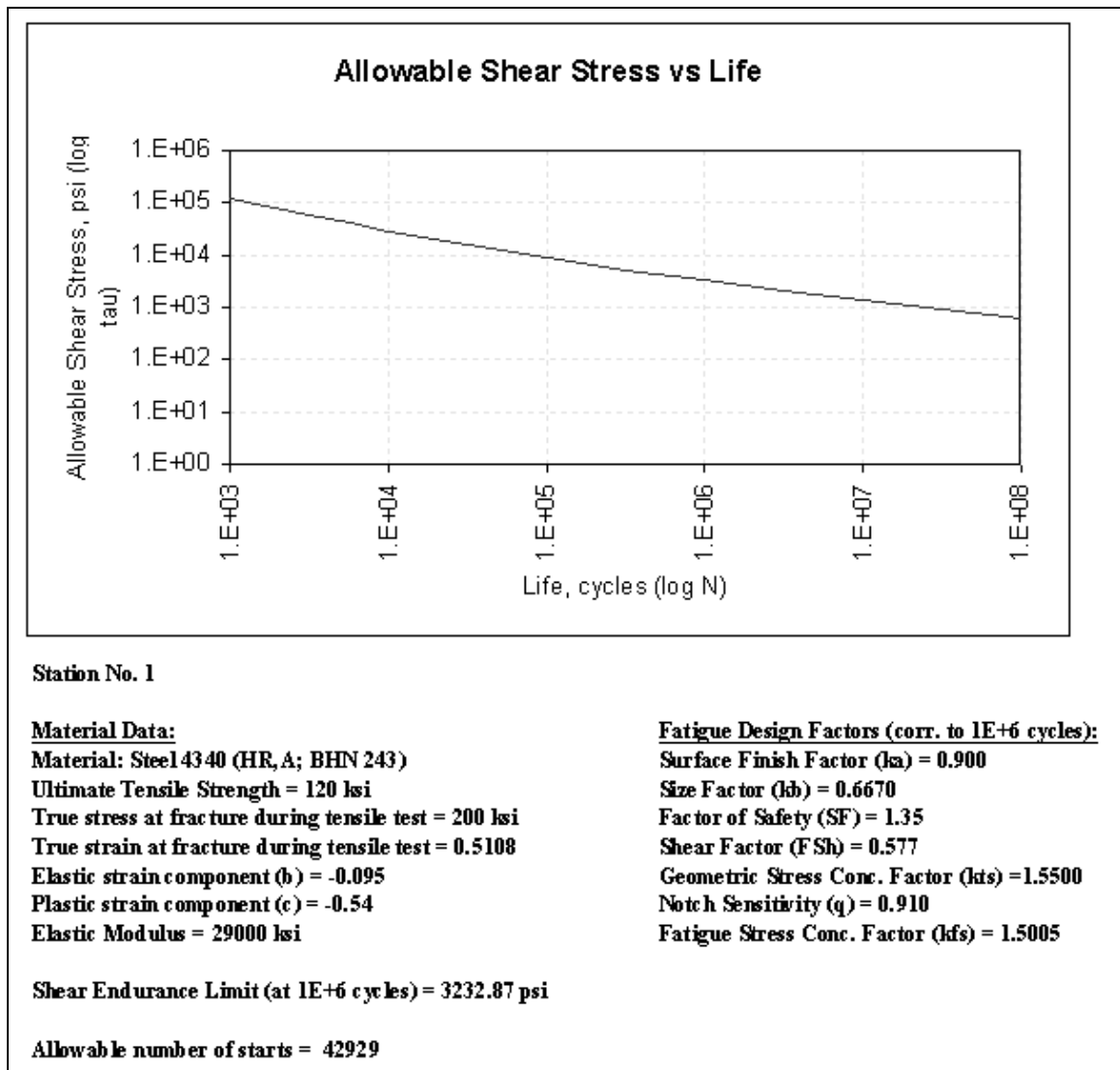


Fig. 51 Fatigue analysis results for 5 inertia, Transfer Matrix model at station No. 1 (motor rotor) with diameter = 21.069”

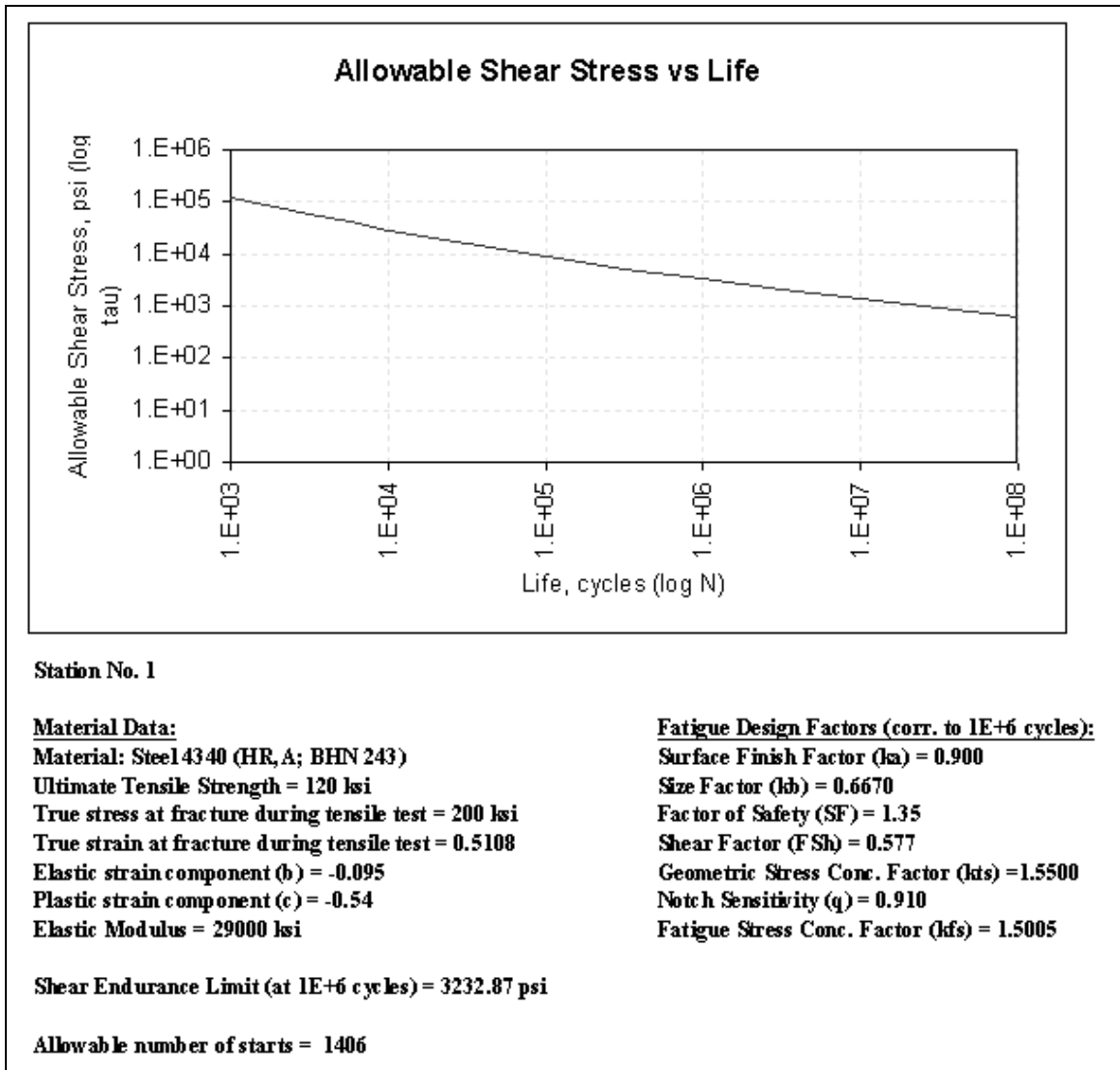


Fig. 52 Fatigue analysis results for 5 inertia, Transfer Matrix model at station No. 1 (motor rotor) with diameter = 13.17"

Figures 51 and 52 show the results of the fatigue analysis performed on the five inertia, Transfer Matrix model using diameters of 21.069” and 13.17” respectively for the motor rotor using results of the transient torque analysis. In order to harmonize the results with Corbo et al. [16], following data were used for performing fatigue analysis:

Shaft Material: Steel 4340 (Hot Rolled and Annealed, BHN 243)

(a) *Ultimate tensile strength* = 120 ksi

(b) *Modulus of elasticity* = 29000 ksi

(c) *True stress at fracture during tensile test* = 200 ksi

(d) *True strain at fracture during tensile test* = 0.5108

(e) *Elastic strain component “b”* = -0.095

(f) *Plastic strain component “c”* = -0.54

Surface finish factor (ka) = 0.9

Size factor (kb) = 0.667

Factor of safety (SF) = 1.35

Shear factor (Fsh) = 0.577

Geometric stress concentration factor (kts) = 1.55

Notch sensitivity (q) = 0.91

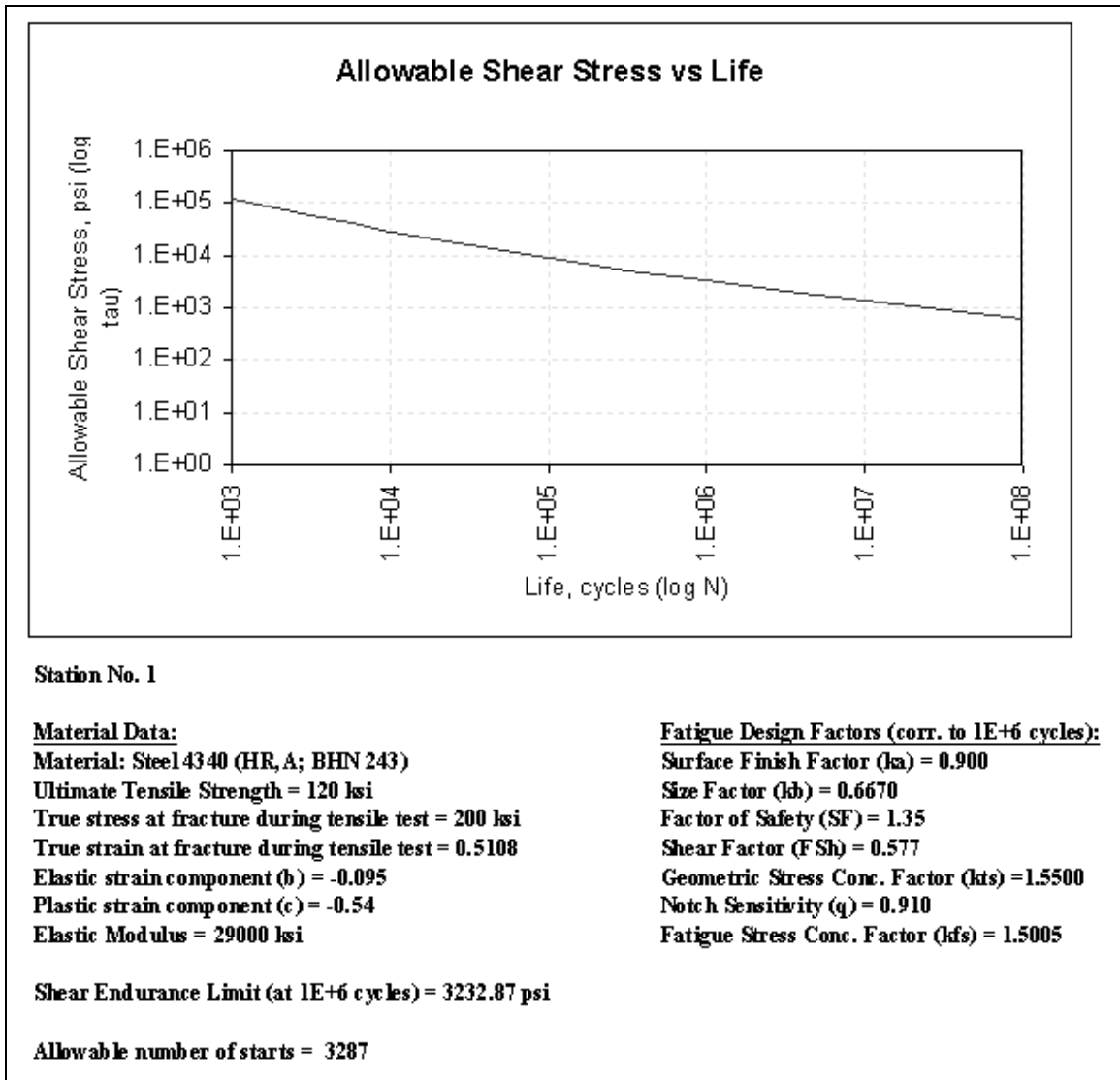


Fig. 53 Fatigue analysis results for experimental transients applied on 5 inertia, Transfer Matrix model at station No. 1 (motor rotor) with diameter = 13.17”

Fatigue analysis was also performed on the five inertia, Transfer Matrix model by using the transient torque data from experiments to station no. 1 with the modified diameter of 13.17". Results for the same are available in Fig. 53.

Results for the fatigue analysis performed at station no. 27 (diameter = 13.17") of the seventy four inertia, Transfer Matrix model using calculated transient torque data are illustrated in Fig. 54. As with the case of the five inertia, Transfer Matrix model, measured transient torques were also applied to station no. 27 and fatigue analysis was performed. Results for the same can be discerned from Fig. 55.

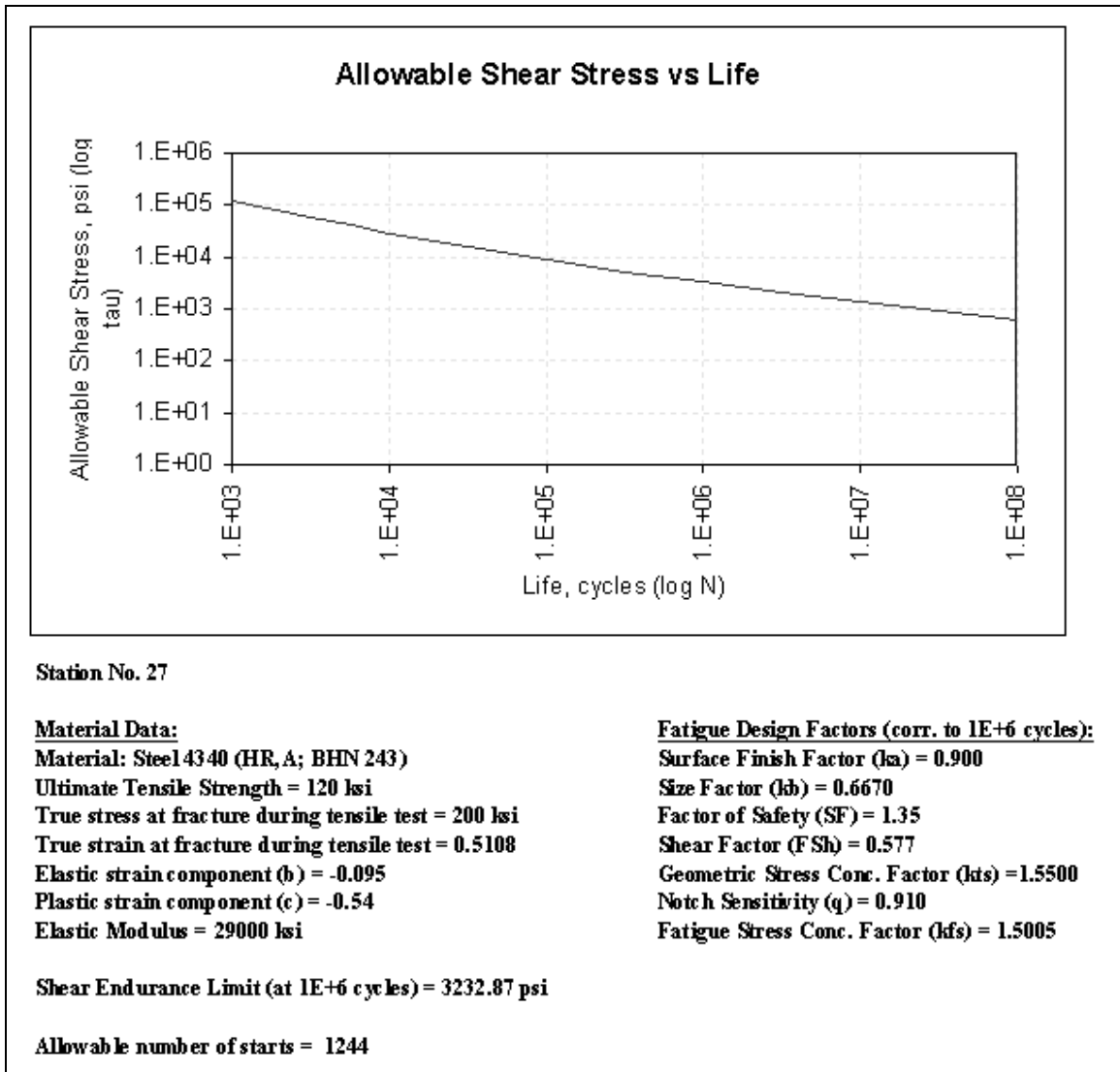


Fig. 54 Fatigue analysis results for 74 inertia, Transfer Matrix model at station No. 27 (motor rotor) with diameter = 13.17"

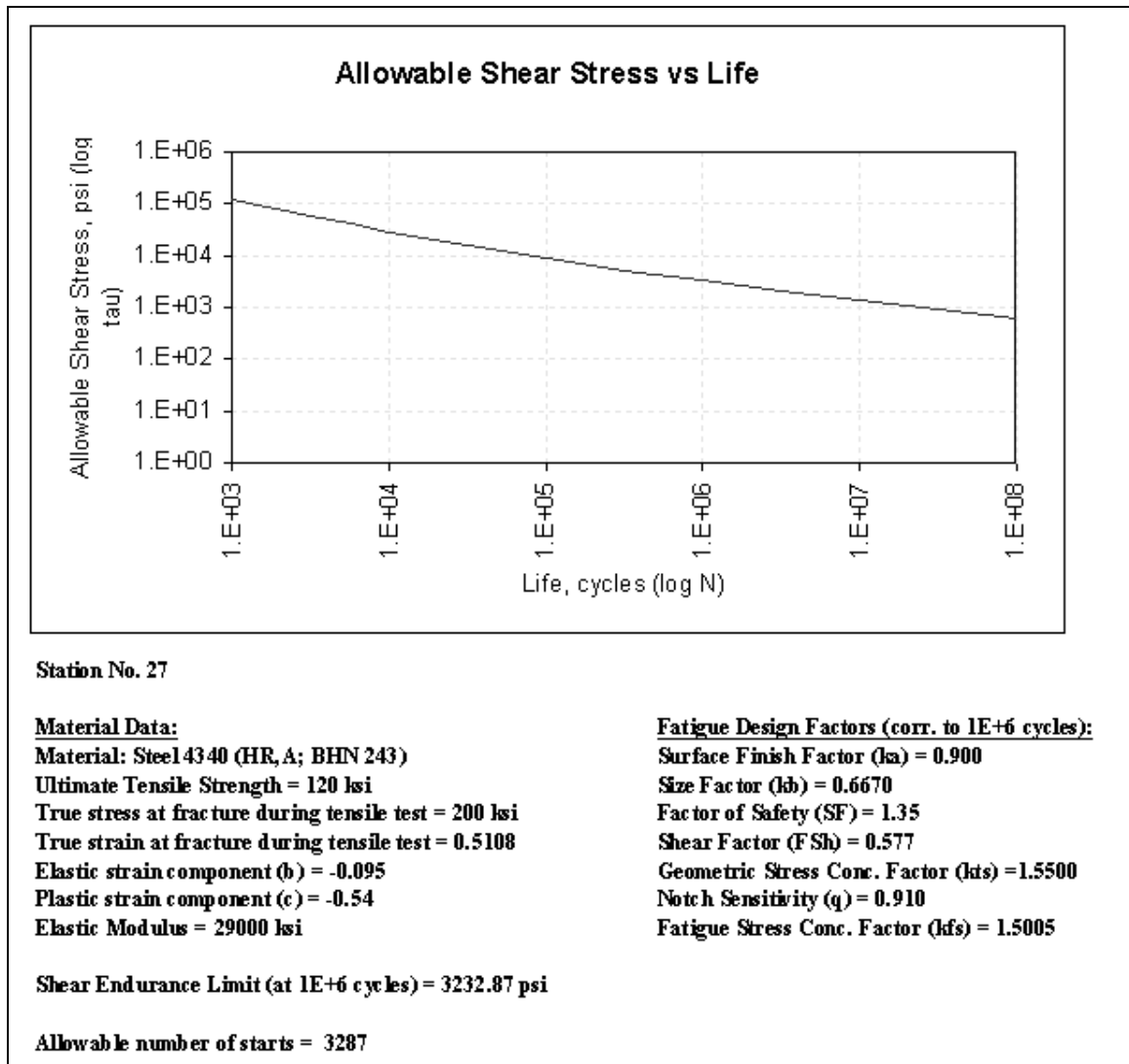


Fig. 55 Fatigue analysis results for experimental transients applied on 74 inertia, Transfer Matrix model at station No. 27 (motor rotor) with diameter = 13.17”

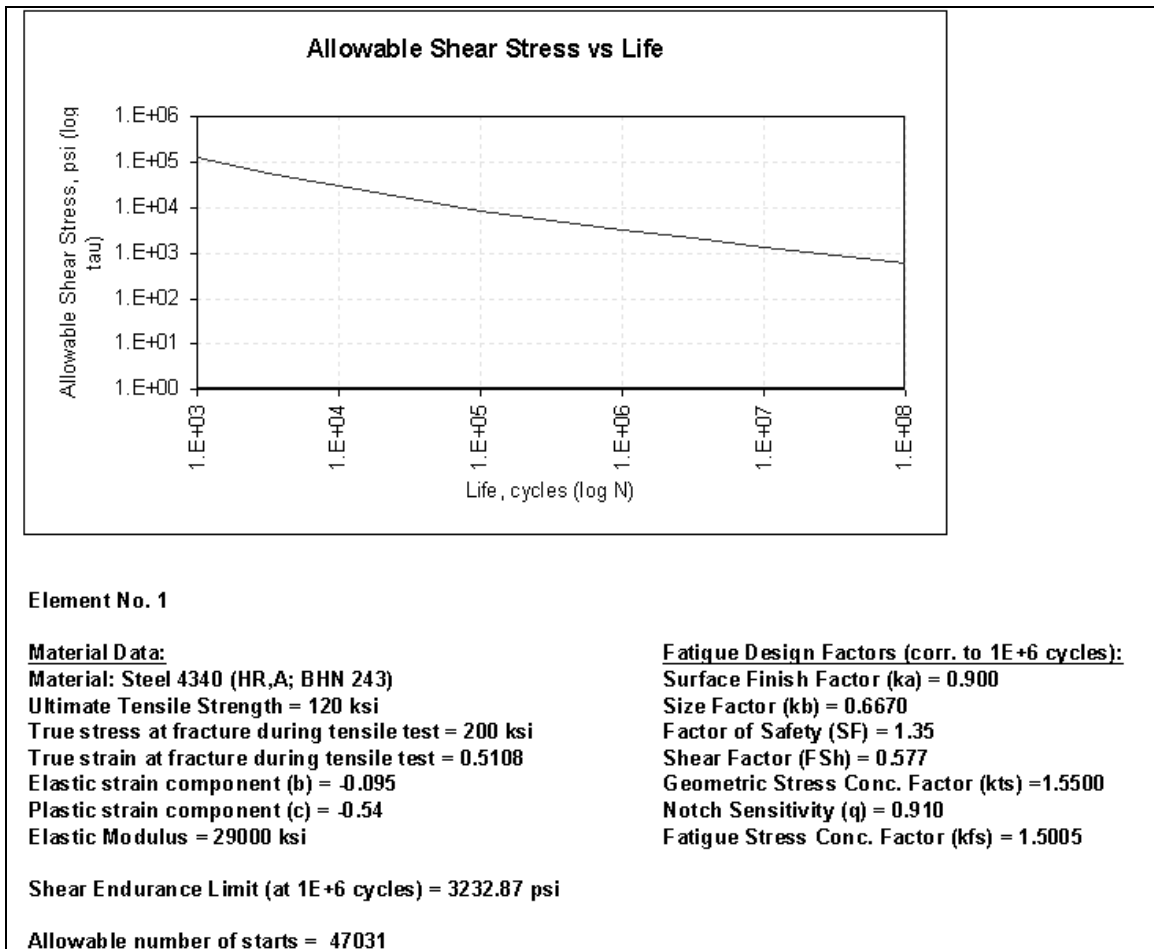


Fig. 56 Fatigue analysis results for 5 inertia, Finite Element model at element No. 1 (motor rotor) with diameter = 21.069”

Similar to the Transfer Matrix case, fatigue analysis was performed at element no. 1 of the five inertia model in the Finite Element module, using both diameters of 21.069” and 13.17”. Calculated torque data obtained via transient torque analysis was used for predicting the number of machine startups using both the diameters. Corresponding results are available in Figures 56 and 57.

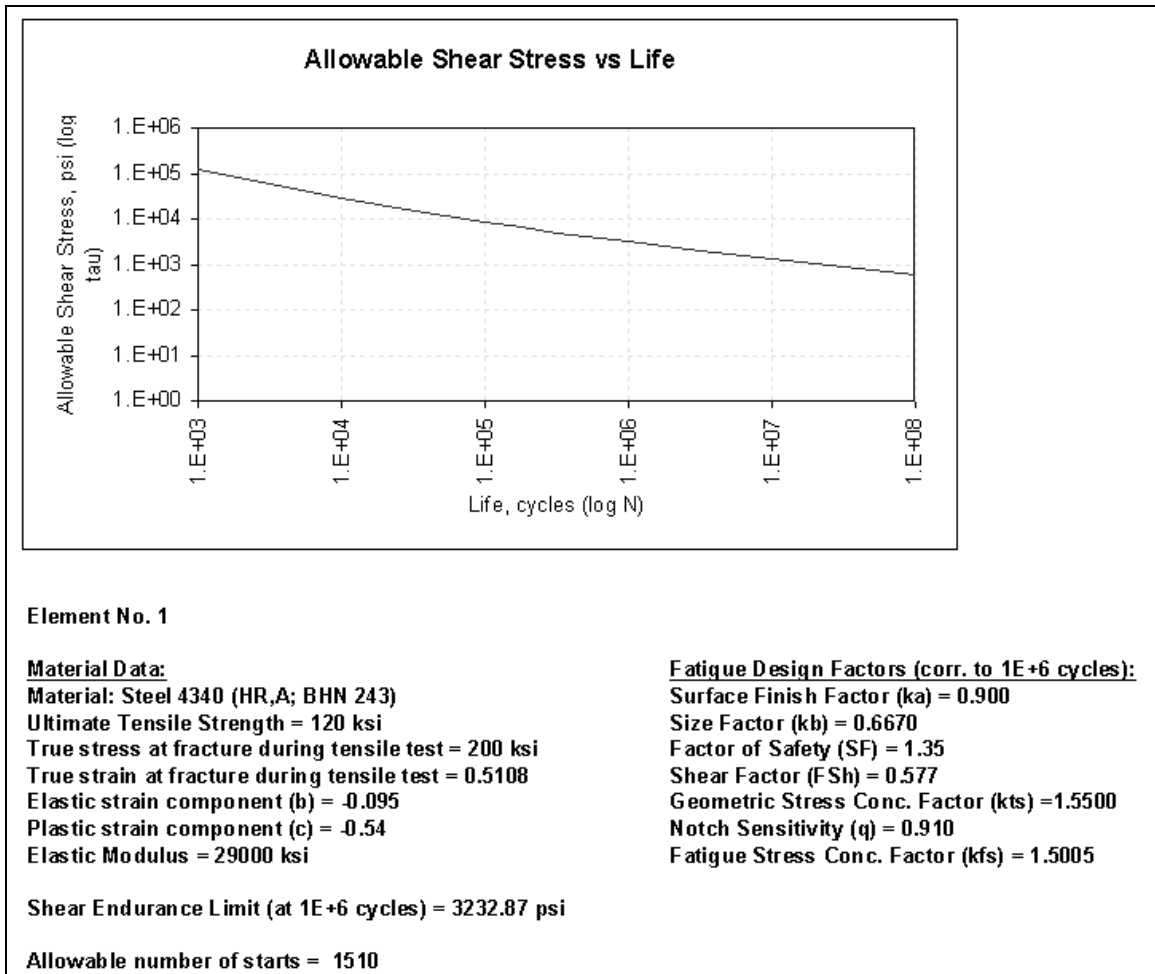


Fig. 57 Fatigue analysis results for 5 inertia, Finite Element model at element No. 1 (motor rotor) with diameter = 13.17"

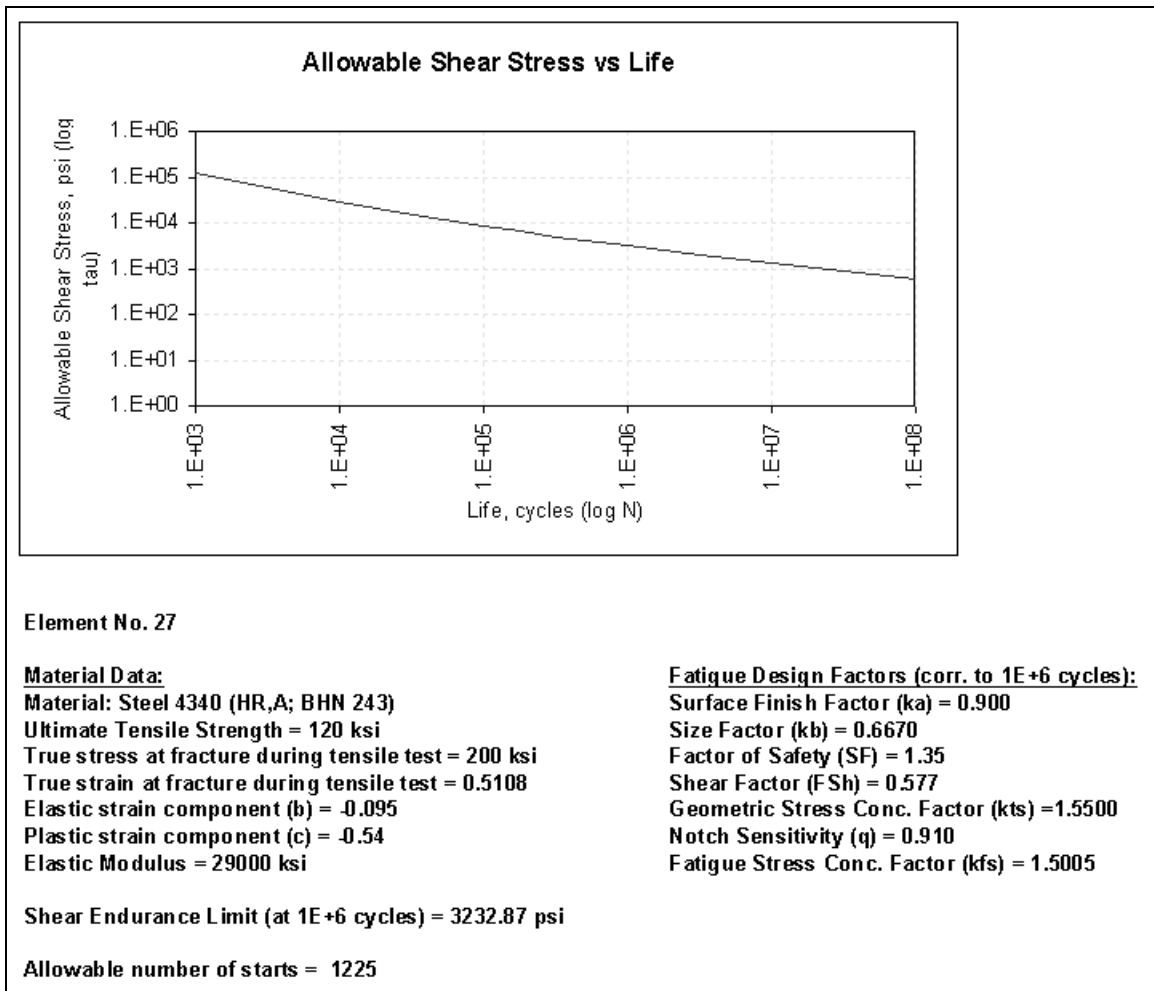


Fig. 58 Fatigue analysis results for 74 inertia, Finite Element model at element No. 27 (motor rotor) with diameter = 13.17”

Figure 58 shows results obtained after using the seventy-four inertia, Finite Element model for predicting the number of startups. The torque data obtained from transient analysis was applied at element no. 1 using a diameter of 13.17” for consistency with Corbo et al. [16].

It is important to note that both the Transfer Matrix and Finite Element models with equal number of inertias are dimensionally equivalent. Hence, prediction of life of both the Finite Element models using test data would have been redundant since the same code had been used for predicting the number of startups on all the models. Table 12 shows a summary of the results for the transient torque and fatigue analyses. The value of the shear endurance limit, which is the allowable shear stress corresponding to $N= 1.0E+06$ cycles, for all the four models was found to be 3232.87 lb/in^2 , whereas Corbo et al. [15] estimate it to around 11194 lb/in^2 .

Table 12 Comparison of predicted lives calculated using fatigue analysis

No.	Model used	Torque Values Used	Station/ Element No.	Dia. of Station/ Element	Predicted No. of Startups
1	5 Inertia, TM	Calculated	1	21.069"	42,929
2	5 Inertia, TM	Calculated	1	13.17"	1,406
3	5 Inertia, TM	Actual	1	13.17"	3,287
4	74 Inertia, TM	Calculated	27	13.17"	1,244
5	74 Inertia, TM	Actual	27	13.17"	3,287
6	5 Inertia, FE	Calculated	27	21.069"	47,031
7	5 Inertia, FE	Calculated	1	13.17"	1,510
8	74 Inertia, FE	Calculated	1	13.17"	1,225
9	Corbo et al. [15]	Calculated	1	13.17"	7,307
10	Corbo et al. [15]	Actual	1	13.17"	34,482

CONCLUSION

A comparative validation of results generated by computer codes using both the Transfer Matrix and Finite Element approaches was made using experimental results. Transient torque data for a 66,000 HP air compressor from the industry was requested and utilized for this purpose. Four different analytical models were prepared for the same rotor, two for analysis using the Transfer Matrix approach and two for analysis using the Finite Element approach. Each such group included models with five and seventy-four inertias for analysis. The following analyses were run on these four models: undamped torsional frequency analysis, transient torque analysis and cumulative fatigue analysis. Subsequent results were then compared to the experimentally measured data and results of the analysis performed by Corbo et al. [16]. On the basis of this comparison, the following conclusions have been drawn:

1. One can infer that undamped torsional frequency analysis on all the four models gave good results for the first two modes when compared with the experimental data. However, the actual third mode was higher than that predicted by all the four models, with the seventy-four inertia model giving greater proximity (less than 6.7%) to the third mode as compared to the five inertia model. Since the fourth mode could not be clearly identified from the experimental data, no comparison was made with experimental data.
2. Campbell diagrams plotted from the undamped eigenvalues looked similar for the two five inertia models and the two seventy-four inertia models having four and three “encounter” speeds respectively corresponding to their natural frequencies.

3. Mode shapes for the first two modes predicted for all four models showed good compatibility amongst themselves and with the results of Corbo et al. [15]. Though eigenvectors for the third mode appeared similar for all the four models, it was noted that they occurred at different frequencies. Mode shapes corresponding to the fourth mode for models with equal number of inertias looked similar.
4. Preliminary run-up analysis on all the four models predicted the time to reach the motor synchronous speed to be around 27 s, which compared well with the experimental results that showed this time to be around 28 s.
5. Results for the transient torque analysis showed good conformance with the test data. Large resonant response on the actual torque-time graph, corresponding to the resonant speed to first natural frequency, was found to occur 1.6 s later than that predicted by all the four models and Corbo et al [16], besides giving lower torque values than predicted. The shapes of the predicted torque curves looked remarkably similar.
6. The strain-life approach [15] was used for the cumulative fatigue analysis of the weak links in the drive train in order to predict the number of startups for the different configurations under study.
7. Cumulative fatigue analysis was performed on eight configurations, which were essentially variations of the four analytical models discussed earlier. These results were then compared with the number of machine startups predicted by Corbo et al. [16]. Excepting configurations using the equivalent diameter of 21.069", which was used to prove that the actual diameter of a shaft element should be used instead of

equivalent diameter for fatigue analysis, the predicted number of machine startups on all the models, including the ones on which the actual torque data from experiments were used, were much lower than that predicted in [16].

8. Shaft material properties, which influence the value of the shear endurance limit, have not been vividly stated in Corbo et al. [16]. Hence, the material Steel 4340 (Hot Rolled and Annealed, BHN 243), whose properties matched closest to the material employed in [16], was used for analysis. It may be noted here that minor changes in input values for fatigue analysis could account for major differences in the predicted number of startups. Besides, due to the log-log nature of the strength vs. life curve, small errors in calculated strengths would lead to large errors in life prediction. Extreme care was, thus, exercised while selecting material properties before running the fatigue analysis.
9. The method for prediction of machine life [15, 16] reveals characteristically large changes in the predicted number of machine startups resulting from small alterations to the values of elastic and plastic strain components for the material. Information regarding the values selected for these components has not been provided by Corbo et al. [15, 16].
10. It is safe to infer that except for a few differences with [15, 16] in the results for the predicted life, the overall conformance of results generated by the computer codes (*XLTRC-Torsion*) with the available analytical and experimental results is good, and hence, acceptable.

NOMENCLATURE

- b = elastic strain component (slope of the elastic strain line)
- bka = intercept of $ka(N)$ vs N line on log-log scale
- bbk = intercept of $kb(N)$ vs N line on log-log scale
- bkf = intercept of $kfs(N)$ vs N line on log-log scale
- c = plastic strain component (slope of the plastic strain line)
- $[C]$ = tri-diagonal damping matrix
- $[CC] = [P]^T [C] [P]$ = cross-coupled modal damping matrix
- C_i = coefficients in shape functions
- C_L = load coefficient
- $[C_m]$ = diagonal matrix whose diagonal elements are $2\zeta_i\omega_i$
- d = shaft section diameter, in
- d_i = inside diameter, in
- D_o = outside diameter, in
- E = modulus of elasticity of material, lb/in²
- $\{F\}$ = complex amplitude of excitation torque
- FSh = shear factor
- $\{F(t)\}$ = external torque vector
- f = power source frequency, Hz
- g = acceleration due to gravity, 386.06 in/s²

- G = shear modulus, lb/in²
- G_n = speed ratio of station n to station 1 $\left(= \frac{N_n}{N_1} \right)$.
- $[I]$ = diagonal matrix of polar moment of inertia
- $[Iden]$ = identity matrix
- I_i = modal inertia of the i^{th} mode
- I_n = effective inertia referred to the speed of station n , lb·in²
- I'_n = actual inertia of station n , lb·in²
- J = polar area moment of inertia of section, in⁴
- $kfs(N)$ = fatigue stress concentration for a life of N cycles
- kts = geometric stress concentration factor
- K'_n = actual stiffness of station n , lb·in/rad
- K_n = effective stiffness referred to the speed of station n , lb·in/rad
- $[K]$ = tri-diagonal stiffness matrix
- $[K_m]$ = diagonal matrix whose diagonal elements are the square of the system natural frequencies
- \hat{K} = shifted stiffness, lb·in/rad
- $ka(N)$ = surface finish factor for a life of N cycles
- $kb(N)$ = size factor for a life of N cycles
- l = shaft section length, in

- mka = slope of $ka(N)$ vs N line on log-log scale
 mkb = slope of $kb(N)$ vs N line on log-log scale
 mkf = slope of $kfs(N)$ vs N line on log-log scale
 n = allowable number of starts for the machine
 N_j = number of cycles for each shear stress value j above the shear endurance limit
 N_i = shape or interpolation function
 N = life of machine, cycles
 $[P]$ = modal matrix
 $[P_R]$ = modal matrix consisted of rigid body modes
 $[P_O]$ = modal matrix consisted of oscillatory modes
 $[P_m]$ = modal matrix whose columns are the mode shapes which are normalized with respect to the inertia matrix
 q = notch sensitivity
 $\{q\}$ = vector of the generalized modal coordinates
 R = radius of the shaft element under consideration ($=d/2$), in
 $S(N)$ = allowable tensile stress corresponding to a life of N cycles, lb/in²
 SF = factor of safety
 $T(t)$ = kinetic energy, lb·in

$$\{T\} = [P]^T \{F(t)\} = \text{vector of modal external torque}$$

$$T_m = \text{motor excitation torque, lb}\cdot\text{in}$$

$$T_a = \text{accelerating unidirectional (average) motor torque, lb}\cdot\text{in}$$

$$T_p = \text{oscillating component of motor torque due to magnetic saliency and non-uniform rotor windings, lb}\cdot\text{in}$$

$$T_L = \text{load torque, lb}\cdot\text{in}$$

$$V(t) = \text{potential energy, lb}\cdot\text{in}$$

Greek Symbols

$$\alpha = \text{angular acceleration, rad/s}^2$$

$$\gamma = \text{material density, lb/in}^3$$

$$\varepsilon_f' = \text{true strain at fracture during tensile test}$$

$$\varepsilon(N) = \text{true strain corresponding to a life of } N \text{ cycles}$$

$$\zeta_i = \text{modal damping factor for the } i^{\text{th}} \text{ normal mode}$$

$$\theta = \text{angular displacement, rad}$$

$$\dot{\theta} = \text{angular velocity, rad/s}$$

$$\ddot{\theta} = \text{angular acceleration, rad/s}^2$$

$$\{\theta\} = \text{vector of angular displacement}$$

$$\sigma_f' = \text{true stress at fracture during tensile test, lb/in}^2$$

$$\tau = \text{torsional shear stress, lb/in}^2$$

τ_{cyclic} = cyclic shear stress, lb/in²

τ_{max} = maximum shear stress, lb/in²

τ_{min} = minimum shear stress, lb/in²

$\tau(N)$ = allowable shear stress corresponding to a life of N cycles,
lb/in²

Φ = phase, degrees (°)

$\phi_j(x)$ = j^{th} undamped normal mode

ϕ_{im} = i^{th} mode shape normalized with respect to the inertia matrix

Ω = excitation torque frequency, Hz

ω_s = slip frequency, Hz

ω_e = motor excitation frequency, Hz

ω_t = i^{th} torsional natural frequency, Hz

ω_m = motor frequency (varies from 0 to ω_{sync} during start-up), Hz

ω_{sync} = synchronous frequency, Hz

Subscripts

a, avg = average

$cyclic$ = recurrent

e = excitation

f = at fracture

L	=	due to load
m	=	modal
M	=	motor
max	=	maximum
min	=	minimum
osc	=	oscillating
O	=	oscillatory modes
p, pul	=	pulsating
$sync, S$	=	synchronous

REFERENCES

- [1] Vance, J. M., 1987, *Rotordynamics of Turbomachinery*, John Wiley and Sons, New York, pp. 57-113.
- [2] Wilson, W. K., 1956, *Practical Solution of Torsional Vibration Problems*, Volume One: Frequency Calculations, 3rd Ed., John Wiley and Sons, New York, pp. xiii–xxxii.
- [3] Pestel, E. C. and Leckie, F. A., 1963, *Matrix Methods in Elastomechanics*, McGraw-Hill Book Company, New York, pp. 51–129.
- [4] Lund, J. W., 1974, "Modal Response of a Flexible Rotor in Fluid-Film Bearings," *ASME Journal of Engineering for Industry*, Vol. 96, No. 2, pp. 525-533.
- [5] Childs, D. W., 1974, "A Rotor Fixed Model Simulation Model for Flexible Rotating Equipment," *ASME Journal of Engineering for Industry*, Vol. 96, No. 2, pp. 359-369.
- [6] Childs, D. W., 1975, "Two Jeffcott Based Modal Simulation Models for Flexible Rotating Equipment." *ASME Journal of Engineering for Industry*, Vol. 97, No. 3, pp. 1000-1014.
- [7] Childs, D. W., 1976, "A Modal Transient Rotor Dynamic Model for Dual Rotor Jet Engine Systems," *ASME Journal of Engineering for Industry*, Vol. 98, No. 3, pp. 876-882.
- [8] Eshleman, R. L., 1974, "Torsional Resonance of Internal Combustion Engines," *ASME Journal of Engineering for Industry*, Vol. 96, pp. 441-449.

- [9] Anwar, I. and Colsher, R., 1979, "Computerized Time Transient Torsional Analysis of Power Trains," ASME Paper 79-DET-74, ASME Design Engineering Division.
- [10] Rao, S. S., 1995, *Mechanical Vibrations*, Addison-Wesley Publishing Company, Boston, MA, pp. 725-749.
- [11] Bathe, K. J., 1996, *Finite Element Procedures*, Prentice Hall, Englewood Cliffs, NJ, pp. 887-937.
- [12] Squires, D. C., 1984, "Transient Analysis of Torsional Vibrations in Rotor Systems", M.S. Thesis, Univ. of Virginia, Charlottesville.
- [13] Corbo, M. A. and Malanoski, S. B., 1996, "Practical Design Against Torsional Vibration," Proceedings, 25th Turbomachinery Symposium, Texas A&M Univ., College Station.
- [14] Wachel, J. C. and Szenasi, F. R., 1993, "Analysis of Torsional Vibrations in Rotating Machinery," Proceedings, 22nd Turbomachinery Symposium, Texas A&M Univ., College Station.
- [15] Corbo, M. A. and Cook, C.P., 2000, "Torsional Vibration Analysis of Synchronous Motor-driven Turbomachinery," Proceedings, 29th Turbomachinery Symposium, Texas A&M Univ., College Station.
- [16] Corbo, M. A., Cook, C. P., Yeiser, C. W. and Costella, M. J., 2002, "Torsional Vibration Analysis and Testing of Synchronous Motor-driven Turbomachinery", Proceedings, 31st Turbomachinery Symposium, Texas A&M Univ., College Station.

- [17] Shigley, J. E. and Mischke, C. R., 2001, *Mechanical Engineering Design*, 6th Ed., McGraw-Hill Book Company, New York.
- [18] *ASM Metals Reference Book*, 2nd Ed., 1983, American Society for Metals, Metals Park, OH.
- [19] Lipson, C. and Juvinall, R. C., 1963, *Handbook of Stress and Strength*, The Macmillan Company, New York.
- [20] Nestorides, E. J., 1958, *A Handbook on Torsional Vibration*, Cambridge University Press, Cambridge.
- [21] Murphy, B. T., 1984, "Eigenvalues of Rotating Machinery," Ph.D. Dissertation, Texas A&M Univ., College Station.
- [22] Harris, C. M., 1996, *Shock and Vibration Handbook*, 4th Ed., McGraw-Hill Book Company, New York, pp. 38.1-38.16.
- [23] Evans, B. F., Smalley, A. J. and Simmons, H. R., 1985, "Startup of Synchronous Motor Drive Trains: The Application of Transient Torsional Analysis to Cumulative Fatigue Assessment," Transactions of the ASME, Paper No. 85-DET-122.
- [24] Orsey, R. S., Brockett, T. S. and Barrett, L. E., 1994, "Transient Torsional Analysis, A Manual for Use with Computer Program TORTRAN2 - Version 1.0," Technical Report UVA/64 3092/MAE94/477, Univ. of Virginia, Charlottesville.
- [25] Khurmi, R. S. and Gupta, J. K., 1999, *A Textbook of Machine Design*, Eurasia Publishing House (Pvt.) Ltd., New Delhi, India.

- [26] Rolovic, R. D., Tipton, S. M. and Sorem, J. R., Jr., 2001, "Multiaxial Stress Concentration in Filleted Shafts," ASME Journal of Mechanical Design. Vol. 123, No. 2, pp. 300-303.
- [27] Ganatra, N. K., Singhal, A., Conkey, A. and Vance, J. M., 2001, "Torsional Vibration Analysis Computer Code: *XLTRC-Torsion*," Report TRC-RD-2-01, Report to the Turbomachinery Research Consortium (TRC), Texas A&M Univ., College Station.
- [28] Ganatra, N. K., Singhal, A., Conkey, A. and Vance, J. M., 2002, "Torsional Vibration Analysis Computer Code: *XLTRC-Torsion*," Report TRC-RD-2-02, Report to the Turbomachinery Research Consortium (TRC), Texas A&M Univ., College Station.
- [29] Hoyt, S. L., 1952, *Metal Data*, Reinhold Publishing Corporation, New York.
- [30] Peterson, R. E., 1974, *Stress Concentration Factors*, John-Wiley & Sons, New York.
- [31] Rothbart, H. A., 1996, *Mechanical Design Handbook*, McGraw-Hill Book Company, New York.
- [32] Sankar, S., 1978, "On the Torsional Vibration of Branched Systems Using Extended Transfer Matrix Method," ASME Paper 77-WA/DE-4.
- [33] *Source Book on Industrial Alloy and Engineering Data*, 1978, American Society for Metals, Metals Park, OH.
- [34] Griffin, T. R., 1998, "Computer-Aided Design Software for Torsional Analysis," M.S. Thesis, Virginia Polytechnic Institute and State Univ., Blacksburg.

- [35] Spotts, M.F. and Shoup, T.E., 1998, *Design of Machine Elements*, 7th Ed., Prentice Hall, Upper Saddle River, NJ.
- [36] Szenasi, F. R. and Von Nimitz, W. W., 1978, "Transient Analysis of Synchronous Motor Trains," Proceedings, 7th Turbomachinery Symposium, Texas A&M Univ., College Station, pp. 111-117.

VITA

Nirmal Kirtikumar Ganatra, born May 23, 1978, was brought up in Bombay, India, from where he also acquired a major part of his education. In 1993, he graduated at the top of his matriculating Grade X class at St. Joseph's High School. He attended pre-degree college at K. J. Somaiya Polytechnic, Bombay from 1993-1996, and graduated with a Diploma in Mechanical Engineering. He joined Fr. Conceicao Rodrigues Institute of Technology, affiliated to the University of Bombay, and graduated college with Distinction in 1999. Later, he worked as an Automation Engineer with Matrix Electronics in New Bombay for one year. In the Fall of 2000, he began graduate studies at Texas A&M University, College Station, TX, where he worked with Dr. John Vance at the Turbomachinery Laboratory as a Research Assistant. Midway through his graduate studies, he joined Flow Products, Inc. at Brookshire, TX, as a Design Engineer performing design, rotordynamic and computational fluid dynamics (CFD) analyses for vertical pumps. Upon completion of his M.S. degree, Nirmal plans to continue his job with Flow Products, Inc.

Nirmal may be contacted at his parent's permanent address and telephone number in Bombay at:

Nirmal K. Ganatra
D/32 Rameshwar Apts.
Murar Road, Mulund (West)
Bombay – 400080
INDIA
Phone: 91-22-25676223